Copyright Warning & Restrictions

The copyright law of the United States (Title 17, United States Code) governs the making of photocopies or other reproductions of copyrighted material.

Under certain conditions specified in the law, libraries and archives are authorized to furnish a photocopy or other reproduction. One of these specified conditions is that the photocopy or reproduction is not to be "used for any purpose other than private study, scholarship, or research." If a, user makes a request for, or later uses, a photocopy or reproduction for purposes in excess of "fair use" that user may be liable for copyright infringement,

This institution reserves the right to refuse to accept a copying order if, in its judgment, fulfillment of the order would involve violation of copyright law.

Please Note: The author retains the copyright while the New Jersey Institute of Technology reserves the right to distribute this thesis or dissertation

Printing note: If you do not wish to print this page, then select "Pages from: first page # to: last page #" on the print dialog screen

UMI Number: 9539582

UMI

300 North Zeeb Road
Ann Arbor, MI 48103

ABSTRACT

COMPOSITE BEAM ANALOGY FRACTURE MODEL (CBAFM): A NON-LINEAR FRACTURE MECHANICS MODEL FOR CONCRETE

by

Mohammed Enamul Haque

The main objective of this dissertation is to develop a simple non-linear fracture mechanics model for the determination of fracture mechanics parameters for concrete, such as fracture process zone length (rp), critical fracture energy release rate (G_{IC}), critical stress intensity factor (K_{IC}) and fracture energy (G_F). The fracture process zone (FPZ) is modeled as a damaged non-elastic cohesive band where the extent of damage due to microcracking varies from no damage at the boundary of FPZ to complete crack surface separation at the notch or macro-crack tip. The proposed method can predict theoretically both the pre-peak and post-peak load versus crack mouth opening displacement (P-CMOD) and load versus load point deflection (P-δ) behaviors for a three point bend (3-PB) single-edge notch (SEN) beam. To apply this method, one only needs to measure peak load (P_u) and corresponding crack mouth opening displacement ($CMOD_u$) of a 3-PB SEN beam, and cylinder compressive strength. This method does not require post-peak load-deflection or CMOD data. Furthermore, it does not require information as to the unloading characteristics of a beam. The testing machine need not be very stiff. This makes the testing procedure greatly simplified and makes it suitable not only for the testing laboratory but also for work sites where a closed-loop testing machine is not available. A microcomputer

based simple numerical model is also developed based on the proposed fracture model. This model is verified by comparison with numerous experimental results as well as with other available methods from the literature.

COMPOSITE BEAM ANALOGY FRACTURE MODEL (CBAFM): A NON-LINEAR FRACTURE MECHANICS MODEL FOR CONCRETE

by
Mohammed Enamul Haque

A Dissertation
Submitted to the Faculty of
New Jersey Institute of Technology
in Partial Fulfillment of the Requirements for the Degree of
Doctor of Philosophy

Department of Civil and Environmental Engineering

May 1995

APPROVAL PAGE

COMPOSITE BEAM ANALOGY FRACTURE MODEL (CBAFM):
A NON-LINEAR FRACTURE MECHANICS MODEL FOR CONCRETE

Mohammed Enamul Haque

Prof. Farhad Ansari, Dissertation Advisor — Date
Professor of Civil Engineering, NJIT

Prof. Edward Dauenheimer, Committee Member — Date
Professor and Graduate Advisor of Civil Engineering, NJIT

Prof. C. T. Thomas Hsu, Committee Member — Date
Professor of Civil Engineering, NJIT

Prof. John Schuring, Committee Member — Date
Professor of Civil Engineering, NJIT

Prof. Ali Maher, Committee Member — Date
Associate Professor of Civil Engineering
Rutgers, State University of New Jersey

BIOGRAPHICAL SKETCH

Author: Mohammed Enamul Haque

Degree: Doctor of Philosophy in Civil Engineering

Date: May, 1995

Undergraduate and Graduate Education:

- Doctor of Philosophy in Civil Engineering,
  New Jersey Institute of Technology, Newark, New Jersey, 1995

- Master of Science in Civil Engineering,
  New Jersey Institute of Technology, Newark, New Jersey, 1986

- Bachelor of Science in Civil Engineering
  Bangladesh University of Engineering and Technology, Dhaka, Bangladesh, 1982

Major: Civil Engineering

Presentation and Publications:

Hussein, Rafaat, and Mohammed E. Haque, "Computer Aided Analysis and Design of Open System Multistory Reinforced Concrete Building" Presented at *Structure Congress '86 by the Structure Division of ASCE*, held in Louisiana, September, 1986.

Haque, Mohammed E., and Jamilur R. Choudhury, "Comparative Study of Seismic Analysis of Multistory Buildings using different Codes", Presented at the *27th Annual Convention of the Institution of Engineers, Bangladesh*, held in Dhaka in December, 1982.

Alam, M.K., and Mohammed E. Haque, "Comparative Influence of the Ganges and the Brahmaputra in the southern parts of Bangladesh", Presented at the *27th Annual Convention of the Institution of Engineers, Bangladesh*, held in Dhaka in December, 1982.

This thesis is dedicated
to
memory of my beloved son,
Mohammed Ziaul Haque (Zia)
(1991-1994)

ACKNOWLEDGMENT

I wish to express my gratitude to my thesis advisor, Dr. Farhad Ansari, for his encouragement, for making valuable suggestions, for his guidance, friendship and for his time spent for reviewing the manuscript. It was always comforting to know that Dr. Ansari was available when I needed him. I would also like to thank the thesis committee members, Prof. E. Dauenheimer, Prof. C.T. Thomas Hsu, Prof. J. Schuring and Prof. A. Maher (Rutgers, State University of New Jersey) for their interest in this work.

Finally, I wish to thank my family for their patience, support and encouragement during the work.

TABLE OF CONTENTS

Chapter	Page
1 INTRODUCTION AND OBJECTIVES	1
1.1 Introduction	1
1.2 Objectives	5
2 SURVEY OF LITERATURE	8
2.1 Fracture Mechanics of Concrete	8
2.1.1 Fictitious Crack Model (FCM)	9
2.1.2 Crack Band Model (CBM)	14
2.1.3 Two Parameter Fracture Model (TPFM)	17
2.1.4 Go Method	18
2.1.5 The Australian Method	21
2.2 Stress-Displacement Relationships	23
2.3 Fracture Energy	25
3 PROPOSED FRACTURE MODEL (CBAFM)	27
3.1 General	27
3.2 Modeling Assumptions and Boundary Conditions	28
3.3 Determination of Fracture Process Zone Length	31
3.4 Determination of Fracture Parameters	38
3.5 Theoretical P-CMOD Curve	45
3.5.1 Descending P-CMOD Curve	45
3.5.2 Ascending P-CMOD Curve	47
3.6 Theoretical Load-Deflection Curve	54
3.7 Estimation of Fracture Energy	55
3.8 Computer Model based on CBAFM	55

TABLE OF CONTENTS
(Continued)

Chapter	Page
4 RESULTS AND DISCUSSION	62
4.1 General	62
4.2 Experimental Verification	62
4.3 Comparison with Available Models	67
4.3.1 Comparison of Calculated K_{IC} and G_{IC} from Different Methods	67
4.3.2 Comparison among CBAFM, TPFM and Experimental Data	68
4.3.3 Comparison among CBAFM, FCM and Experimental Data	68
4.4 Comparison of Fracture Energy	73
4.5 Behavior of Crack Propagation	73
5 CONCLUSIONS AND RECOMMENDATIONS FOR FUTURE RESEARCH	79
5.1 Summary and Conclusions	79
5.2 Recommendations for Future Research	80
APPENDIX A FORMULAE DERIVATION	82
APPENDIX B COMPUTER PROGRAM BASED ON CBAFM.	88
APPENDIX C SI UNIT CONVERSION FACTORS	94
REFERENCES	95

LIST OF FIGURES

Figures **Page**

1.1 A loaded Concrete Beam with a crack and a fracture zone. No well-defined crack tip exists 1

1.2 Schematic Flow Chart for the proposed methodology 6

2.1 The principles for division of the deformation properties into σ–ε diagram and σ-w diagram, where w is the additional deformation due to formation of a fracture zone (Hillerborg, 1983) 10

2.2 The simplified description of the fracture zone as a "fictitious crack" with width w Hillerborg, 1983) 11

2.3 Energy dissipation related to the σ–ε and σ-w diagrams. The values of the shaded area represent the energy dissipation per unit material volume and per unit crack area respectively (Hillerborg, 1983) 12

2.4 Stress distribution in front of a crack tip before and after growth of real crack (Hillerborg, 1983) 13

2.5 Simple approximate assumption for use in numerical calculations (Hillerborg, 1983) 14

2.6 The Cartesian coordinate for Crack Band Model (Bazant, 1983) 14

2.7 Stress-Strain for fracture process zone (Bazant, 1983) 15

2.8 Two-parameter Fracture Model 19

2.9 (a) The σ-w curve approximated to a single straight line; (b) A two-line approximation of the σ-w curve (Petersson, 1981) 25

3.1 (a) Three-point load beam geometry, (b) Section 29

3.2 Partial beam section showing parameters at (P_u, $CMOD_u$) 29

3.3 Stress-Strain and linear softening stress-separation 29

3.4 (a) Actual beam section; (b) Actual stress diagram; (c) Linear strain-COD 30

LIST OF FIGURES
(Continued)

Figures **Page**

3.5 (a) Composite beam section; (b) Composite stress diagram; (c) Linear strain-COD 30

3.6 Schematic Flow Chart for Estimating Fracture Process Zone 32

3.7 P_u and P_e are identified on typical P-CMOD curve 33

3.8(a)Force and Moment Equilibrium 37

3.8(b)Force and Moment Equilibrium for Equivalent Composite Section 37

3.9 Schematic Flow Chart for Estimating Fracture Parameters 39

3.10(a) Actual Stress and Composite Stress in the Fracture Process Zone 40

3.10(b) Stress Loss within the Fracture Process Zone 41

3.11(a)Linear Crack Opening Displacement 42

3.11(b)Total and Recoverable Crack Opening Displacement Curves 43

3.12 Stress distribution before the Process zone becomes fully developed 48

3.13 Stress diagrams during the Process Zone developing stages 50

3.14 Composite Section and Composite Stress Diagram During the Process Zone Developing Stage 52

3.15(a) Computer Flow chart for the Proposed Model 57

3.15(b) Flow Chart for Program Module-1 58

3.15(c) Flow Chart for Program Module-2 59

3.15(d) Flow Chart for Program Module-3 60

3.15(e) Flow Chart for Program Module-4 61

LIST OF FIGURES
(Continued)

Figures **Page**

4.1(a) Comparison of computed (CBAFM), and experimental load-CMOD relations for small size beam (Beam No. 1) 64

4.1(b) Comparison of computed (CBAFM), and experimental load-deflection relations for small size beam (Beam No. 1) 64

4.2(a) Comparison of computed (CBAFM), and experimental load-CMOD relations for mid-size beam (Beam No. 2) 65

4.2(b) Comparison of computed (CBAFM), and experimental load-deflection relations for mid-size beam (Beam No. 2) 65

4.3(a) Comparison of computed (CBAFM), and experimental load-CMOD relations for large size beam (Beam No. 3) 66

4.3(b) Comparison of computed (CBAFM), and experimental load-deflection relations for large size beam (Beam No. 3) 66

4.4 Load versus CMOD curves - Theoretical prediction by CBAFM, TPFM and experimental Results (Jenq and Shah, 1985) for Beam No. 4 70

4.5 Load versus CMOD curves - Theoretical prediction by CBAFM, TPFM and experimental Results (Jenq and Shah, 1985) for Beam No. 5 70

4.6 Load versus CMOD curves - Theoretical prediction by CBAFM, FCM and experimental Results (Refai and Swartz, 1987) for Beam No. 6 71

4.7 Load versus CMOD curves - Theoretical prediction by CBAFM, FCM and experimental Results (Refai and Swartz, 1987) for Beam No. 7 71

4.8 Load versus CMOD curves - Theoretical prediction by CBAFM, FCM and experimental Results (Ratanalert and Wecharatana, 1990) for Beam No. 8 72

4.9 Load versus CMOD curves - Theoretical prediction by CBAFM, FCM and experimental Results (Ratanalert and Wecharatana, 1990) for Beam No. 9 72

4.10 Plot of $[P/P_u]$ versus Crack Growth $[(a_i+rp_i)/h]$ for different sizes of beams. 76

LIST OF FIGURES
(Continued)

Figures **Page**

4.11 Plot of [CMOD/$CMOD_u$] versus Crack Growth [(a_i+rp_i)/h] for different sizes of beams 76

4.12 Plot of [P/P_u] versus [$CMOD/CMOD_u$] for different sizes of beams 77

4.13 Plot of [P/P_u] versus [rp/rp_u] for different sizes of beams 77

4.14 Plot of [$CMOD/CMOD_u$] versus [rp/rp_u] for different sizes of beams 78

LIST OF TABLES

Table **Page**

2.1 Regression Coefficients 23

4.1 Beam Dimensions and Data from Experiments for use with the Proposed Model 63

4.2 Pre-cracked Beam Dimensions and Data from Experiments for use with the Proposed Model 63

4.3 Comparison of computed K_{IC} and G_{IC} values by different methods 67

4.4 Comparison of Fracture Energy values, G_F 73

LIST OF SYMBOLS

A_c	= area of the composite section
a_o	= initial notch length
a_i	= pre-crack length or crack length at i =1,2,3... during crack proceeding stage
b, B	= beam width
CCO	= cohesive crack opening
CMOD	= crack mouth opening displacement
$CMOD_F$	= crack mouth opening displacement at complete failure
$CMOD_u$	= crack mouth opening displacement at peak load
CTOD	= crack tip opening displacement
E	= Young's modulus of elasticity
E_v	= variable Young's modulus of elasticity
f_c'	= compressive strength of concrete
f_t'	= direct tensile strength of concrete
FPZ	= fracture process zone
G_F	= fracture energy
G_{IC}	= critical fracture energy release rate
h , H	= beam height
I_c	= composite moment of inertia
K_{IC}	= critical stress intensity factor or critical fracture toughness
l , L	= span length
$MCOD_{rc}$	= recoverable crack opening displacement of the process zone
$MCOD_t$	= total crack opening displacement of the process zone

LIST OF SYMBOLS
(Continued)

$MCOD_{ir}$ = irrecoverable crack opening displacement of the process zone

M_e = elastic moment capacity

M_u = maximum moment

N_v = variable modulur ratio

P = load

P_e = elastic load capacity

P_u = peak load

rp = fracture process zone length

S_c = section modulus of the composite section

W_c = fracture process zone band width

δ = load point deflection

σ = stress

σ_c = composite stress

γ = unit weight of concrete

CHAPTER 1

INTRODUCTION AND OBJECTIVES

1.1 Introduction

The formation and propagation of cracks play an important role in the behavior of all cementitious materials. Realistic design procedures require considerations as to the analysis of crack formation and crack propagation in concrete. In a cementitious material like concrete, due to microcracking, the stresses in front of a crack tip may have a stress distribution similar to the one shown in Figure 1.1. The concentration of the fracture zone in a small area, compared to the specimen dimensions as idealized in small scale yielding of metals, does not conform with the size of the fracture process zone in concrete. The microcracking zone is relatively large in concrete, and therefore calculation of fracture parameters should include the effect of this zone. The material in this fracture zone is far from being linear elastic, and if the zone length is not small compared with the specimen dimension and the notch or pre-crack depth, one has to consider the properties of the zone when studying the crack propagation.

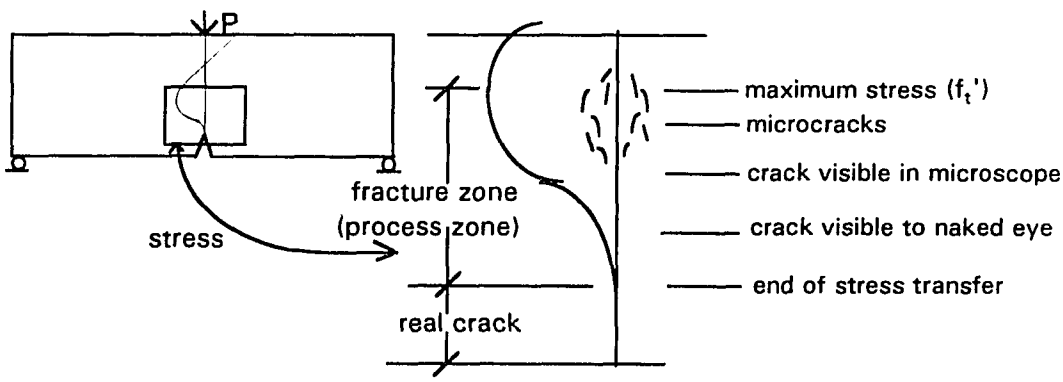

Figure 1.1 A Loaded Concrete Beam with a crack and a fracture zone.
No well-defined crack tip exists.

Application of linear elastic fracture mechanics (LEFM) to concrete was first attempted by Kaplan in 1961. Since then, a large number of test programs have been conducted to examine the applicability of LEFM to concrete. Results of these experiments show that when Mode I fracture toughness, K_{IC}, is evaluated for notched concrete specimen using LEFM (measured peak load and initial notch length), a significant size effect is observed. This size effect is attributed to nonlinear slow crack growth that occurs prior to peak load; and as a result the concepts of LEFM are not directly applicable. Different parameters have been proposed to describe the fracture behavior in concrete subjected to mode I deformation, such as the fracture toughness, K_{IC}, the critical strain energy release rate, G_{IC}, the fracture energy, G_F, the J integral, the critical tip opening displacement, $CTOD_c$ and the crack resistance, R. Many fracture mechanics models have been proposed in recent years to account for the non-linear behavior of concrete around the crack tip region. Among them, three of the most well-known fracture models are the Fictitious Crack Model (FCM) by A.E. Hillerborg (1976), the Crack Band Model (CBM) by Z.P. Bazant (1983), and the Two-Parameter Fracture Model (TPFM) by Jenq and Shah (1985a). The first two models represented the fracture process zone with a damage band or a band of crack closing pressure, which depends on the crack opening displacement (i.e. the post- peak stress-displacement relationship). The accuracy of these models relies significantly on the selected post-peak stress-displacement relationship, and since they are primarily using numerical finite element method, a non-linear stress-displacement relationship further complicates the computational process. The fracture energy, G_F, which is defined as the area under the post-peak stress versus the crack opening displacement curve, the Young's modulus of elasticity, E, and uniaxial tensile strength, f_t', are the material properties required to describe the tensile fracture behavior of concrete. On

the other hand, the TPFM does not require the post-peak constitutive relation, instead it calculates critical stress intensity factor at the tip of effective crack in such a way that the measured elastic crack-mouth-opening displacement equals the one calculated using LEFM formula. Since both the fracture mechanics parameters, (K_{IC} and $CTOD_C$) are directly determined from LEFM, crack tip singularity is automatically incorporated in the TPFM. Although, TPFM does not require post-peak stress-displacement relationship for calculating critical stress-intensity factor, but it requires cyclic P-CMOD relationship for estimating inelastic coefficients, (α , β). These inelastic coefficients are considered as material properties in TPFM, and employed for predicting theoretical P-CMOD and P-δ diagrams.

Two other well-known methods - Go Method (Go, Cheer and Swartz, 1983) and the Australian Method (Nallathambi and Karihaloo, 1985) are also used for calculating fracture parameters. The Go Method is based on bending analogy and is a finite element method. In this method, the William's stress function was applied to the single-edge notch beam specimen and evaluated at twenty-three boundary stations using boundary collocation method. On the other hand, the Australian method provides a set of regression formulae based on various experimental results and finite element analysis of a "fictitious beam". The fictitious beam containing a notch of effective depth and having unchanged stiffness was introduced to be equal to the real beam with original notch length and reduced stiffness. The accuracy of these two methods significantly depends on experimental results and boundary conditions of the finite element analysis.

None of these models developed a theoretical constitutive model that is able to describe softening behavior in terms of post-peak stress-displacement variables and the crack closing pressure. On the other hand, experimental determination of stable post-peak stress - crack mouth opening displacements and deflections require a very stiff

closed-loop servo-controlled materials testing machine. Stable post-peak displacements in beams are achieved by maintaining a constant rate of increase of CMOD through the closed-loop system. Even though, CMOD increases at a controlled rate, local deformation immediately across the crack increases drastically, sometimes resulting in a premature and unstable failure. Certainly, the complete testing procedure is complicated, time consuming, and above all, costly.

Fracture energy, G_F has been considered to be a reliable fracture mechanics parameter which can describe the process of cracking in concrete. To determine the fracture energy, the RILEM Technical Committee 50-FMC (1985) has put forward a recommendation, which specifies a method for the determination of the fracture energy of concrete and mortar by means of a stable three-point bend test on notched beams. Keeping the importance of G_F in mind, a simple theoretical methodology for the estimation of fracture energy is proposed in this dissertation.

1.2 Objectives

The main objective of this research is to develop a simple non-linear fracture mechanics methodology for the determination of fracture mechanics parameters, such as fracture process zone length (rp), critical fracture energy release rate (G_{IC}), critical stress intensity factor (K_{IC}) and fracture energy (G_F), and for predicting theoretically Load-CMOD and Load-Deflection behaviors for a three-point bend (3-PB) single-edge-notch (SEN) concrete beam. The main advantage of the proposed methodology is simplicity. Unlike previously developed cohesive models, the present approach does not require the post-peak load-deflection or CMOD data. Furthermore, the present approach does not require information as to the unloading characteristics of the beam. Therefore, the testing machine need not be very stiff. No closed-loop displacement control is needed. This makes the testing procedure greatly simplified and makes it suitable not only for the testing laboratory but also for work sites where a closed-loop testing machine is not available. The proposed methodology is shown schematically in the Flow Chart (Figure 1.2).

In the process of developing the proposed fracture mechanics model, the following are achieved:

1. The fracture process zone (FPZ) is modeled as a damage band where the extent of damage due to microcracking varies from no damage at the tip of FPZ to complete crack separation at the notch tip or macro-crack. Hence, in the proposed model, it is assumed that the FPZ possess a continuously variable Young's modulus of elasticity, E_V, where $E_V = 0$ at the notch and $E_V = E$ (uncracked modulus) at the boundary of FPZ.

2. The fracture process zone for a 3-PB SEN beam is analyzed using composite beam analysis and by satisfying equations of static equilibrium and stress boundary conditions.

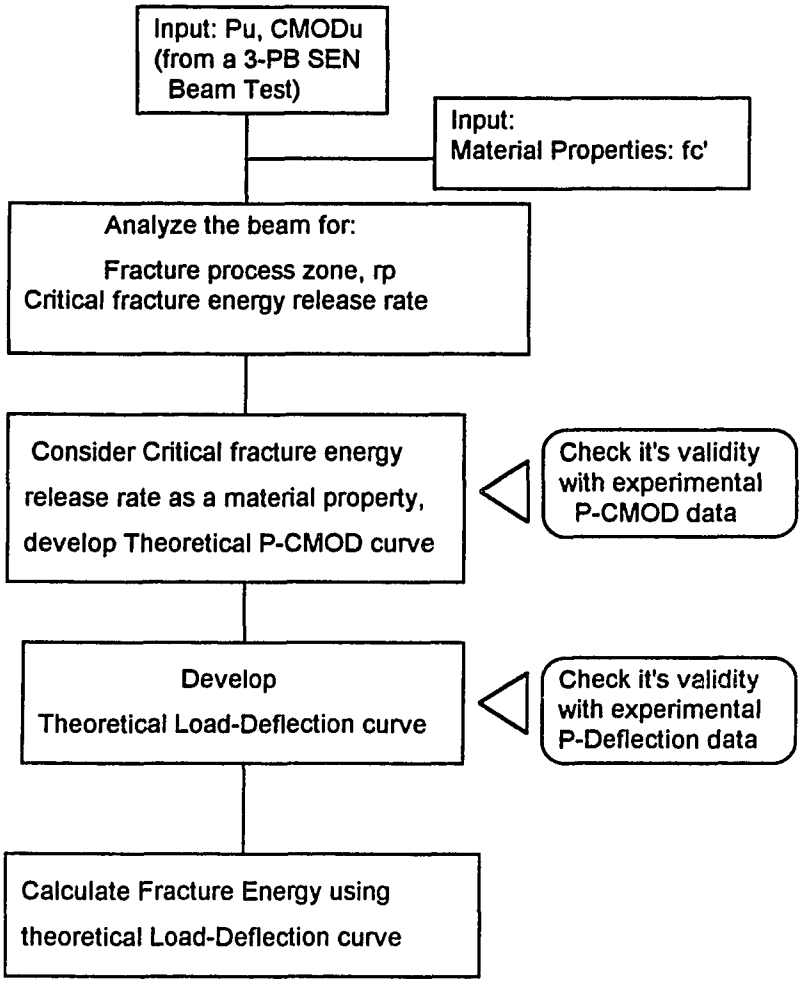

Figure 1.2 Schematic flow chart for the proposed methodology

3. A set of mathematical equations are derived to determine the fully developed process zone length (rp), unrecoverable stress or stress loss during the process of developing fracture zone, unrecoverable crack mouth opening displacement, critical fracture toughness K_{IC} , and critical fracture energy release rate, G_{IC}.

4. The entire Load-CMOD relationship is developed theoretically based on the knowledge of peak load (P_u) and corresponding crack-mouth opening displacement ($CMOD_u$).

5. Theoretical Load-Deflection relationship is developed from the theoretical Load-CMOD results obtained above.

6. Fracture energy, G_F is calculated from the theoretical Load-Deflection curve.

7. The validity of the theoretical Load-CMOD and Load-Deflection are examined with the available experimental data.

8. The proposed model is compared with the other available models, such as Fictitious Crack Model (FCM) and Two-Parameter Fracture Model (TPFM).

CHAPTER 2

SURVEY OF LITERATURE

2.1 Fracture Mechanics of Concrete

Linear elastic fracture mechanics (LEFM) considers the stress distribution in the vicinity of the crack tip to be related to a constant K, known as the stress intensity factor. The stress at the crack tip theoretically approaches infinity, while the stress in reality can never exceed the cohesive strength of the material. Since no real materials can withstand infinitely large stress, an inelastic zone is usually present in front of the crack tip. If size of the inelastic zone is much smaller than the dimension of a structure, linear elastic fracture mechanics (LEFM) can be approximately used. Nevertheless, the size of the inelastic fracture zone, also termed the fracture process zone, is small for usual dimensions of concrete structures. The material in the fracture process zone is partly destroyed due to micro-cracks, but still able to transfer stress. The stress transferring capability normally decreases when the local deformation of the zone increases, i.e. when the number of micro-cracks increases. At present, models with more than one fracture parameter have been proposed to explain the fracture process in concrete. Many fracture mechanics models have been proposed in recent years to account for the non-linear behavior of concrete around the crack tip region. The Fictitious Crack Model, FCM (Hillerborg, et al., 1976), the Crack Band Model, CBM (Bazant, et al., 1983), the Two-Parameter Fracture Model, TPFM (Jenq and Shah, 1985a, 1985b), the Go Method (Go, Cheer and Swartz, 1983) and the Australian Method (Nallathambi and Karihaloo, 1985) are reviewed in the literature survey.

Fracture energy, G_F has been considered to be a reliable fracture mechanics parameter which can describe the energy dissipation in the process of fracture. The RILEM method (RILEM TC-50 FMC 1985) which has been widely used by many

researchers for calculating the fracture energy is discussed in this literature survey. The basic concept of this method for calculating G_F, is to utilize the calculated area under the load-load point displacement curve for a three-point bend notched beam test.

2.1.1 Fictitious Crack Model (FCM)

Fictitious Crack Model (FCM) was proposed by A.E. Hillerborg (1976). In FCM, the fracture energy (GF) which is defined as the area under the post-peak stress vs. crack opening displacement (σ-COD) curve, uniaxial tension strength (f_t') and the shape of σ-COD curve (obtained from the uniaxial tension test) are the material parameters required for the FCM. The fracture process zone is modeled as an extension of the actual crack subjected to a closing pressure which depends on the crack opening displacement. The FCM assumes the effect of microcracked zone to be confined to a narrow band of line cracks where the total fracture energy is consumed.

The fundamental idea of FCM is best demonstrated by means of a tension test, Figure 2.1. The test is assumed to be deformation-controlled and stable, so that it is possible to follow the descending branch of stress-deformation curve all the way down to zero load. The test bar is assumed to be homogeneous and to have a constant cross-section. Before the maximum force F_{max} is reached, the deformations at A and B are identical. When F_{max} is reached, the deformation has a value ΔL_e. When the deformation is increased still further, the force starts decreasing due to the fact that a fracture zone develops somewhere along the bar. Consequently, as the force decreases, the deformation also decreases everywhere except within the fracture zone.

In Figure 2.1, it is assumed that the whole fracture zone falls within gauge length A. The deformation within gauge length B can then be described by means of a stress-strain curve, including the unloading branch. The deformation within gauge length A includes also the deformation of the fracture zone. The additional

deformation, w, due to the fracture zone is the difference between the descending branches of curves A and B. It is possible to describe the deformation properties of the test bar by means of two diagrams:

- The stress-strain (σ–ε) diagram, including the unloading branch, Figure 2.1c.
- The stress-deformation (σ-w) diagram for the fracture zone, Figure 2.1d.

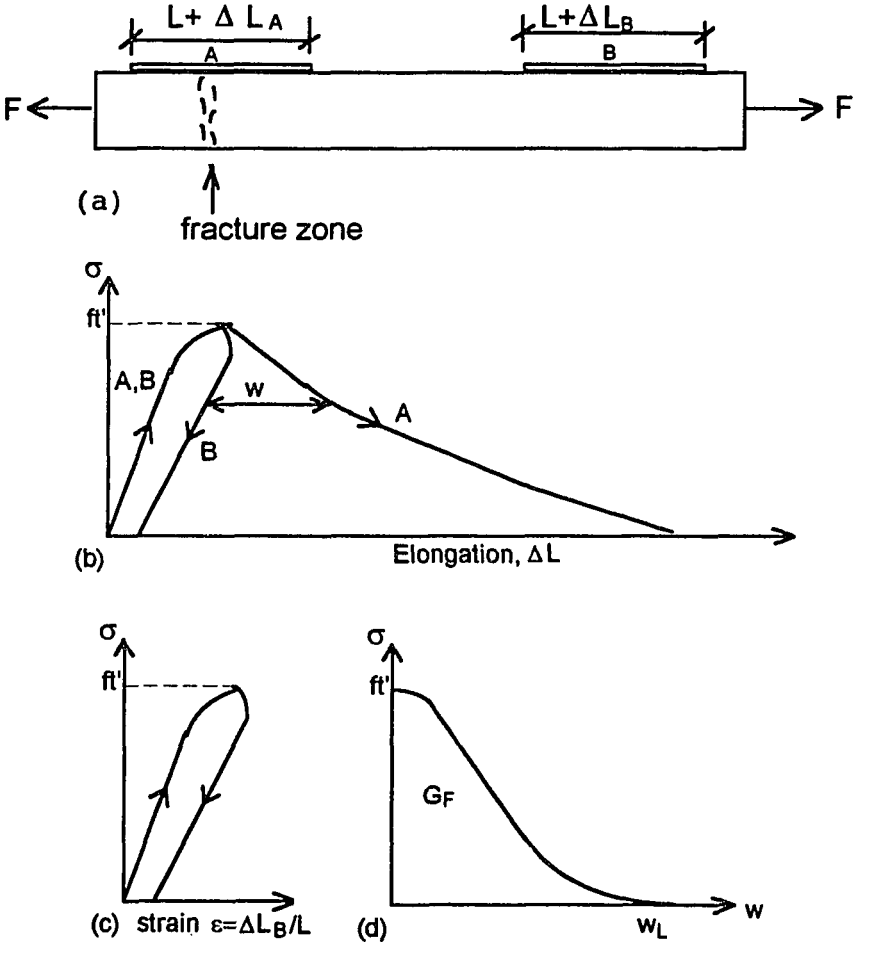

Figure 2.1 The principles for division of the deformation properties into a σ–ε diagram and σ-w diagram, where w is the additional deformation due to formation of a fracture zone (Hillerborg, 1983).

By these two diagrams, one can calculate the deformation ΔL of any gauge length L_o, where the gauge end is not situated within a fracture zone. If there is no fracture zone within the gauge length, the deformation is,

$$\Delta L = \varepsilon L_o. \tag{2.1}$$

If a fracture zone is situated within the gauge length, the deformation is,

$$\Delta L = \varepsilon L_o + w \tag{2.2}$$

It has to be noted that w is a length contrary to ε, which is a strain. The width of the fracture zone does not enter into the equation above. The simplest possible assumption can be that the original width of the fracture zone is zero. The total width of the fracture zone then equals w. According to the assumption of zero original width, the fracture zone can be described as a tied crack with width w, i.e. a crack which can transfer a stress, σ according to the σ-w curve when its width is w. As the fracture zone in reality has a certain width, the tied crack which is introduced as simplified description is not a real crack. It has therefore been called a fictitious crack.

The application of FCM to the description of the tensile test is shown in Figure 2.2.

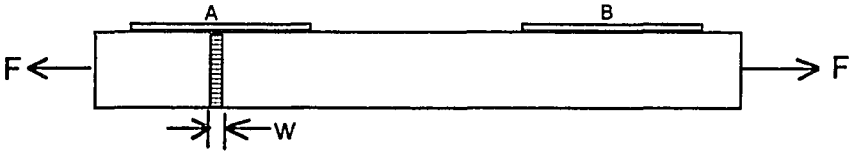

Figure 2.2 The simplified description of the fracture zone as a "fictitious crack" with width w (Hillerborg, 1983).

During the tensile test to complete separation, energy is absorbed inside and outside the fracture zone. With the FCM the energy absorbed in the fictitious crack is

$$A\int_0^{w_l} \sigma \cdot dw = AG_F \tag{2.3}$$

where A=cross sectional area; w_l=w-value for σ=0; G_F=area below the σ-w curve, Figure 2.3.

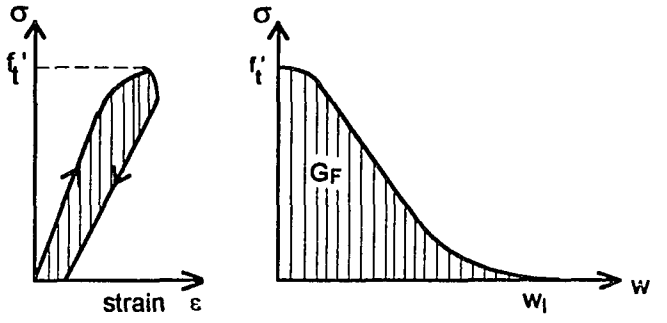

Figure 2.3 Energy dissipation related to the σ–ε and σ-w diagrams. The values of the shaded area represent the energy dissipation per unit material volume and per unit crack area respectively (Hillerborg, 1983)

G_F thus is the absorbed energy per unit crack area for the complete separation of the crack surface. The crack area in question is the projected area, not the total area of the irregular crack surface. The energy absorption outside the fictitious crack is determined in the usual way as the volume of the specimen times the area below the σ–ε curve. For a purely elastic material, this energy absorption is zero.

Figure 2.4 shows the stress distribution in front of a notch or a crack tip in a beam under the action of a growing imposed deformation (or load). The fracture zone that has developed is described as the fictitious crack. Within the fictitious crack the relation between the stress σ and the crack width w is given by σ-w curve. Everywhere outside the fictitious crack the σ–ε curve for the material is valid. As the deformation increases, the stress in front of the fictitious crack tip increases. No stress is assumed to be higher than the tensile strength, f_t'. As soon as a stress has reached f_t', any increase in deformation cause the development of a fictitious crack at that point. Thus the stress at the fictitious crack tip is f_t' as long as the fictitious crack grows.

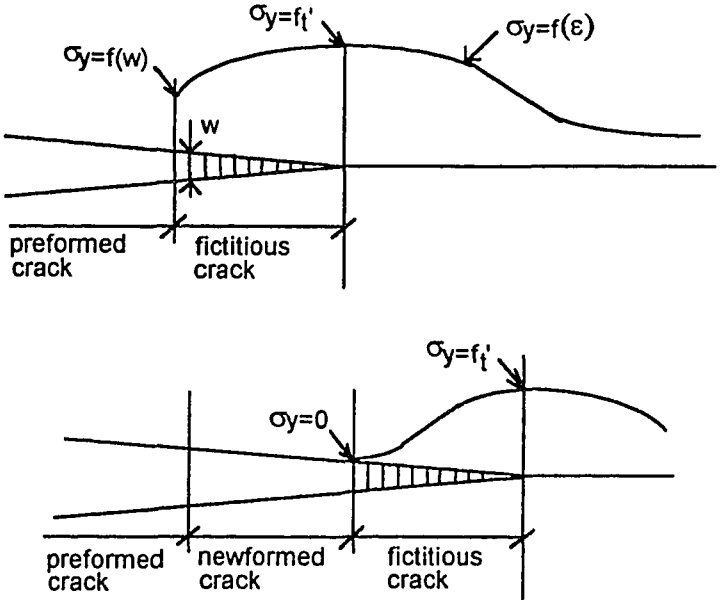

Figure 2.4 Stress Distribution in front of a crack tip before and after growth of real crack (Hillerborg, 1983)

Although the FCM has a very general applicability, it is hardly ever possible to find analytical solutions based on the FCM. Thus finite element method (FEM) is necessary to implement the model. In this method it is easy to follow the growth of fictitious and real cracks, which coincide with the sides of elements. The elements are just separated by distances w and forces corresponding to σ from σ-w curve are introduced across the crack.

In FEM calculations it is very time-consuming and extensive to use non-linear σ–ε and σ-w curves. It is however relatively inexpensive to use stepwise linear σ-w curves. The simplest possible assumptions regarding σ–ε and σ-w curves to be used in FEM analyses are according to Figure 2.5, i.e. , straight line approximations for both curves. Most of the analyses performed so far have been based on these assumptions.

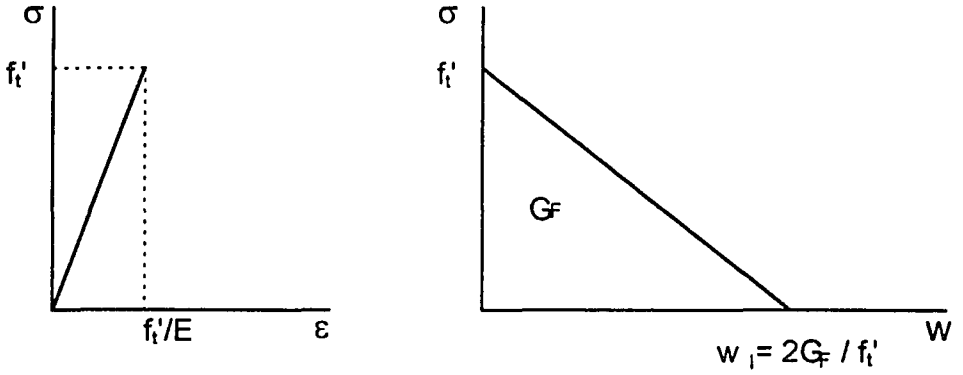

Figure 2.5 Simple approximate assumption for use in numerical calculations (Hillerborg, 1983)

2.1.2 Crack Band Model (CBM)

In concrete, as well as mortars, fracture is preceded by a gradual dispersed microcracking that occurs within a relatively large fracture process zone ahead of the tip of a continuous crack. In CBM, fracture of this type is modeled as the propagation of a band of uniformly and continuously distributed (smeared) cracks with a fixed width w_c at the fracture front, with w_c assumed to represent a material property (Figure 2.6).

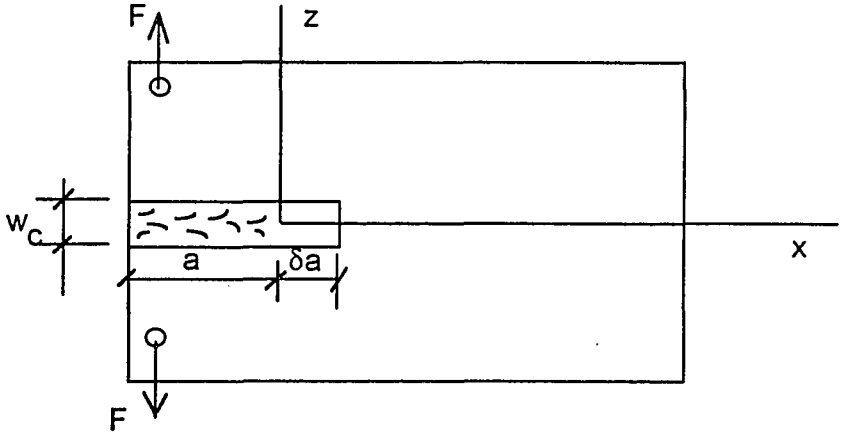

Figure 2.6 The Cartesian Coordinate for Crack Band Model (Bazant, 1983)

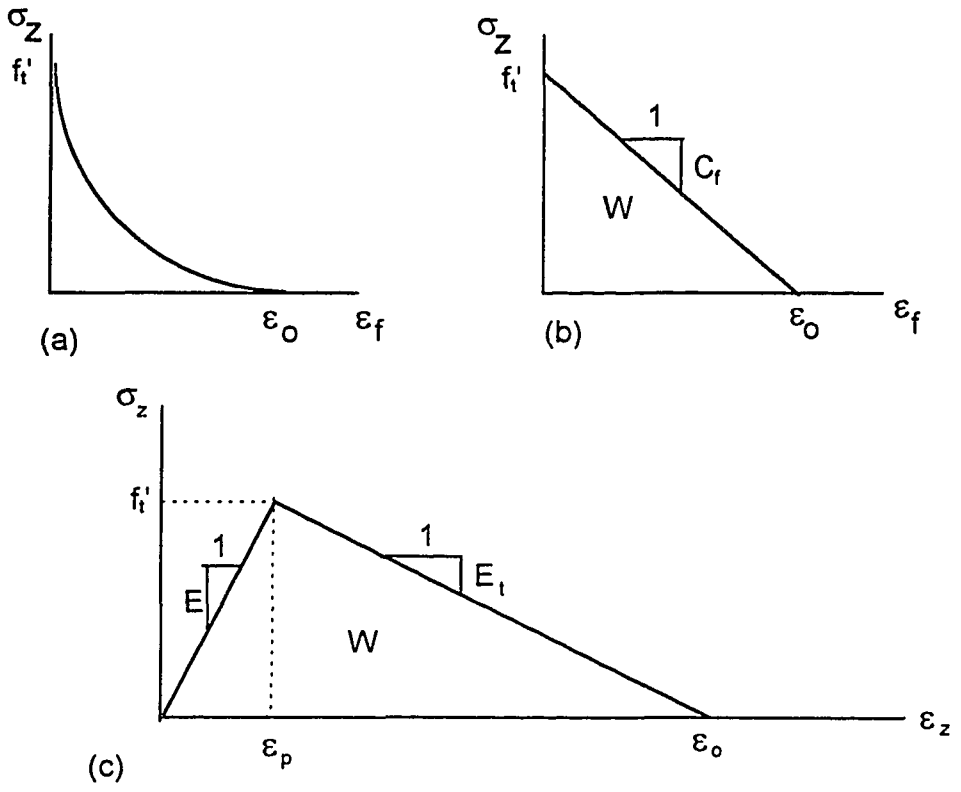

Figure 2.7 Stress-Strain for fracture process zone (Bazant, 1983)

The fracture energy, G_F, which is defined as the energy consumed in the formation and opening of all microcracks per unit area of plane (x,y) (Figures 2.6 and 2.7):

$$G_F = w_c \int_0^{\varepsilon_0} \sigma_z d\varepsilon_f \tag{2.4}$$

Referring to Figure 2.7(b)

$$G_F = 0.5 w_c \left(f_t' \varepsilon_0\right), \quad \varepsilon_0 = f_t' / C_f \tag{2.5}$$

where

w_c = the effective width of the fracture process zone (or crack band) over which the microcracks are assumed to be uniformly spread.

ε_f = the fracture strain, i.e., the additional strain caused by the opening of the microcracks.

f_t' = the direct tensile strength

$\varepsilon_o = \delta_f / w_c$, ($\delta_f$ = sum of the openings of individual microcracks), is the strain at the end of strain-softening and $\sigma_z = 0$.

C_f = the slope of strain-softening curve.

The pre-peak and post-peak behavior are both described by a stress-strain relationship as shown in Figure 2.7c, characterized by elastic modulus E, strength (peak stress) f_t', and strain-softening modulus E_t, which is negative.

$$\frac{1}{E_t} = \frac{1}{E} - \frac{1}{C_f} \le 0 \tag{2.6}$$

The energy consumed per unit advance of the crack band, called the fracture energy, may then be simply expressed as:

$$\begin{aligned} G_F &= w_c \left(1 - \frac{E}{E_t}\right) \frac{f_t'^2}{2E} \\ &= 0.5\left(f_t' \cdot \varepsilon_p + f_t'\left(\varepsilon_0 - \varepsilon_p\right)\right) w_c = W \cdot w_c \end{aligned} \tag{2.7}$$

where $W = \int \sigma_z \cdot d\varepsilon_z$

By analyzing numerous test data (Bazant and Oh, 1983), it was shown that G_F may be predicted (with a coefficient of variation about 16%) from the empirical formula,

$$G_F = 0.0214\left(f_t' + 127\right) f_t'^2 d_a / E \tag{2.8}$$

where E, f_t' are in pound per square inch; d_a=maximum aggregate size in inch.

Both the Fictitious Crack Model and the Crack Band Model, mentioned above, irrespective of the approaches adopted, require a complete stress-crack opening relationship.

2.1.3 Two Parameter Fracture Model (TPFM)

Two-Parameter Fracture Model (TPFM) was proposed by Jenq and Shah (1985a,b). The TPFM does not require post-peak (or strain softening) constitutive law. The TPFM includes the non-linear slow crack growth prior to peak load. The two parameters are the critical stress intensity factor (K_{IC}) and the critical crack tip opening displacement ($CTOD_c$). The concept behind this model can be explained from P-CMOD relationship (Figure 2.8). Initially, the P-CMOD plot is linear up to about half the maximum load ($0.5P_m$), and the corresponding CTOD is zero. Then, a significant inelastic displacement and slow crack growth occur during the load increase from 0.5 P_m on the ascending branch to $0.95P_m$ on the descending one. The latter loading station defines the critical point, often called point of instability. At this point, the crack tip opening displacement reaches a critical value ($CTOD_c$) and $K_I = K_{IC}$.

To determine the stress intensity factor, the effective crack length, a_e should be calculated first. The effective crack length is the sum of the initial notch (a_o) plus an effective crack extension at the peak load. An iterative numerical scheme is necessary to evaluate a_e. First an initial value of $a = a_o + \Delta l_e$ was assumed. For this assumed value of a, the measured value of maximum load and using the following LEFM equation (Tada, et al. 1976), $CMOD^e$ was calculated. This procedure was repeated until the calculated and measured CMOD values agree.

$$CMOD^e = \frac{6P \cdot l \cdot a}{h^2 \cdot b \cdot E} V_1\left(\frac{a}{h}\right) \qquad (2.9)$$

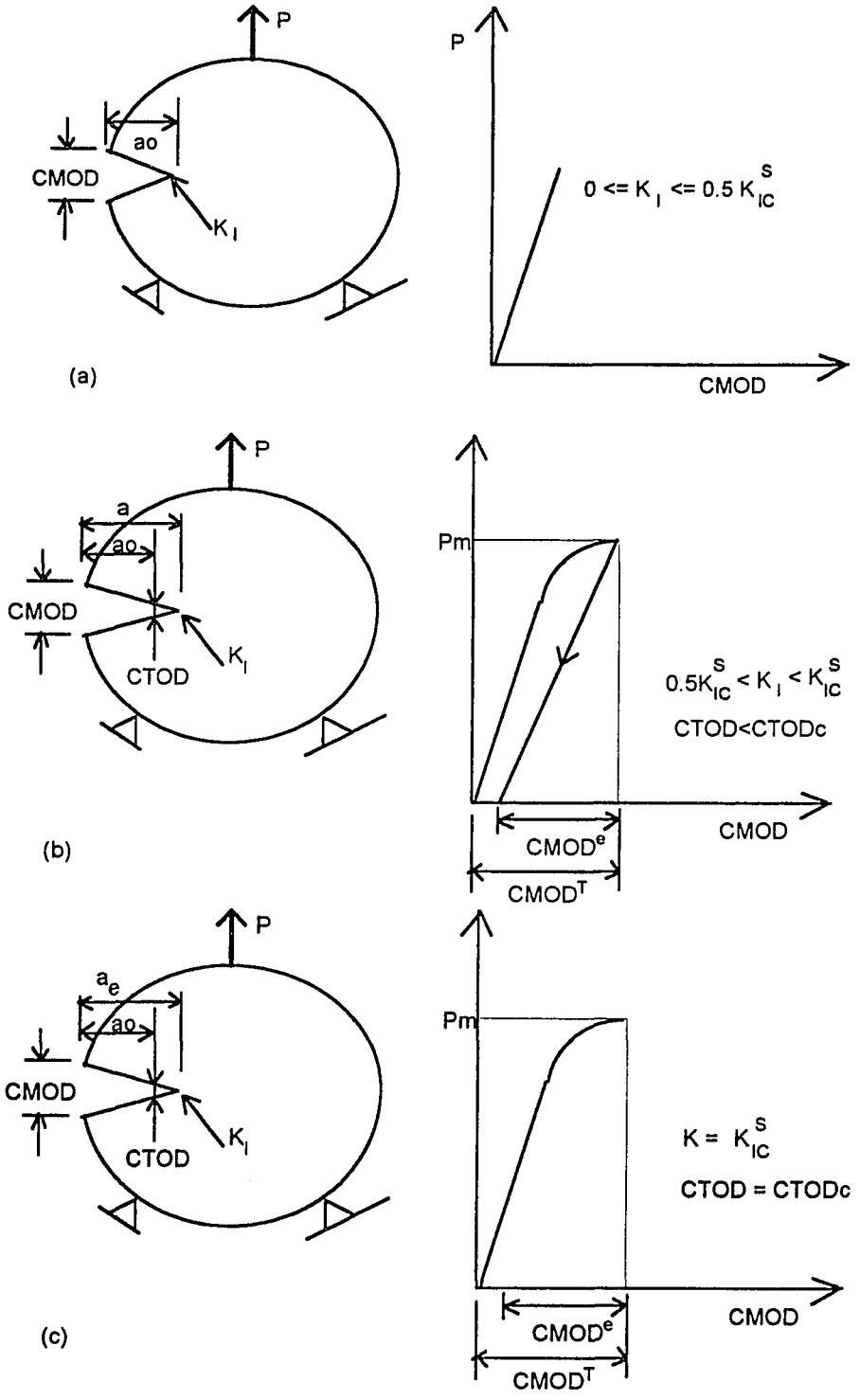

Figure 2.8 Two-Parameter Fracture Model

where

$$V_1(A) = 0.76 - 2.28A + 3.87A^2 - 2.04A^3 + \frac{0.66}{(1-A)^2}$$

for $\frac{l}{h} = 4; \quad A = \frac{a}{h}$

The critical stress intensity factor was calculated using the following LEFM equation:

$$K_{IC} = \frac{1.5P \cdot l\sqrt{a}}{h^2 \cdot b} F_1\left(\frac{a}{h}\right) \tag{2.10}$$

where $F_1\left(\frac{a}{h}\right) = \frac{1}{\sqrt{\pi}} \frac{1.99 - A(1-A)(2.15 - 3.93A + 2.7A^2)}{(1+2A)(1-A)^{3/2}}$,

$A = \frac{a}{h}$

The P-CMOD curves for the descending part were calculated using a constant value of K_{IC}. For a given beam, a given value of a, P and $CMOD_e$ can be calculated using LEFM equations (2.9) and (2.10). The value of $CMOD^T$ was computed using the following equation:

$$CMOD^T = CMOD^e\left(\frac{\beta}{\beta - 1}\right) + CMOD^T_{max}\left(\frac{\beta - \alpha}{\alpha\beta - \alpha}\right), \text{ for } CMOD^T \geq CMOD^T_{max} \tag{2.11}$$

where $CMOD^T_{max} = CMOD$ at peak load, P_m. The inelastic coefficients, α and β are considered material properties and determined from cyclic P-CMOD curves.

2.1.4 Go Method (Go, Cheer and Swartz, 1983)

This method calculates critical stress intensity factor based on bending analogy, finite element method. The William's stress function

$$\Phi = \sum_{n=1}^{N} r^{\frac{n}{2}+1} \left\{ \begin{array}{l} a_n \left[\sin\left(\frac{n}{2}-1\right)\theta - \frac{n-2}{n+2}\sin\left(\frac{n}{2}+1\right)\theta \right] \\ +b_n \left[\cos\left(\frac{n}{2}-1\right)\theta - \cos\left(\frac{n}{2}+1\right)\theta \right] \end{array} \right\} \qquad (2.12)$$

was applied to the single-edge-notch beam and evaluated at twenty-three boundary stations, using the boundary collocation method. The constant of those obtained by this method, a_1 is used to evaluate stress-intensity factor, K_I as

$$K_I = -a_1\sqrt{2\pi} \qquad (2.13)$$

An equation for estimating K_I was derived (Refai and Swartz, 1987) using the least squares method and was as following:

$$K_{IC} = \frac{M}{b \cdot h^{1.5}}\overline{A} \qquad (2.14)$$

$$M = \frac{P_u \cdot l}{4}$$

where for $\frac{l}{h} = 3.75$

$$\overline{A} = -0.065z^2 - 3.483z - 0.12 + 5.706z^{-1} + 0.166z^{-2}$$

$$z = \left(1 - \frac{a_e}{h}\right)$$

Other expressions for different l/h are given in Reference (Go, Cheer and Swartz, 1983).

Using the LEFM relation and neglecting Poisson's ratio, the critical energy release rate is found as following:

$$G_{IC} = \frac{K_{IC}^2}{E} \qquad (2.15)$$

In order to obtain the critical stress intensity factor, K_{IC}, using Equation. (2.14), the crack length must be evaluated at the point of instability. In Reference (Refai and Swartz, 1987), this point was estimated on the descending portion of the P-CMOD curved and at 0.95 of the maximum load. The effective crack length was estimated from the maximum load calibration curves.

2.1.5 The Australian Method

Nallathambi and Karihaloo (1985) proposed an analytical expression for determining critical stress intensity factor, K_{IC} and critical energy release rate, G_{IC} for plain concrete in 3-P bending. In developing these expressions, extensive use has been made of their experimental data and full allowance has been considered for slow crack preceding fracture and for the complex state of stress existing at the growing crack front. The determination of the extended crack growth is based on the results of a series of tests and on a self-consistent approximation to the non-linear response of the slow crack growth prior to fracture. In this method, a fictitious beam containing a notch of effective depth, a_e and having unchanged stiffness E was introduced to be equal to the real beam with the reduced stiffness and the original crack length. This concept with the help of a finite element program and the use of various experimental results led to a regression formula that represents the process zone as follows:

$$(a_e - a)/h = \frac{f_c'}{E}\left[\beta_o + \beta_1\left(\frac{g}{g+1}\right)^2 + \beta_2\left(\frac{g}{g+1}\right)\left(\frac{a}{h}\right) + \beta_3\left(\frac{a}{h}\right)\left(\frac{l}{h}\right) + \beta_4\left(\frac{h}{h+1}\right)\right] \qquad (2.16)$$

where the regression coefficients are

$\beta_o = 3960;\ \beta_1 = 144;\ \beta_2 = -88.2;\ \beta_3 = 8.7;\ \beta_4 = -3950;$

In Equation (2.16), $a=a_o$ for notched beams, and $a=a_i$ for precracked beams. The maximum aggregate size is denated by g.

In order to calculate the stress intensity factors and the energy release rates at the tip of an advancing crack, the true stress state ahead of the crack tip was considered. The stress state consists of a tensile stress normal to the crack front and also a tensile stress in the plane of the crack and a shear stress. Plane stress finite element calculations were performed on the test beams and a regression analysis was performed on the critical stress intensity factors and the critical energy release rates were calculated using the effective crack length. It follows that

$$K_{IC} = \sigma_o \sqrt{a_e}\, y_1\left(\frac{a_e}{h}\right) y_2\left(\frac{a_e}{h}, \frac{l}{h}\right) \tag{2.17}$$

$$G_{IC} = \sigma_o^2 \cdot \frac{a_e}{E} z_1\left(\frac{a_e}{h}\right) z_2\left(\frac{a_e}{h}, \frac{l}{h}\right) \tag{2.18}$$

$$\sigma_o = 1.5 \frac{P \cdot l}{b \cdot h^2} \tag{2.19}$$

The various functions appearing in Equations (2.17) and (2.18) are defined as following:

$$y_1\left(\frac{a_e}{h}\right) = A_0 + A_1\left(\frac{a_e}{h}\right) + A_2\left(\frac{a_e}{h}\right)^2 + A_3\left(\frac{a_e}{h}\right)^3 + A_4\left(\frac{a_e}{h}\right)^4 \tag{2.20}$$

$$z_1\left(\frac{a_e}{h}\right) = C_0 + C_1\left(\frac{a_e}{h}\right) + C_2\left(\frac{a_e}{h}\right)^2 + C_3\left(\frac{a_e}{h}\right)^3 + C_4\left(\frac{a_e}{h}\right)^4 \tag{2.21}$$

$$y_2\left(\frac{a_e}{h}, \frac{l}{h}\right) = B_0 + B_1\left(\frac{l}{h}\right) + B_2\left(\frac{l}{h}\right)^2 + B_3\left(\frac{l}{h}\right)^3 + B_4\left(\frac{l}{h}\right)\left(\frac{a_e}{h}\right) + B_5\left(\frac{l}{h}\right)^2\left(\frac{a_e}{h}\right) \tag{2.22}$$

$$z_2\left(\frac{a_e}{h},\frac{l}{h}\right) = D_0 + D_1\left(\frac{l}{h}\right) + D_2\left(\frac{l}{h}\right)^2 + D_3\left(\frac{l}{h}\right)^3 + D_4\left(\frac{l}{h}\right)\left(\frac{a_e}{h}\right) + D_5\left(\frac{l}{h}\right)^2\left(\frac{a_e}{h}\right) \qquad (2.23)$$

The regression coefficients A_i, C_i, B_j, D_j are given in the following Table 2.1.

Table 2.1 Regression Coefficients

i / j	A_i	C_i	B_j	D_j
0	3.6460	1.5640	0.4607	1.9560
1	-6.7890	-8.3200	0.0484	0.3982
2	39.2400	52.9500	-0.0063	-0.0553
3	-76.8200	-124.900	0.0003	0.0027
4	74.3300	122.900	-0.0059	0.0202
5	--	--	0.0003	-0.0055

In order to apply this method to the precracked beams, it was assumed (Refai and Swartz, 1987) that the initial crack depth - excluding any microcracking, i.e., outside the process zone, stress free surface - is equal to distance from the crack "mouth" to the root of the "V-shape" revealed by the dye penetration, a_i .

2.2 Stress-Displacement Relationships

The stress-crack opening displacement (σ-w) relationship will significantly affect the prediction of the load-CMOD and load-deflection responses using the FCM. The most reliable stress-displacement relation is supposed to be the one directly obtained from the uniaxial tension test. Conducting a direct tension test to observe the post-peak tensile response of concrete and other brittle materials is difficult. Different empirical

stress-displacement relationships have been proposed for mortar and concrete of various mix-proportions. A few of the experimentally observed σ-w relationships are described as follows:

Reinhardt conducted a direct tension test using a prism specimen with both ends glued to steel plates which were pulled apart under strain control (Reinhardt, Cornelissen and Hordijk, 1986), and proposed an empirical σ-w relation as:

$$\frac{\sigma}{f_t'} = \left(1 + (c_1\xi)^3\right)e^{(-c_2\xi)} - \xi\left(1 + c_1^{\,3}\right)e^{-c_2}. \qquad (2.24)$$

where

σ is the closing pressure

f_t' is the maximum tensile strength

ξ represents the ratio of crack opening displacement to maximum crack opening displacement at $\sigma = 0$;

$\xi = w / w_c$

c_1 and c_2 for concrete equals 3.0 and 6.93 respectively.

Wecharatana and Chiou (1986) also conducted direct tension test using closed-loop strain control to observe the post-peak responses. Two types of tension specimens, i.e. dog bone and tapered specimen, were used. They obtained an empirical σ-w relationship as follows:

$$\frac{\sigma}{f_t'} = \frac{A}{\xi}\left(1 - e^{-B\xi^C}\right)(1 - \xi)^D \qquad (2.25)$$

where σ, f_t' and ξ are the same as defined above.

A,B,C and D are empirical constants which for mortar and concrete are equal to 0.052, 400, 1.75 and 0.5 respectively.

The simplest σ-w relation is the linear one (Figure 2.9a) proposed and used by Petersson (1981). The two-line approximation of the σ-w relation (Figure 2.9b) was also proposed and used by Petersson (1981). Since the FCM requires extensive numerical computation, selecting a linear σ-w relation reduces enormously the tedious analysis. The linear σ-w function can be written as follows:

$$\frac{\sigma}{f_t'} = (1 - \xi) \tag{2.26}$$

where σ, f_t' and ξ are the same as defined above.

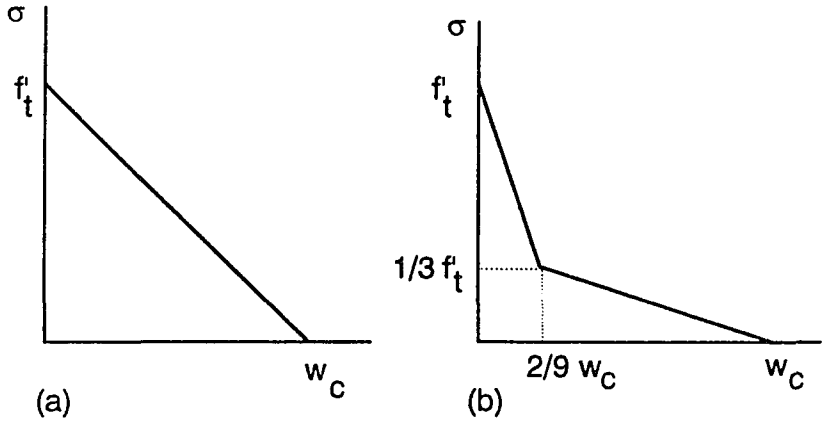

Figure 2.9 (a) The σ-w curve approximated to a single straight line; (b) A two-line approximation of the σ-w curve (Petersson, 1981)

2.3 Fracture Energy

The RILEM Technical Committee 50 FMC (1985) proposed a method for calculating fracture energy, G_F per unit surface area of real crack. The RILEM proposed formula is

$$G_F = (W_o + mg \cdot \delta_0) / A_{lig} \tag{2.27}$$

where

W_o = the area under the load versus load-point displacement (P-δ) curve from P=0 to P=0 again.

mg = self weight of the beam between supports plus twice the weight of fixtures supported by the beam.

δo = measured displacement at P=0 of the unloaded portion of the (P-δ) curve.

A_{lig} = Uncracked cross-sectional area of the beam at mid-span.

CHAPTER 3

PROPOSED FRACTURE MODEL (CBAFM)

3.1 General

According to the theory of elasticity, the stress intensity factor K_I is a measure of the stress intensity near the crack tip. When K_I reaches a critical values K_{IC}, the fracture toughness, the crack propagates. K_I and K_{IC} have to be used instead of stress and strength because according to the theory of elasticity the stress approaches infinity at the crack tip. As infinite stresses do not exist in reality, this way of treating the problem of crack stability never gives an exact description of the reality. When a notched or pre-cracked 3-P bend concrete beam as shown in Figure 3.1 subjected to load P_u, a zone of micro-cracks will be developed in front of the notch or the pre-crack front as shown in Figure 3.2. In-elastic deformations take place within this micro-cracked zone. It has been established that the stress transfer mechanism in the microcracked zone is govern by the stress-softening relationship. Since this in-elastic deformation zone can transfer stresses according to stress-softening relation (Figure 3.3), this in-elastic deformation zone are treated in this research as a cohesive crack opening (CCO) zone or fracture process zone (FPZ). The extent of this zone results in the observed nonlinearities.

In this dissertation, the fracture process zone (FPZ) is modeled as a damage band where the extent of damage due to microcracking varies from no damage at the tip of FPZ to complete separation at the notch or macro crack. Hence, in the proposed model, it is assumed that the FPZ possess a continuously variable Young's modulus of elasticity, E_V, where E_V=0 at the notch or macrocrack, and E_V=E (the modulus of elasticity of uncracked zone) at the end of fracture process zone. Because of E_V, it is possible to consider the microcracked section as a composite, and analyzed

it as such. Considering variable Young's modulus of elasticity within FPZ and analysis as a composite beam, the proposed fracture mechanics model has given a name as **C**omposite **B**eam **A**nalogy **F**racture **M**odel (CBAFM).

3.2 Modeling Assumptions and Boundary Conditions

Assumptions and boundary conditions employed for the analysis of the microcracked section according to the Composite Beam Analogy Fracture Model (CBAFM) are given in the following:

1. For simplicity, it is assumed that the stress-strain ($\sigma - \varepsilon$) and stress-displacement ($\sigma - u$) curves follow straight lines according to Figure 3.3. Before any micro-crack develops, the material follows stress-strain, and once micro-crack develops, the material follows stress-displacement. The strain portion of the horizontal axis in Figure 3.3 corresponds to the elastic stage, and the displacement portion corresponds to the microcracking stage.
2. Unloading-reloading within the stress-strain zone occurs along the original loading line. Within the stress-displacement zone unloading-reloading follows lines parallel to the loading elastic zone straight line according to Figure 3.3.
3. Fracture process zone is assumed to have fully developed first, at the peak load (P_u).
4. Young's Modulus of Elasticity (E) within the fracture process zone (or the cohesive crack opening zone) varies linearly from zero at the notch tip to E at the process zone boundary (Figure 3.4).
5. The fracture process zone is a cohesive zone and able to transfer stress.
6. Plane sections before bending remain plane after bending (Figs. 3.4(c) and 3.5 (c)).

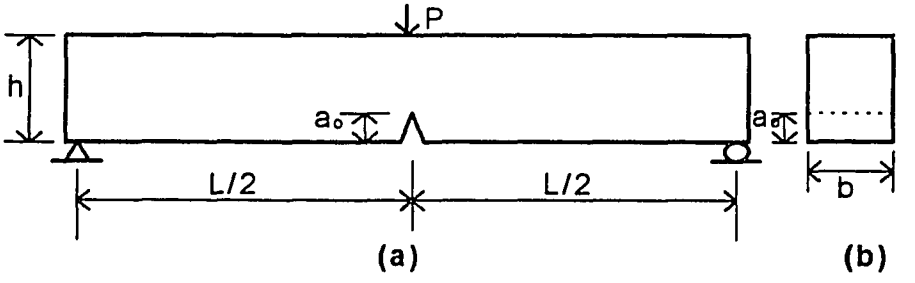

Figure 3.1 (a) Three Point Load Beam Geometry; (b) Section

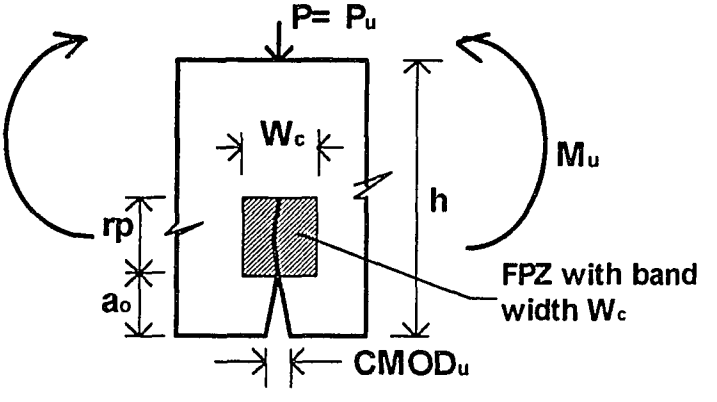

Figure 3.2 Partial Beam Section showing parameters at (P_u, $CMOD_u$)

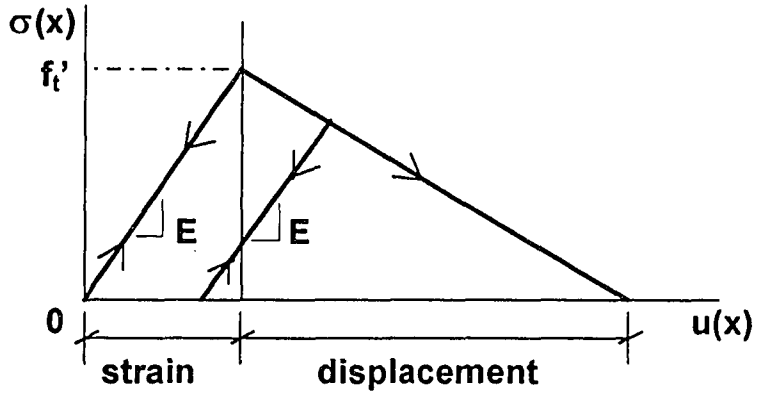

Figure 3.3 Stress-Strain and Linear Softening Stress-Separation

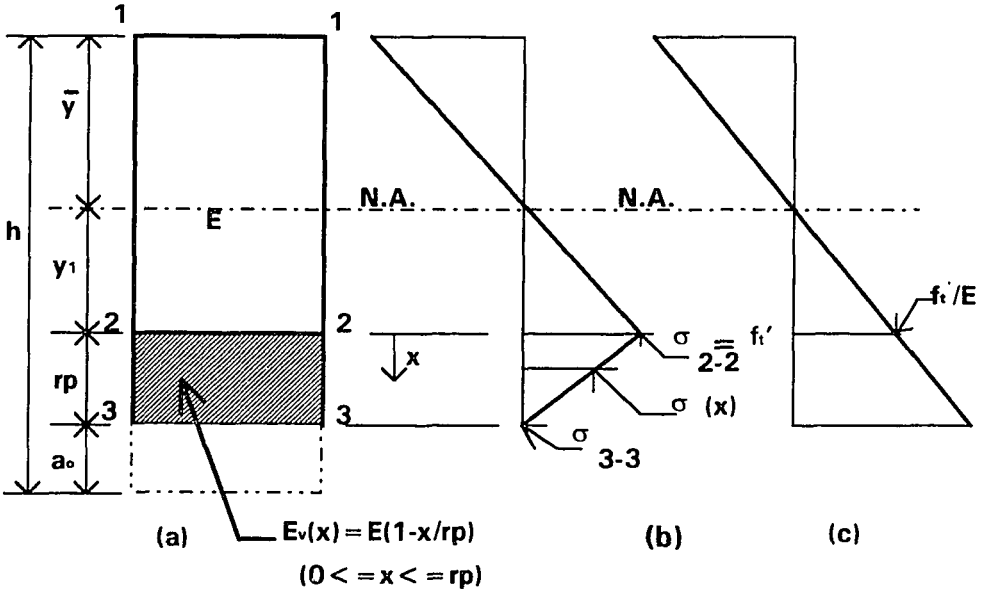

Figure 3.4 (a) Actual Beam Section; (b) Actual Stress Diagram; (c) Linear Strain-COD

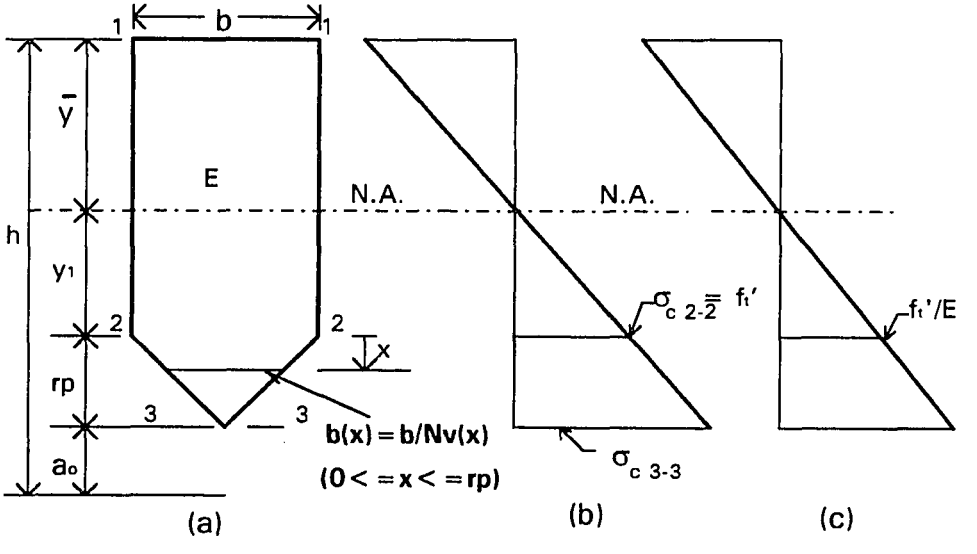

Figure 3.5 (a) Composite Beam Section; (b) Composite Stress Diagram; (c) Linear Strain-COD

3.3 Determination of Fracture Process Zone Length

Based on model assumptions, at peak load, P_u, the FPZ will be fully developed. Beyond this critical point, the real crack will begin to develop and load starts to decrease. The peak load, P_u is the only parameter needed for the computation of fully developed process zone, rp. The schematic flow chart for estimating fracture process zone length is shown in Figure 3.6.

The proposed model requires material properties of concrete which are direct tensile strength (f_t') and Young's Modulus of Elasticity (E), and they can be calculated from compressive strength (f_c') using the following Equations:

For Normal weight concrete,

$$E = 57000\sqrt{f_c'} \tag{3.1}$$

$$f_t' = 6\sqrt{f_c'} \tag{3.2}$$

where units for f_c', f_t' and E are in PSI.

The Equation for the direct tensile strength, f_t' (which is lower than the modulus of rupture, $f_r = 7.5\sqrt{f_c'}$) shown above is an empirical equation which has been widely used by many researchers.

In order to obtain a non-linear fracture process zone (i.e. microcracking zone), the peak-load, P_u must be greater than the elastic load carrying capacity of the section, P_e (Figure 3.7). This means that the peak-load moment, M_u should be greater than the elastic moment capacity of the section, M_e . The peak-load moment, M_u can be calculated from P_u, and the elastic moment capacity, M_e can be calculated using the following Equations: (for derivation, see Appendix A-1 and A-2)

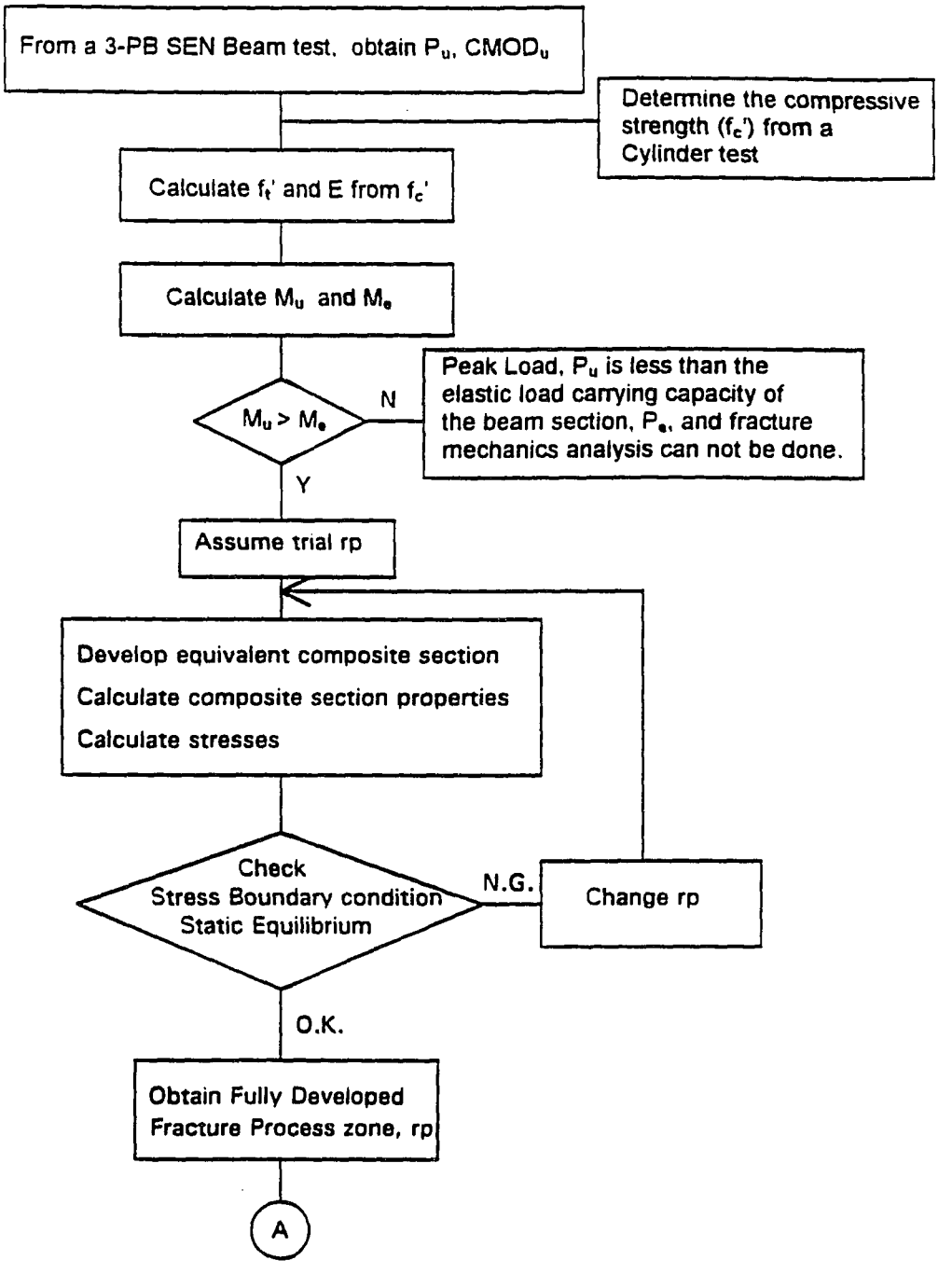

(Note: "A" is the connector for Figure 3.9)

Figure 3.6 Schematic Flow Chart for Estimating Fracture Process Zone

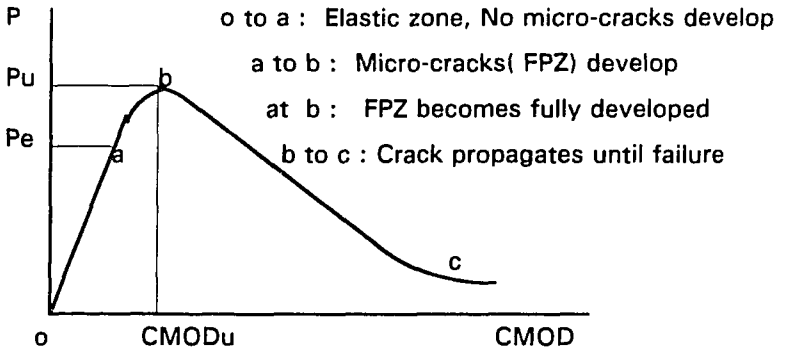

Figure 3.7 P_u and P_e are identified on a typical P-CMOD Curve

$$M_u = \frac{1}{4}(P_u \cdot L) + \frac{1}{8}(\gamma \cdot b \cdot h)L^2 \tag{3.3}$$

where γ = unit weight of concrete

= 150 lb./Cu.ft. for Normal Weight Concrete.

Beam dimensions, span (L), height (h) and width (b) are shown in Figure 3.1.

Elastic Moment Capacity, M_e can be expressed as

$$M_e = \frac{1}{6} f_t' b(h - a_0)^2 \tag{3.4}$$

Elastic load capacity, P_e can be calculated as

$$P_e = \frac{4}{L}\left[\frac{1}{6} f_t' b(h - a_o)^2 - \frac{1}{8}(\gamma \cdot b \cdot h)L^2\right] \tag{3.5}$$

If $M_u < M_e$, the peak load (P_u) will be less than the elastic load carrying capacity (P_e) of the section, and there will be no fracture process zone. In that case, the fracture mechanics analysis can not be done.

The fully developed fracture process zone (rp) is evaluated in an iterative manner according to the following steps:

(i) A trial rp within the limiting values, $0 < rp < 0.634(h\text{-}a_o)$ is chosen to start the iteration, where the upper limit for rp is evaluated according to the derivations given in Appendix A-3.

(ii) The variable modular ratio, $N_V(x)$ as shown in Figure 3.5 is defined as:

$$N_v(x) = \frac{E}{E_v(x)} \tag{3.6}$$

$$\text{where } E_v(x) = E\left(1 - \frac{x}{rp}\right); \quad (0 \le x \le rp)$$

(iii) Based on the variable modular ratio as defined in step (ii), the composite section (Figure 3.5a) is developed, and composite section properties, $A_c, \bar{y}, I_c, S_{c1\text{-}1}, S_{c2\text{-}2}$ and $S_{c3\text{-}3}$ are calculated using the following equations: (for derivation, see Appendix A-4)

Area of the Composite section:

$$A_c = (b \cdot h_1 - 0.5b \cdot rp) \tag{3.7}$$

where ligament length $h_1 = (h - a_0)$

Location of N.A. :

$$\bar{y} = \frac{3h_1^2 + rp^2 - 3h_1 rp}{6(h_1 - 0.5rp)} \tag{3.8}$$

Composite Moment of Inertia:

$$I_c = \frac{b(h_1 - rp)^3}{12} + b(h_1 - rp)(\frac{h_1 - rp}{2} - \bar{y})^2 + \frac{b \cdot rp^3}{36} + \frac{b \cdot rp}{2}(h_1 - 0.6667rp - \bar{y})^2 \quad (3.9)$$

Section Modulus for the composite section:

$$\begin{aligned} S_{c1-1} &= I_c / \bar{y} \\ S_{c2-2} &= I_c / (h_1 - rp - \bar{y}) \\ S_{c3-3} &= I_c / (h_1 - \bar{y}) \end{aligned} \quad (3.10)$$

(iv) Composite and actual stresses at different levels, 1-1, 2-2 and 3-3 are calculated using the following set of equations:

Composite stresses are calculated by using composite section moduli (Figure 3.5b):

$$\begin{aligned} \sigma_{c1-1} &= M_u / S_{c1-1} \\ \sigma_{c2-2} &= M_u / S_{c2-2} \\ \sigma_{c3-3} &= M_u / S_{c3-3} \end{aligned} \quad (3.11)$$

Actual stresses are calculated from composite stresses using modular ratios (Figure 3.4b):

$$\begin{aligned} \sigma_{1-1} &= \sigma_{c1-1} \\ \sigma_{2-2} &= \sigma_{c2-2} \\ \sigma_{3-3} &= \frac{\sigma_{c3-3}}{N_v(x = rp)} = \frac{\sigma_{c3-3}}{\infty} = 0.0 \end{aligned} \quad (3.12)$$

It should be noted that the modular ratios at levels 1-1 and 2-2 are 1.

(v) The stress boundary condition at the tip of process zone rp, requires:

$$\sigma_{2\text{-}2} = \sigma_{c2\text{-}2} = f_t' \tag{3.13}$$

(vi) The compressive force (C), tensile force (T) and moment capacity ($M_{CAPACITY}$) are calculated using the following set of equations (Figure 3.8b):

(for derivation, see Appendix A-6)

$$\begin{aligned} C &= 0.5 \cdot \sigma_{c1\text{-}1} \cdot b \cdot \bar{y} \\ T_1 &= 0.5 \cdot \sigma_{c2\text{-}2} \cdot b(h - a_0 - \bar{y} - rp) \\ T_2 &= \frac{1}{3} b \cdot rp(\sigma_{c2\text{-}2} + \frac{1}{2}\sigma_{c3\text{-}3}) \\ T &= T_1 + T_2 \\ M_{CAPACITY} &= C \cdot Z \\ or &= T \cdot Z \end{aligned} \tag{3.14}$$

Where moment arm, $Z = 0.6667\bar{y} + \bar{y}_1$,

Where $\bar{y}_1 = \frac{1}{T}\left[\frac{2}{3}T_1(h - a_0 - \bar{y} - rp) + T_2\left\{(h - a_0 - \bar{y} - rp) + \frac{1}{2}rp\left(\frac{\sigma_{c2\text{-}2} + \sigma_{c3\text{-}3}}{2\sigma_{c2\text{-}2} + \sigma_{c3\text{-}3}}\right)\right\}\right]$

and by substituting, $\frac{\sigma_{c3\text{-}3}}{\sigma_{c2\text{-}2}} = \frac{h - a_0 - \bar{y}}{h - a_0 - \bar{y} - rp}$

$$\bar{y}_1 = \frac{1}{T}\left[\frac{2}{3}T_1(h - a_0 - \bar{y} - rp) + T_2\left\{(h - a_0 - \bar{y} - rp) + \frac{1}{2}rp\left(\frac{2(h - a_0 - \bar{y}) - rp}{3(h - a_0 - \bar{y}) - 2rp}\right)\right\}\right]$$

(v) Check the static equilibrium, $\sum H = 0, \sum M = 0$

$$T = C$$

$$M_u = M_{CAPACITY}$$

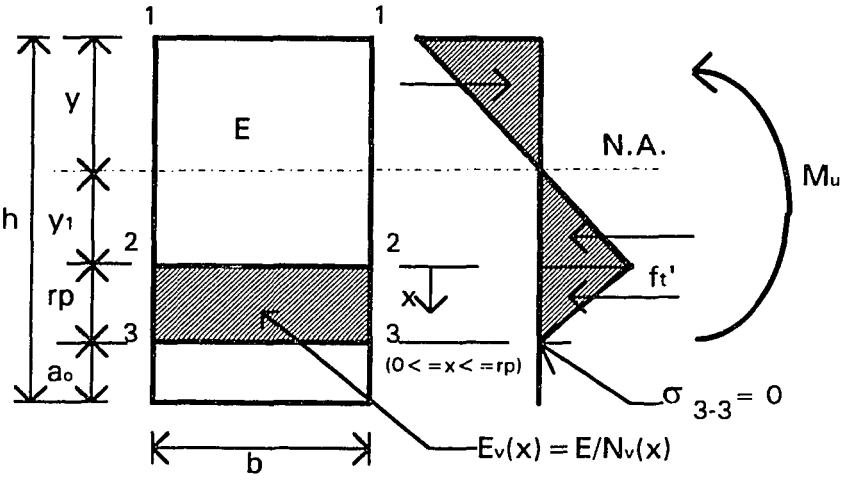

Figure 3.8 (a) Force and Moment Equilibrium

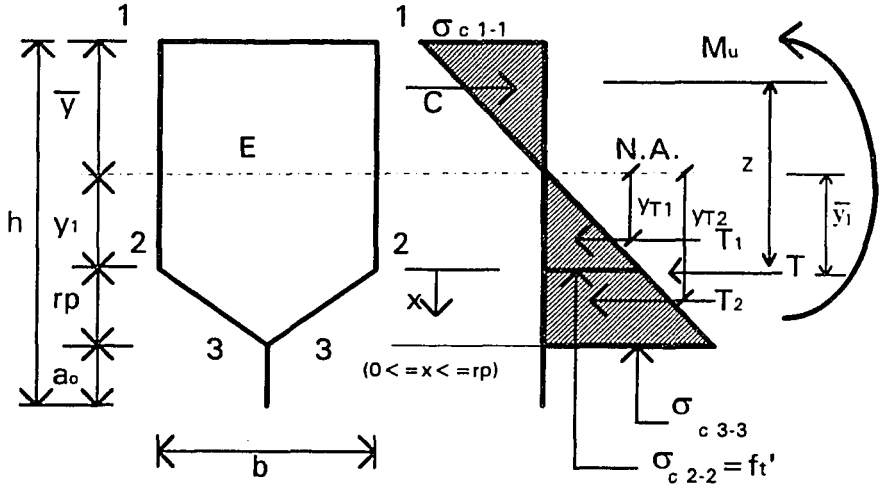

Figure 3.8(b) Force and Moment Equilibrium for Equivalent Composite Section

This iterative procedure (steps (i) through (v)) is continued by changing rp values until the stress boundary condition and the equations of static equilibrium are satisfied. The rp which satisfies both the stress boundary condition and static equilibrium is the correct process zone length.

3.4 Determination of Fracture Parameters

The methodology to be used to determine fracture parameters, such as critical fracture energy release rate, G_{IC} and critical stress intensity factor, K_{IC} is shown in a schematic flow chart (Figure 3.9). Before calculating fracture parameters, one must obtain the fully developed fracture process zone length, rp using the procedure as described in previous section and in Figure 3.6.

G_{IC} is the critical energy release rate per unit width per unit crack extension at the peak. It corresponds to the situation when the process zone is fully developed, and any further increase in deformation results in growth of macrocrack and a corresponding drop in load. Unlike the LEFM based G_{IC}, the energy release rate here is not elastic, since it consists of the energy consumed during the formation of the process zone. G_{IC} is the irrecoverable energy absorbed during crack formation. It is evaluated by integrating the product involving the consumed stress (irrecoverable stress) and the irrecoverable opening displacement of the process zone:

$$G_{IC} = \frac{1}{b}\int_{x=0}^{x=rp} \sigma_{ir}(x) \cdot MCOD_{ir}(x)dx \qquad (3.15)$$

where,

$\sigma_{ir}(x)$ = consumed stress distribution, or the irrecoverable stress within the process zone.

$MCOD_{ir}(x)$ = irrecoverable opening displacement of the microcracked or the process zone.

Irrecoverable stress is defined as the difference between the composite and actual stresses within the microcracked region (Figure 3.10), and is evaluated in the following manner:

At a distance x (within the FPZ)

$$\text{Composite stress distribution} = \sigma_c(x) = \frac{M_u(y_1 + x)}{I_c} = f_t'\left(1 + \frac{x}{y_1}\right) \tag{3.16}$$

$$\text{Actual stress distribution} = \sigma(x) = \frac{1}{N_v(x)}\sigma_c(x) = \left(1 - \frac{x}{rp}\right)\sigma_c(x) \tag{3.17}$$

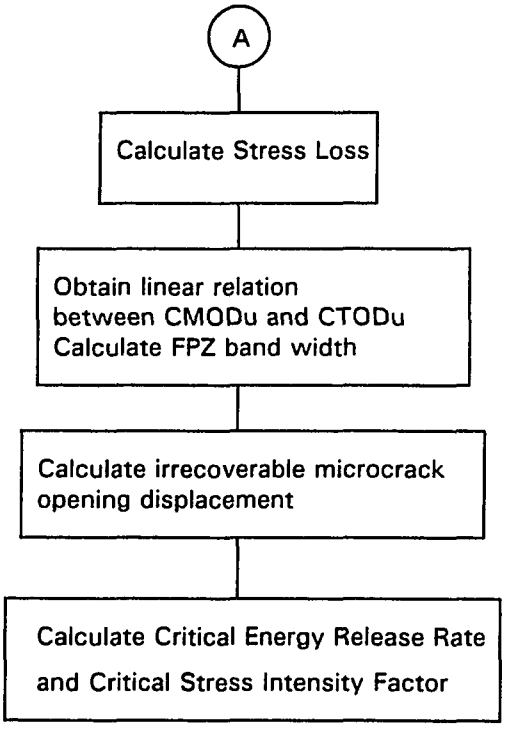

(Note: "A" is the connector for Figure 3.6)

Figure 3.9 Schematic Flow Chart for determining Fracture Parameters

Stress loss (Irrecoverable stress) = $\sigma_{ir}(x) = \sigma_c(x) - \sigma(x)$

$$= \sigma_c(x)\left[1 - \frac{1}{N_v(x)}\right]$$

$$= \sigma_c(x)\left[1 - 1 + \frac{x}{rp}\right]$$

$$= \sigma_c(x)\left(\frac{x}{rp}\right)$$

$$= \frac{M_u \cdot y_1}{I_c}\left(1 + \frac{x}{y_1}\right)\left(\frac{x}{rp}\right)$$

Since, $\frac{M_u \cdot y_1}{I_c} = \sigma_{c2-2} = f_t'$

Therefore, $\sigma_{ir}(x) = f_t'\left(1 + \frac{x}{y_1}\right)\left(\frac{x}{rp}\right)$, where $0 \le x \le rp$ (3.18)

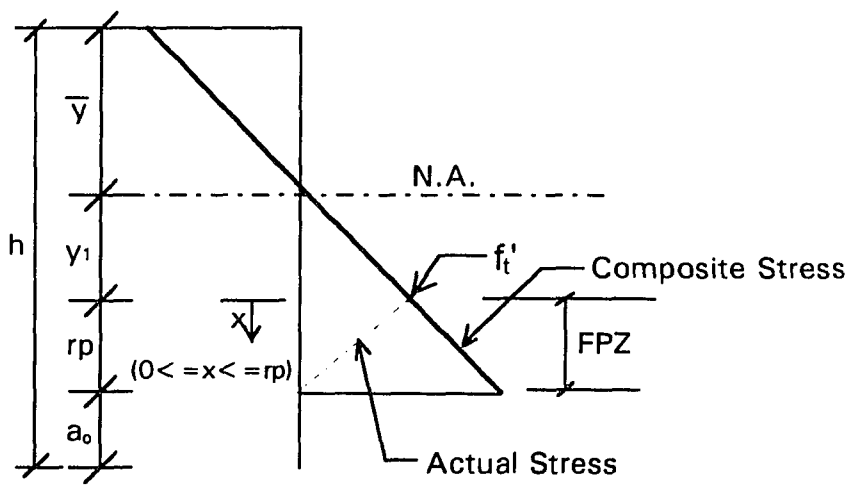

Figure 3.10(a) Actual Stress and Composite Stress in the Fracture Process Zone.

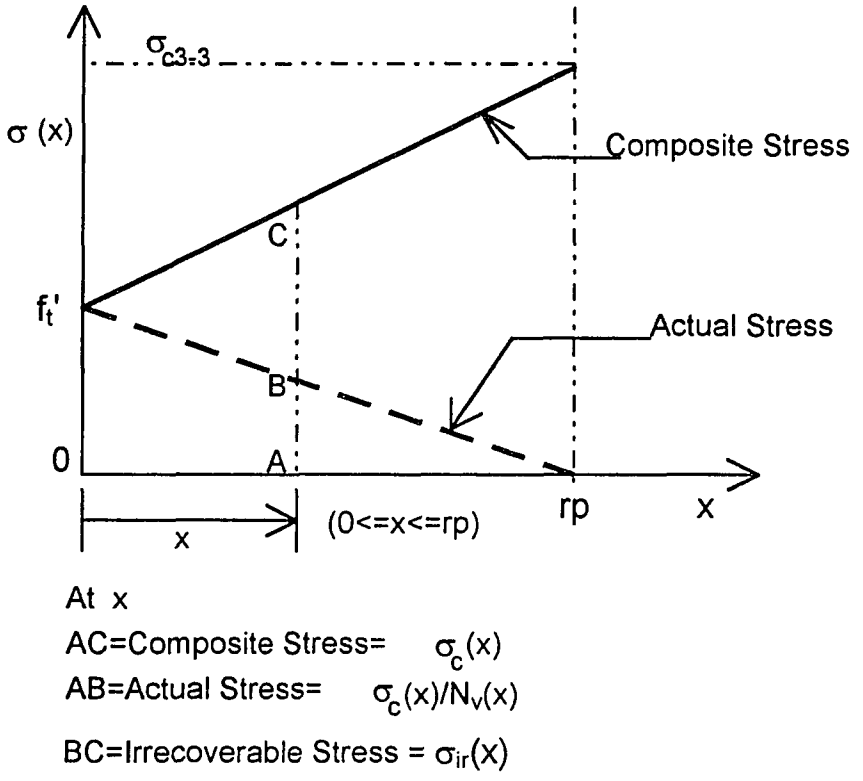

Figure 3.10(b) Stress Loss within the Fracture Process Zone

Figure 3.11(a) shows the linear crack opening displacement which is based on the modeling assumption and boundary condition (6) - Plane sections before bending remain plane after bending. By assuming existence of linear relationship between the crack tip and crack mouth opening at peak load, the crack-tip-opening displacement ($CTOD_u$) can be related to crack-mouth-opening displacement ($CMOD_u$) as following:

$$CTOD_u = CMOD_u\left[\frac{(h-\bar{y}-a_o)}{(h-\bar{y})}\right] \tag{3.19}$$

Similarly, assuming linear relations, the band width W_c can be expressed as:

$$W_c = \left[\frac{CMOD_u}{f_t^{'}/E}\right]\left(\frac{y_1}{h-\bar{y}}\right) \tag{3.20}$$

where $y_1 = (h - \bar{y} - rp - a_o)$

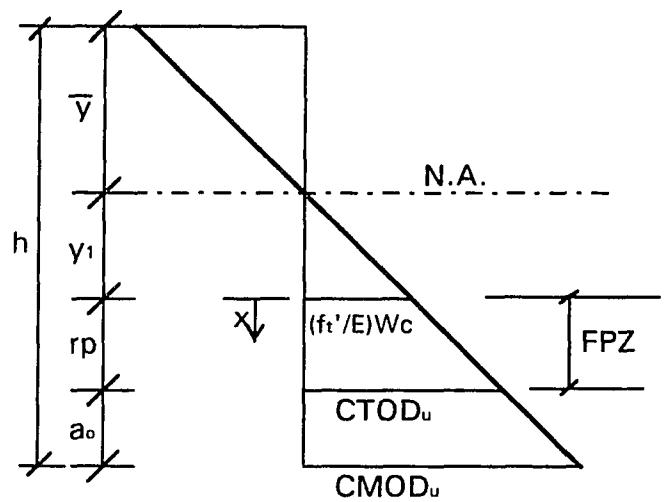

Figure 3.11(a) Linear Crack Opening Displacement

As shown in Figure 3.11(b), the total opening displacement of the process zone, $MCOD_t(x)$ as a function of x (where $0 \le x \le rp$) is derived from the composite stress distribution as:

$$MCOD_t(x) = \frac{M_u}{I_c}(y_1 + x)\left(\frac{W_c}{E}\right) = \left(\frac{f_t^{'}}{E}\right)W_c\left[1 + \frac{x}{y_1}\right] \tag{3.21}$$

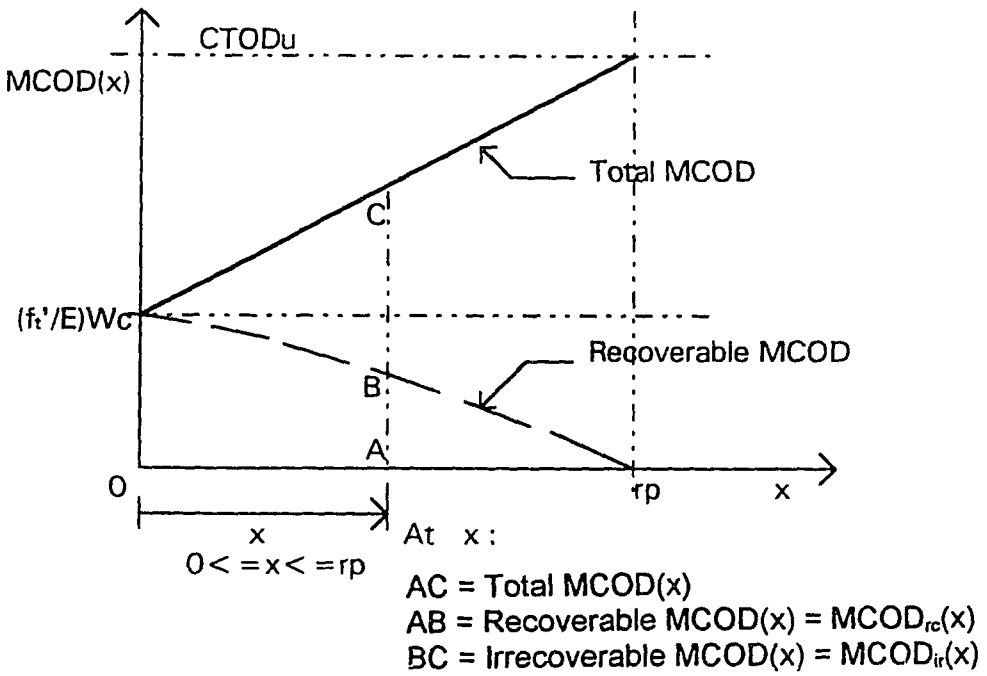

Figure 3.11(b) Total and Recoverable Crack Opening Displacement Curves

A certain portion of the opening displacement within the process zone is due to elastic deformations which can be recovered upon unloading. Based on the stress-softening diagram given in Figure 3.3, the recoverable opening displacement of the microcracked zone, $MCOD_{rc}(x)$ can be obtained from the actual stress distribution as:

$$
\begin{aligned}
MCOD_{rc}(x) &= \frac{\sigma_c(x)}{N_v(x)}\left(\frac{W_c}{E}\right) \\
&= \frac{M_u(y_1+x)}{I_c}\left(1-\frac{x}{rp}\right)\left(\frac{W_c}{E}\right) \\
&= \frac{M_u \cdot y_1}{I_c}\left(1+\frac{x}{y_1}\right)\left(1-\frac{x}{rp}\right)\left(\frac{W_c}{E}\right) \\
&= f_t'\left(1+\frac{x}{y_1}\right)\left(1-\frac{x}{rp}\right)\left(\frac{W_c}{E}\right)
\end{aligned}
$$

Therefore, $$MCOD_{rc}(x) = f_t'\left(\frac{W_c}{E}\right)\left(1+\frac{x}{y_1}\right)\left(1-\frac{x}{rp}\right) \tag{3.22}$$

The irrecoverable opening displacement of the process zone, $MCOD_{ir}(x)$ can be obtained by subtracting Equation (3.22) from Equation (3.21), resulting in:

$$MCOD_{ir}(x) = MCOD_t(x) - MCOD_{rc}(x)$$

$$= f_t'\left(\frac{W_c}{E}\right)\left(1+\frac{x}{y_1}\right)\left(\frac{x}{rp}\right) \tag{3.23}$$

G_{IC} is evaluated by integration of Equation(3.15), and substitutions of $\sigma_{ir}(x)$, and $MCOD_{ir}(x)$ from Equations (3.18) and (3.23). By integration of Equation (3.15), G_{IC} can be expressed as:

$$b \cdot G_{IC} = \int_{x=0}^{x=rp} \sigma_{ir}(x) \cdot MCOD_{ir}(x)dx$$

$$= \int_0^{rp} f_t'^2\left(\frac{W_c}{E}\right)\left(\frac{x}{rp}\right)^2\left(1+\frac{x}{y_1}\right)^2 dx$$

$$= f_t'^2\left(\frac{W_c}{E}\right)\left(\frac{1}{rp}\right)^2\left\{\int_0^{rp} x^2dx + 2\left(\frac{1}{y_1}\right)\int_0^{rp} x^3dx + \left(\frac{1}{y_1^2}\right)\int_0^{rp} x^4dx\right\}$$

$$= f_t'^2\left(\frac{W_c}{E}\right)\left(\frac{1}{rp}\right)^2\left\{\frac{rp^3}{3} + 2\left(\frac{1}{y_1}\right)\frac{rp^4}{4} + \left(\frac{1}{y_1^2}\right)\frac{rp^5}{5}\right\}$$

$$= f_t'^2\left(\frac{W_c}{E}\right)rp\left\{\frac{1}{3} + \frac{1}{2}\left(\frac{rp}{y_1}\right) + \frac{1}{5}\left(\frac{rp}{y_1}\right)^2\right\}$$

Therefore,

$$G_{IC} = \frac{1}{b}\frac{f_t'^2 \cdot rp \cdot W_c}{E}\left[\frac{1}{3} + \frac{1}{2}\left(\frac{rp}{y_1}\right) + \frac{1}{5}\left(\frac{rp}{y_1}\right)^2\right] \tag{3.24}$$

From Equation (3.20), $$f_t'\left(\frac{W_c}{E}\right) = CMOD_u\left(\frac{y_1}{h-\bar{y}}\right)$$

After simplifying Equation (3.24), G_{IC} can be expressed in terms of $CMOD_u$ as:

$$G_{IC} = \frac{f_t' \cdot CMOD_u \cdot rp \cdot y_1}{b \cdot (h-\bar{y})}\left[\frac{1}{3}+\frac{1}{2}\left(\frac{rp}{y_1}\right)+\frac{1}{5}\left(\frac{rp}{y_1}\right)^2\right] \tag{3.25}$$

According to LEFM, critical stress intensity factor, K_{IC} can be expressed as

$$K_{IC} = \sqrt{E \cdot G_{IC}} \quad \text{for plane stress,} \tag{3.26}$$

and

$$K_{IC} = \frac{\sqrt{E \cdot G_{IC}}}{1-\upsilon^2} \quad \text{for plane strain} \tag{3.27}$$

By substituting the Poisson ratio $\upsilon = 0.15$ for ordinary concrete, we get

$$K_{IC} = 1.01\sqrt{E \cdot G_{IC}} \approx \sqrt{E \cdot G_{IC}} \quad \text{for plane strain} \tag{3.28}$$

By substituting G_{IC} from Equation (3.24, or 3.25), K_{IC} can be expressed in different forms.

3.5 Theoretical P-CMOD Curve

3.5.1 Descending P-CMOD Curve

In the proposed model, it is assumed that the process zone length (rp_i) will not remain constant as the crack grows. So, rp_i is an unknown variable during the crack

propagation which will be calculated through an iterative process until static equilibrium is satisfied.

For any new crack length, a_i (where $a_i > a_o$), first assume a trial value of rp_i and calculate composite section properties using Equations (3.7),(3.8),(3.9) and (3.10). Then calculate stresses at different locations (Figure 3.5b) using the following Equations:

$$\begin{aligned} \sigma_{c2-2} &= f_t' \\ \sigma_{c1-1} &= f_t' \cdot \bar{y} / (h - \bar{y} - a_i - rp_i) \\ \sigma_{c3-3} &= f_t' \cdot (h - \bar{y} - a_i) / (h - \bar{y} - a_i - rp_i) \end{aligned} \tag{3.29}$$

Using the stresses calculated above, compute total compression (C) and Tension (T) as following:

In Figure 3.8b

$$C = 0.5 \cdot \sigma_{c1-1} \cdot b \cdot \bar{y} \tag{3.30}$$

$$T = t_1 + t_2 \tag{3.31}$$

where

$t_1 = 0.5 \cdot f_t' \cdot b \cdot (h - a_i - \bar{y} - rp_i)$

$t_2 = b \cdot rp_i \cdot f_t' / 3 + b \cdot rp_i \cdot \sigma_{c3-3} / 6$

Once forces, C and T are calculated, static equilibrium, T=C will be checked. If the equilibrium is not satisfied, assume a new trial value of rp_i and repeat the above procedure.

Then calculate Moment, M_i using the following Equation:

$$M_i = C \cdot \left(\frac{2}{3} \bar{y} + \bar{y}_1 \right) \tag{3.32}$$

where $\bar{y}_1 = \frac{1}{T}\left[\left(2 \cdot t_1 \cdot g_1 / 3\right) + t_2\left(g_1 + g_2\right)\right]$

$g_1 = (h - a_i - \bar{y} - rp_i)$

$g_2 = 0.5 \cdot rp_i \cdot \left(\sigma_{c2-2} + \sigma_{c3-3}\right) / \left(2 \cdot \sigma_{c2-2} + \sigma_{c3-3}\right)$

Calculate P_i using the following Equation:

$$P_i = \frac{4}{l}\left(M_i - \frac{1}{8}\gamma \cdot b \cdot h \cdot l^2\right) \tag{3.33}$$

where γ = unit weight of concrete

= 150 lb./Cu.ft. for Normal weight concrete.

In this research, the critical energy release rate, G_{IC} is considered as a material property which is required to predict the post-peak behavior of the crack-mouth opening displacement. By considering linear proportion of total energy loss based on the process zone length, rp_u at P_u and rp_i at P_i (where $P_i < P_u$) and by rearranging Equation (3.25) for $CMOD_i$ instead of $CMOD_u$, $CMOD_i$ can be expressed as:

$$CMOD_i = G_{IC}\frac{(h - \bar{y}) \cdot b}{f_t' \cdot rp_i \cdot y_1}\left(\frac{1}{3} + \frac{1}{2}\frac{rp_i}{y_1} + \frac{1}{5}\left(\frac{rp_i}{y_1}\right)^2\right)^{-1}\left(\frac{rp_u}{rp_i}\right) \tag{3.34}$$

where $y_1 = \left(h - a_i - \bar{y} - rp_i\right)$

3.5.2 Ascending P-CMOD Curve

Determination of pre-peak load-CMOD relationship is accomplished through an iterative procedure similar to those performed earlier for the post-peak region. The procedure involves determination of proper process zone length, rp, and evaluation of

the load from equilibrium conditions. It is important to know that in this case, the modular ratio for the composite section is different from the one assumed at the post-peak stage. At peak, the process zone is fully developed and the original notch tip is totally separated. This results in a notch tip material of zero modulus, and the variable modular ratio is as given by the linear relationship in Equation (3.6). However, at pre-peak levels, the process zone is not fully developed, and therefore the material at the notch tip is not totally separated. The real stress distribution in front of the notch tip is as shown in Figure 3.12. In this case, the modulus of elasticity of the damaged section at the notch tip is not known, and the modular ratio has to be evaluated accordingly.

During the development for the fracture process zone, the stress diagram and the position of the neutral axis (N.A.) changes which is shown in Figure 3.13.

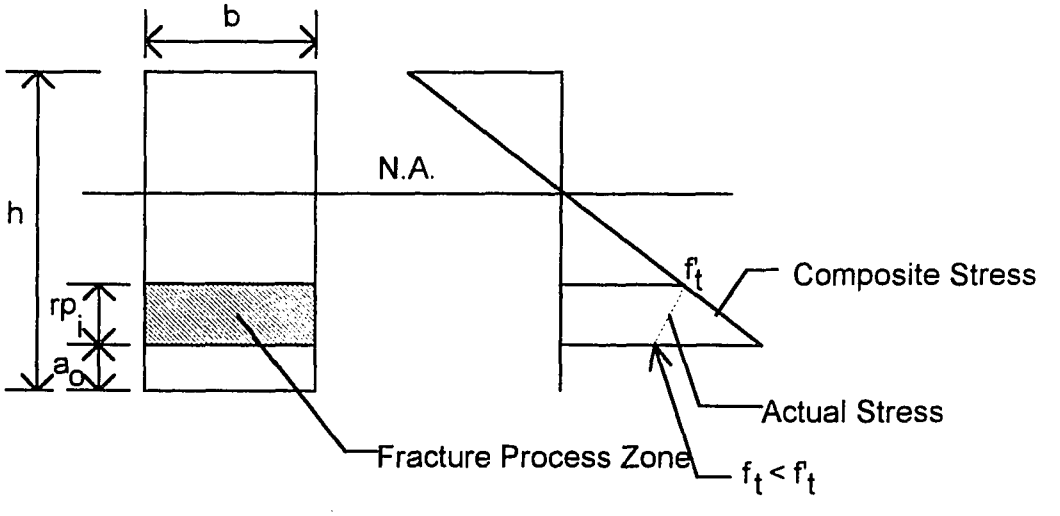

Figure 3.12 Stress distribution before the Process zone becomes fully developed.

For the elastic strength condition (notch tip stress = f_t'), the position of the neutral axis is at $\frac{h_1}{2}$. At peak, the process zone is fully developed, and the position of neutral axis

is at $\bar{y}_u$. Therefore, the pre-peak position of the neutral axis, $\bar{y}_i$, varies within these limits $\left(\bar{y}_u < \bar{y}_i < \frac{h_1}{2}\right)$.

In order to obtain a set of pre-peak P-CMOD coordinates, we need to consider a set of $\bar{y}_i$, where $\bar{y}_u < \bar{y}_i < h_1/2$. For any location of N.A., $\bar{y}_i$, first assume a trial values of rp_i (a very small number, $rp_i < rp_u$) , and using linear relationships and assuming a'b' parallel to ab in Figure 3.13, evaluate the actual and the composite stresses at the notch tip as following:

In Figure 3.13;

$$rp2 = rp_i;\ rp3 = rp_u;\ y2 = \bar{y}_i$$

$$\frac{a'a''}{aa''} = \frac{a'a''}{f_t'} = \frac{rp_i}{rp_u}$$

$$\Rightarrow a'a'' = f_t'\left(\frac{rp_i}{rp_u}\right)$$

$$aa' = aa'' - a'a'' = f_t'\left[1 - \frac{rp_i}{rp_u}\right]$$

$$ad' = f_t' \cdot \frac{(h_1 - \bar{y}_i)}{(h_1 - \bar{y}_i - rp_i)}$$

Therefore, composite stress at notch tip,

$$\sigma_{c,notch} = ad' = f_t' \frac{(h_1 - \bar{y}_i)}{(h_1 - \bar{y}_i - rp_i)} \tag{3.35}$$

and actual stress at notch tip,

$$\sigma_{notch} = aa' = f_t'\left(1 - \frac{rp_i}{rp_u}\right) \tag{3.36}$$

The variable modular ratio can be calculated by taking the ratio of composite stress to actual stress at the tip of notch as following:

$$N_{vi} = \frac{\sigma_{c,notch}}{\sigma_{notch}} = \frac{\dfrac{(h_1 - \bar{y}_i)}{(h_1 - \bar{y}_i - rp_i)}}{\left(1 - \dfrac{rp_i}{rp_u}\right)} \qquad (3.37)$$

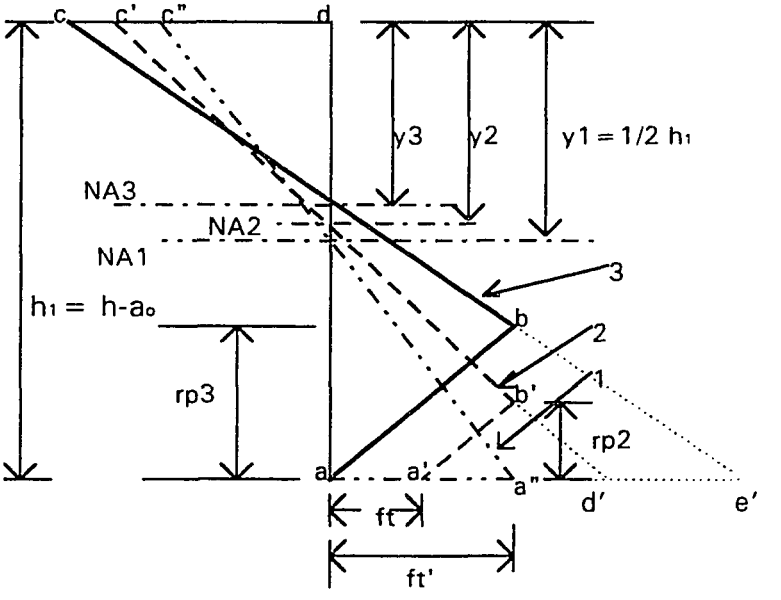

- Stress Diagram 1 (Line a"c"): Elastic Strength Condition with zero process zone length. aa"=dc"=f_t'
- Stress Diagram 2 (Line a'b'c'): Process Zone Developing Stage. Process Zone length rp2<rp_u where rp_u= Fully developed Process Zone. Assumption: Line a'b' is parallel to line ab.
- Stress Diagram 3 (Line abc): Process Zone fully developed. rp3=rp_u.
- Neutral Axis y1>y2>y3

Figure 3.13 Stress diagrams during the Process Zone developing Stages

Using the above modular ratio, N_{vi}, develop the equivalent composite section as shown in Figure 3.14, and calculate the distance of the N.A., $\bar{y}_{i\,calculated}$ from the top of the section using the following Equation:

$$\bar{y}_{icalculated} = \left(\frac{1}{A}\right)\left(A1\cdot\left(h_1 - rp_1\right)/2 + A2\cdot\left(h_1 - rp_i/2\right) + A3\cdot\left(h_1 - 2\cdot rp_i/3\right)\right) \tag{3.38}$$

where

$$A = A1 + A2 + A3$$
$$A1 = b\cdot\left(h_1 - rp_i\right)$$
$$A2 = rp_i\cdot b / N_{vi}$$
$$A3 = 0.5\cdot rp_i\cdot b\left(1 - \frac{1}{N_{vi}}\right)$$

Then compare the calculated distance of the N.A., $\bar{y}_{i\,calculated}$ with the $\bar{y}_i$. If the difference between them is not negligible, assume a new trial value of rp_i and repeat the above procedure.

Once the correct rp_i for $\bar{y}_i$ obtained, develop the composite section and stress diagram (Figure 3.14), and calculate the forces T, C and moment arm Z using the following formulae:

The width of the section within the fracture process zone:

$$\begin{aligned} b(x) &= \frac{b}{N_{vi}} + \left(b - \frac{b}{N_{vi}}\right)\left(1 - \frac{x}{rp_i}\right) \\ &= b\left[\frac{1}{N_{vi}} + 1 - \frac{1}{N_{vi}} - \frac{x}{rp_i} + \frac{x}{N_{vi}\cdot rp_i}\right] \\ &= b\left[1 - \frac{x}{rp_i}\left(1 - \frac{1}{N_{vi}}\right)\right] \end{aligned} \tag{3.39}$$

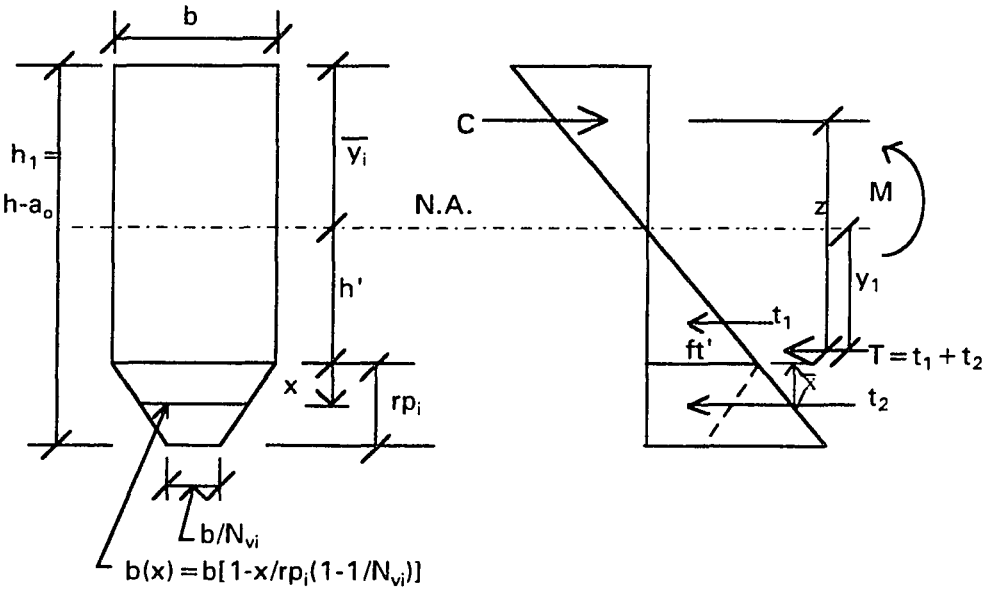

Figure 3.14 Composite Section and Composite Stress Diagram During the Process Zone Developing Stage.

Calculate forces C, t_1, t_2, T (Figure 3.14):

$$C = \frac{1}{2} b \cdot \bar{y}_i \cdot \left(f_t' \cdot \frac{\bar{y}_i}{h'} \right), \text{ where } h' = h - a_0 - rp_i - \bar{y}_i \tag{3.40}$$

$$T = t_1 + t_2 \tag{3.41}$$

where

$$t_1 = \frac{1}{2} b \cdot f_t' \cdot h'$$

$$t_2 = \int_0^{rp_i} f_t' \left(\frac{h' + x}{h'} \right) \cdot b \left[1 - \frac{x}{rp_i} \left(1 - \frac{1}{N_{vi}} \right) \right] dx$$

$$= \left(f_t' \cdot b \right) \left[\int_0^{rp_i} \left(1 + \frac{x}{h'} \right) dx - \left(1 - \frac{1}{N_{vi}} \right) \int_0^{rp_i} \left(1 + \frac{x}{h'} \right) \left(\frac{x}{rp_i} \right) dx \right]$$

$$= \left(f_t' \cdot b \right) \left[rp_i + \frac{rp_i^2}{2h'} - \left(1 - \frac{1}{N_{vi}} \right) \left\{ \frac{rp_i^2}{2rp_i} + \frac{rp_i^3}{3rp_i \cdot h'} \right\} \right]$$

$$= \left(f_t' \cdot b \right) \left[\frac{rp_i}{2} + \frac{1}{6} \frac{rp_i^2}{h'} + \frac{rp_i}{2N_{vi}} + \frac{rp_i^2}{3N_{vi} \cdot h'} \right]$$

$$= \left(f_t' \cdot b \cdot rp_i \right) \left[\frac{1}{2} \left(1 + \frac{1}{N_{vi}} \right) + \frac{rp_i}{6h'} \left(1 + \frac{2}{N_{vi}} \right) \right]$$

Locate C.G. of t_2:

$$t_2 \cdot \bar{x} = \int_0^{rp_i} f_t' \left(\frac{h' + x}{h'} \right) \cdot b \left[1 - \frac{x}{rp_i} \left(1 - \frac{1}{N_{vn}} \right) \right] x \cdot dx$$

$$= \left(f_t' \cdot b \right) \left[\int_0^{rp_i} \left(1 + \frac{x}{h'} \right) x \cdot dx - \left(1 - \frac{1}{N_{vn}} \right) \int_0^{rp_i} \left(1 + \frac{x}{h'} \right) \left(\frac{x^2}{rp_i} \right) dx \right]$$

$$= \left(f_t' \cdot b \right) \left[\frac{rp_i^2}{2} + \frac{rp_i^3}{3h'} - \left(1 - \frac{1}{N_{vn}} \right) \left\{ \frac{rp_i^3}{3rp_i} + \frac{rp_i^4}{4rp_i \cdot h'} \right\} \right]$$

$$= \left(f_t' \cdot b \right) \left[\frac{rp_i^2}{2} + \frac{1}{3} \frac{rp_i^3}{h'} - \left(1 - \frac{1}{N_{vn}} \right) \left\{ \frac{rp_i^2}{3} + \frac{rp_i^3}{4h'} \right\} \right]$$

$$= \left(f_t' \cdot b \cdot rp_i^2 \right) \left[\frac{1}{6} + \frac{1}{12} \left(\frac{rp_i}{h'} \right) + \frac{1}{3N_{vn}} + \frac{rp_i}{4N_{vn} \cdot h'} \right]$$

$$= \left(f_t' \cdot b \cdot rp_i^2 \right) \left[\frac{1}{6} \left(1 + \frac{2}{N_{vn}} \right) + \frac{1}{12} \left(\frac{rp_i}{h'} \right) \left(1 + \frac{3}{N_{vn}} \right) \right]$$

Therefore, C.G. of t_2 from the tip of process zone:

$$\bar{x} = \frac{rp_i \cdot \left[\frac{1}{6} \left(1 + \frac{2}{N_{vn}} \right) + \frac{1}{12} \left(\frac{rp_i}{h'} \right) \left(1 + \frac{3}{N_{vn}} \right) \right]}{\left[\frac{1}{2} \left(1 + \frac{1}{N_{vn}} \right) + \frac{1}{6} \left(\frac{rp_i}{h'} \right) \left(1 + \frac{2}{N_{vn}} \right) \right]} \tag{3.42}$$

Locate C.G. of T

$$y_1 = \frac{1}{T} \left[\frac{2}{3} t_1 \cdot h' + t_2 \left(h' + \bar{x} \right) \right] \tag{3.43}$$

Moment arm, Z

$$Z = \frac{2}{3} \bar{y}_i + y_1 \tag{3.44}$$

Calculate moment, M_i and force, P_i using the following equations:

$$M_1 = T \cdot Z = C \cdot Z \tag{3.45}$$

$$P_i = \frac{4}{l}\left(M_1 - \frac{1}{8}\gamma \cdot b \cdot h \cdot l^2 \right) \tag{3.46}$$

Using W_C from Equation (3.20) calculate $CMOD_i$ as following:

$$CMOD_1 = \frac{f_t'}{E} W_c \cdot (h - \bar{y}_1) / h' \tag{3.47}$$

where

$$h' = h - a_o - rp_1 - \bar{y}_i$$

3.6 Theoretical Load-Deflection Curve

Based on the theoretical Load-CMOD curve as developed above, a simple formulation are derived to predict theoretical Load versus Load-Point Deflection (P-δ).

For 3-PB SEN beam specimen, empirical equations for calculating CMOD and load-Point Displacement are presented by Tada et al (1976) as following:

For span to depth ratio of 4:

$$CMOD = \frac{4\sigma \cdot a}{E} V_1(\xi) \tag{3.48}$$

Load-point deflection, $\delta = \frac{\sigma \cdot L}{E} V_2(\xi)$ (3.49)

Where $\sigma = \frac{6M}{b \cdot h^2}$; $M = \frac{P \cdot L}{4}$; $a = a_0 + rp$; $\xi = \frac{a}{h}$

$$V_1(\xi) = 0.76 - 2.28(\xi) + 3.87(\xi)^2 - 2.04(\xi)^3 + \frac{0.66}{(1-\xi)^2}$$

$$V_2(\xi) = \left(\frac{\xi}{1-\xi} \right)^2 \left\{ 5.58 - 19.57(\xi) + 36.82(\xi)^2 - 34.94(\xi)^3 + 12.77(\xi)^4 \right\}$$

$V_1(\xi)$ and $V_2(\xi)$ for span to depth >4 can be estimated by interpolation from the curves provided by Tada et al. (1976).

From Equations (3.48) & (3.49), one can derive a relationship between CMOD and load-point deflection, δ as following:

$$\delta = 0.25 \cdot CMOD \cdot \left(\frac{L}{a}\right)\left(\frac{V_2(\xi)}{V_1(\xi)}\right) \tag{3.50}$$

By using Equation (3.50), it is possible to relate CMOD to δ at various points along a typical P-CMOD diagram, and therefore develop a load-deflection relationship. In this dissertation, theoretical P-δ curve is developed using Equation (3.50) and the theoretical P-CMOD relation as developed in previous section.

3.7 Estimation of Fracture Energy

Estimation of fracture energy requires computation of the area beneath load-deflection diagram. In this dissertation, the fracture energy, G_F is calculated using RILEM method TC 50-FMC (1985) which is described in literature review, section 2.3. The theoretical P-δ curve as developed in previous section is used to estimate G_F.

3.8 Computer Model based on CBAFM

A simple PC based PASCAL program, named **CBAFM.PAS** is developed based on the proposed fracture model, CBAFM. The Flow Chart is shown in Figure 3.15. The computer model has four main modules, (i) Module-1 for calculating the fully developed process zone length (rp), the critical fracture energy release rate (G_{IC}) and

the critical stress intensity factor (K_{IC}), (ii) Module-2 for developing the descending (post-peak) branch of the theoretical P-CMOD curve, (iii) Module-3 for developing the ascending branch of the theoretical P-CMOD curve and (iv) Module-4 for developing the theoretical Load-Load Point Deflection curve.

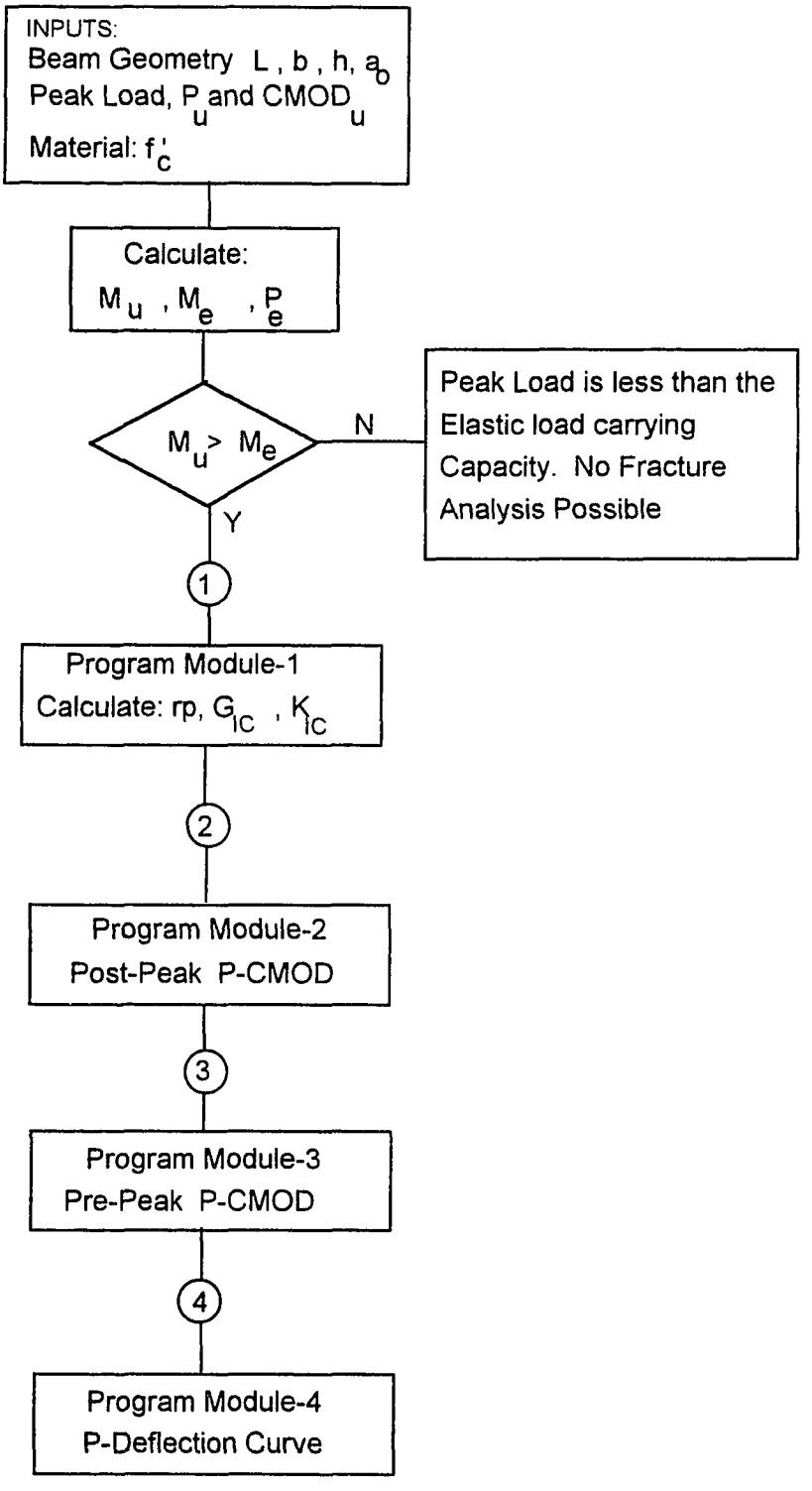

Figure 3.15(a) Computer Flow Chart for the Proposed Model

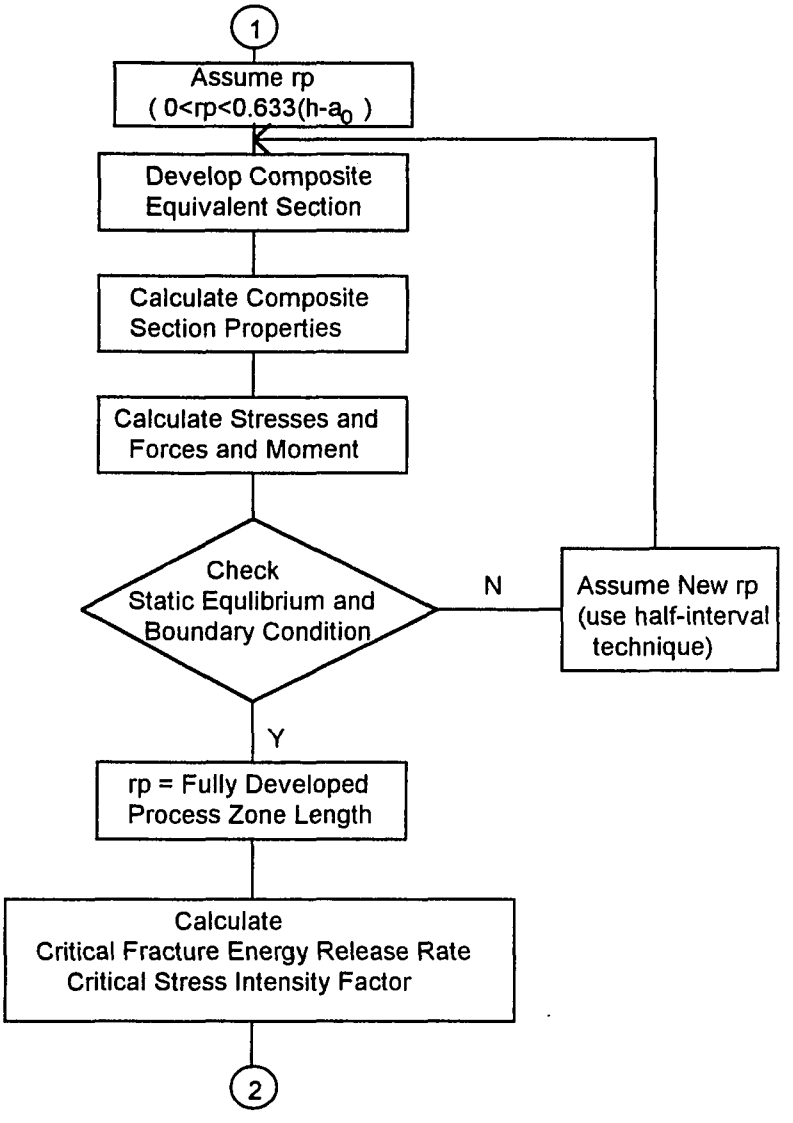

Figure 3.15(b) Flow Chart for Program Module-1

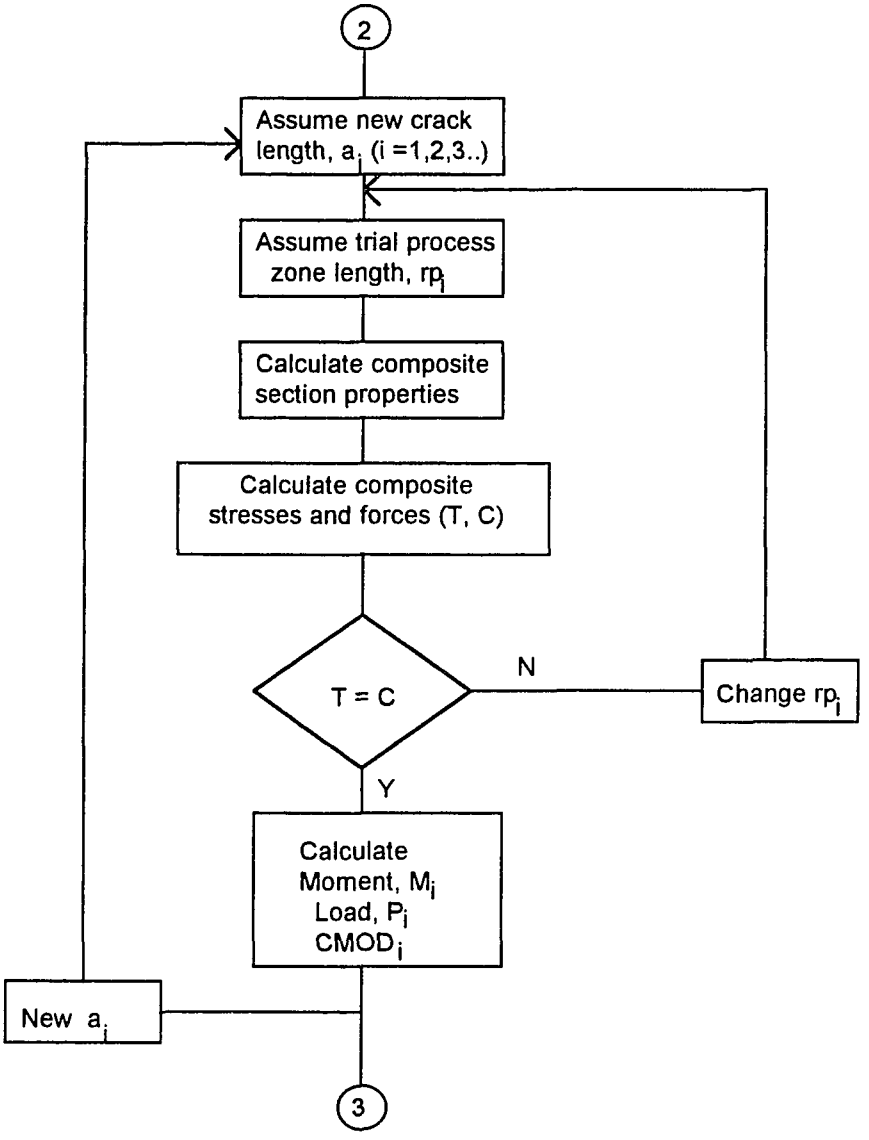

Figure 3.15(c) Flow Chart for Program Module-2

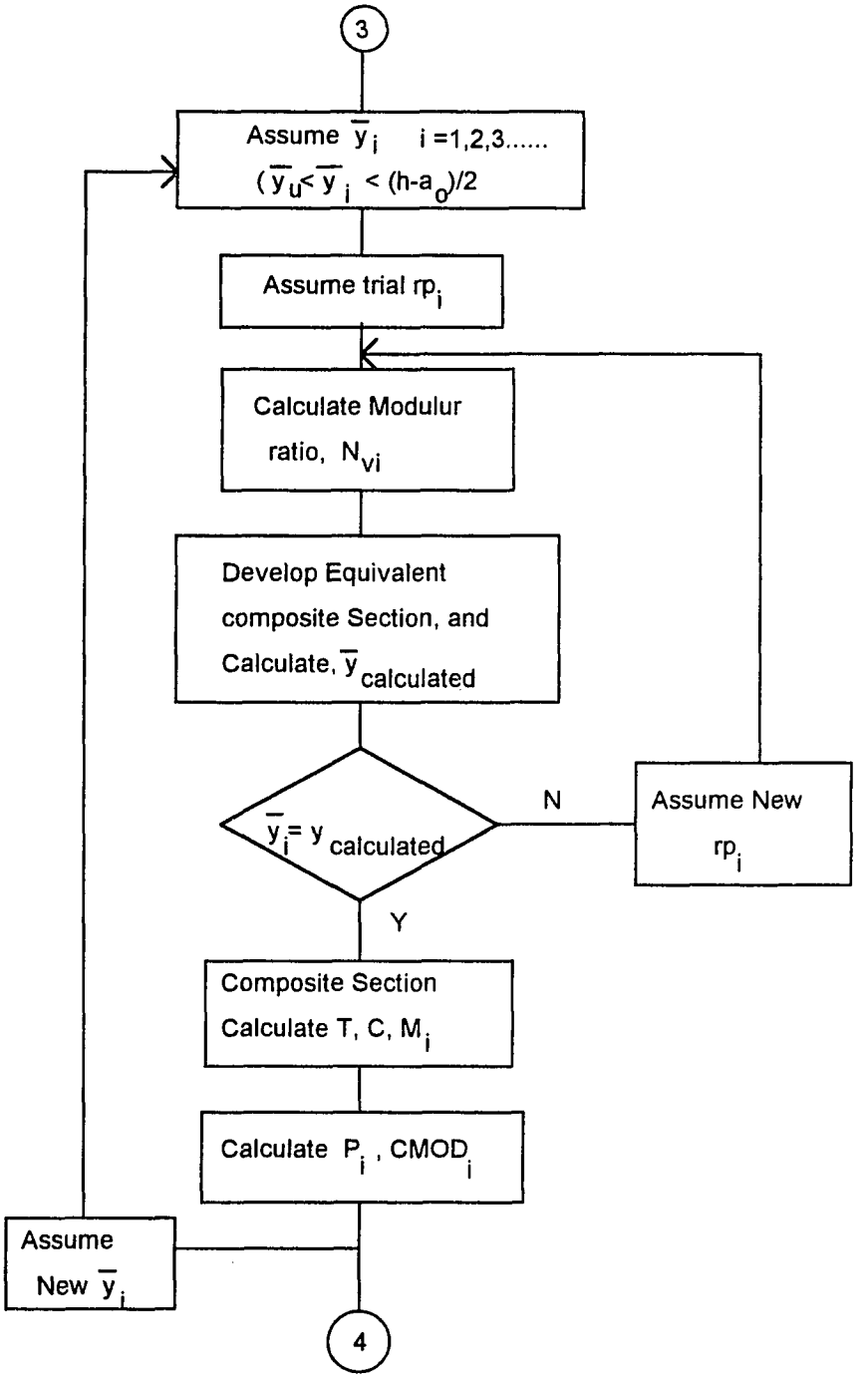

Figure 3.15(d) Flow Chart for Program Module-3

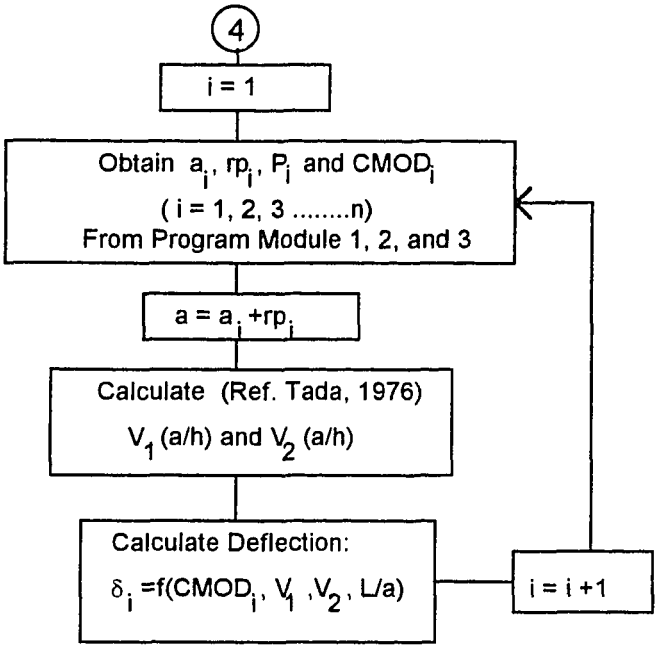

Figure 3.15(e) Flow Chart for Program Module-4

CHAPTER 4

RESULTS AND DISCUSSION

4.1 General

The validity of the proposed model (CBAFM) is examined from the analysis of available experimental data on 3-PB beams. Experimental results involved data on beams from tests by Yu (1995), Refai and Swartz (1987), Jenq and Shah (1985b), Go, Cheer-Germ and Swartz (1983), and Nallathambi and Karihaloo (1985). Table 4.1 and Table 4.2 represent experimental data for 3-PB SEN beams and 3-PB Pre-cracked beams respectively employed by CBAFM for the determination of fracture parameters and load-displacement relationships. Data required for analysis by CBAFM are beam dimensions (L, b, h), initial notch length (a_o) or precracked length (a_i), material property (f_c') or (f_t', E), peak load (P_u) and crack mouth opening displacement corresponding to peak load ($CMOD_u$). Besides Load-CMOD and Load-Deflection relationships, the fracture mechanics parameters acquired from the analysis of data encompassed the fracture process zone length, and it's extent during the fracturing process, G_{IC}, K_{IC}, and G_F. The following sections describe the comparison of the proposed model with the available experimental data and with other models.

4.2 Experimental Verification

Figures 4.1(a) & (b) through 4.3(a) & (b), depict comparison of the experimental Load-CMOD and Load-Deflection data by Yu (1995), and the computed relationships developed by the proposed model. The theoretical results are obtained by using the experimental P_u, $CMOD_u$, and f_c'. Experimental data involved small, medium, and

large size specimens, and as shown in these figures, agreement between the computed and experimental relationships are quite satisfactory.

Table 4.1 Beam Dimensions and Data from Experiments for use with the Proposed Model

Beam No.	Ref.	L x b x h x a_o (mm)	E (MPa)	f_t' (MPa)	P_u (kN)	$CMOD_u$ (mm)
1	[1]	457x76x76x38	$30.44x10^3$	3.20	0.84	0.04
2	[1]	813x102x102x51	$30.44x10^3$	3.20	1.09	0.06
3	[1]	965x102x152x76	$30.44x10^3$	3.20	1.67	0.05
4	[2]	640x160x160x80	$36.03x10^3$	3.78	5.07	0.04
5	[2]	2000x500x500x250	$41.02x10^3$	4.31	56.94	0.11
6	[3]	762x76x203x61	$38.43x10^3$	4.00	5.03	0.05
7	[3]	1143x76x305x92	$39.32x10^3$	3.76	7.56	0.71
8	[4]	572x51x152x48	$24.15x10^3$	2.76	2.00	0.05
9	[4]	203x51x51x24	$24.15x10^3$	2.76	0.62	0.03

[1] Yu, 1995; [2] Jenq/Shah, 1985b; [3] Refai/Swartz, 1987;
[4] Ratanalert/Wecharatana, 1990

Table 4.2 Pre-cracked Beam Dimensions and Data from Experiments for use with the Proposed Model

Beam No.	Beam Id. [1]	L x b x h x a_i (mm)	E (MPa)	f_t' (MPa)	P_u (kN)	$CMOD_u$ (mm)
10	B31	762x76x203x77.2	$38.4x10^3$	4.00	4.85	0.114
11	B25	762x76x203x121.9	$38.4x10^3$	4.00	2.80	0.102
12	B24	762x76x203x144.5	$38.4x10^3$	4.00	1.98	0.097
13	C22	1143x76x305x116.1	$39.4x10^3$	3.76	7.65	0.064
14	C2	1143x76x305x128.9	$39.4x10^3$	3.76	6.05	0.102
15	C24	1143x76x305x132.0	$39.4x10^3$	3.76	6.12	0.071
16	C20	1143x76x305x143.8	$39.4x10^3$	3.76	4.67	0.102
17	C15	1143x76x305x146.0	$39.4x10^3$	3.76	4.89	0.102
18	C5	1143x76x305x160.6	$39.4x10^3$	3.76	4.54	0.102
19	C26	1143x76x305x173.1	$39.4x10^3$	3.76	4.27	0.076
20	C27	1143x76x305x185.3	$39.4x10^3$	3.76	2.89	0.102
21	C10	1143x76x305x205.1	$39.4x10^3$	3.76	2.49	0.117

(a_i = Initial crack length of pre-cracked beam)
[1] Reference- Refai/Swartz (1987)

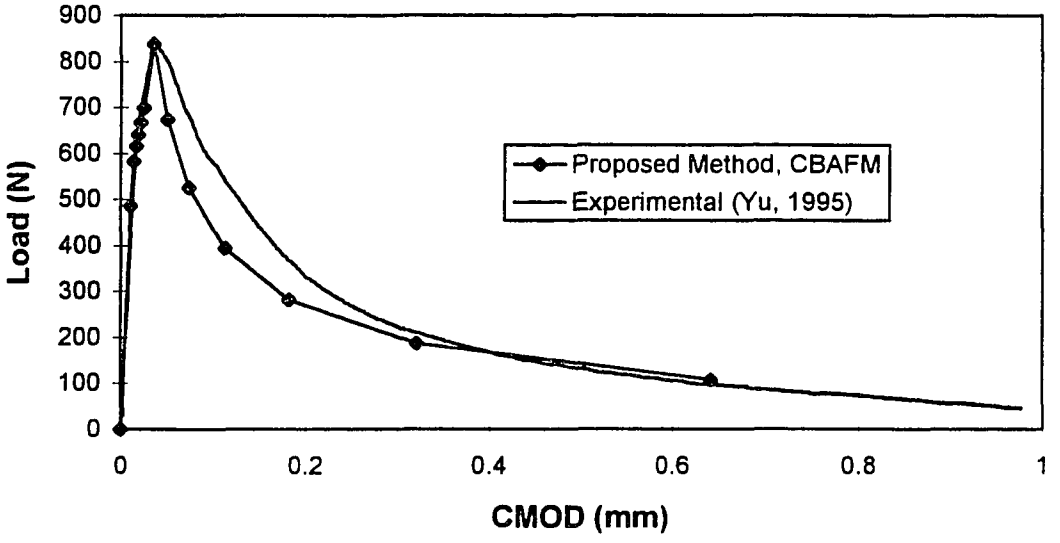

Figure 4.1(a) Comparison of computed (CBAFM), and experimental load-CMOD relations for small size beam (Beam No. 1).

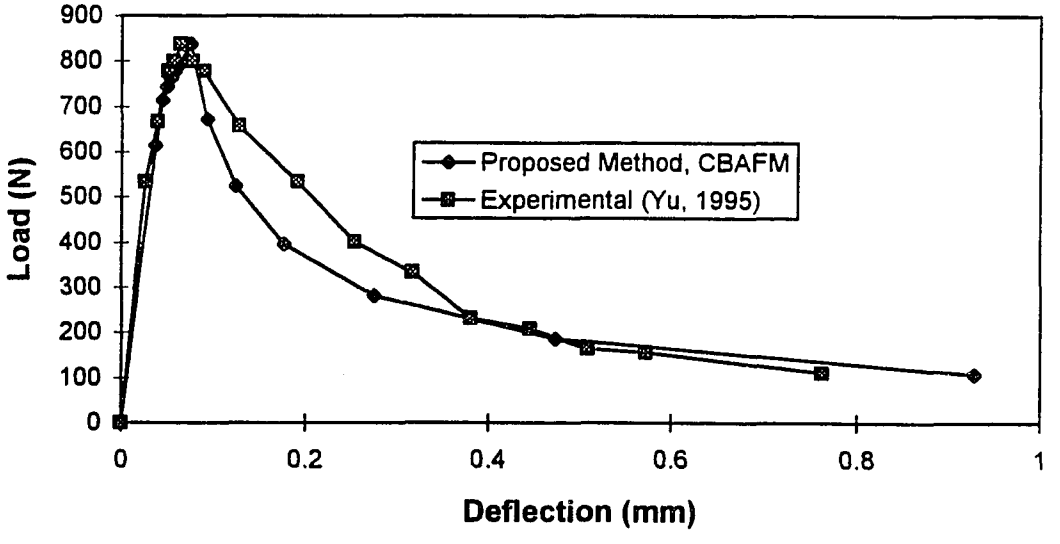

Figure 4.1(b) Comparison of computed (CBAFM), and experimental load-deflection relations for small size beam (Beam No. 1).

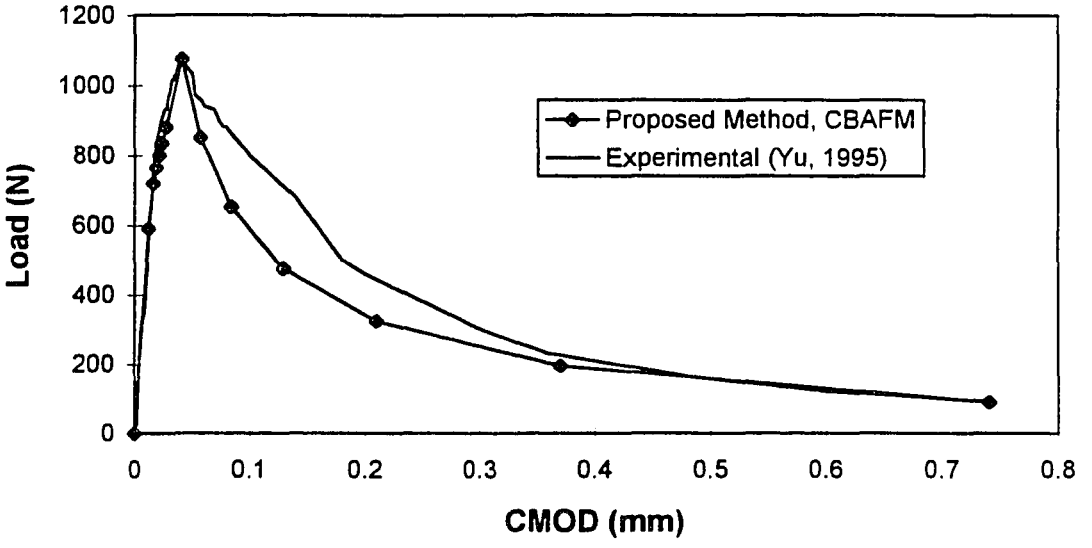

Figure 4.2(a) Comparison of computed (CBAFM), and experimental load-CMOD relations for mid-size beam (Beam No. 2).

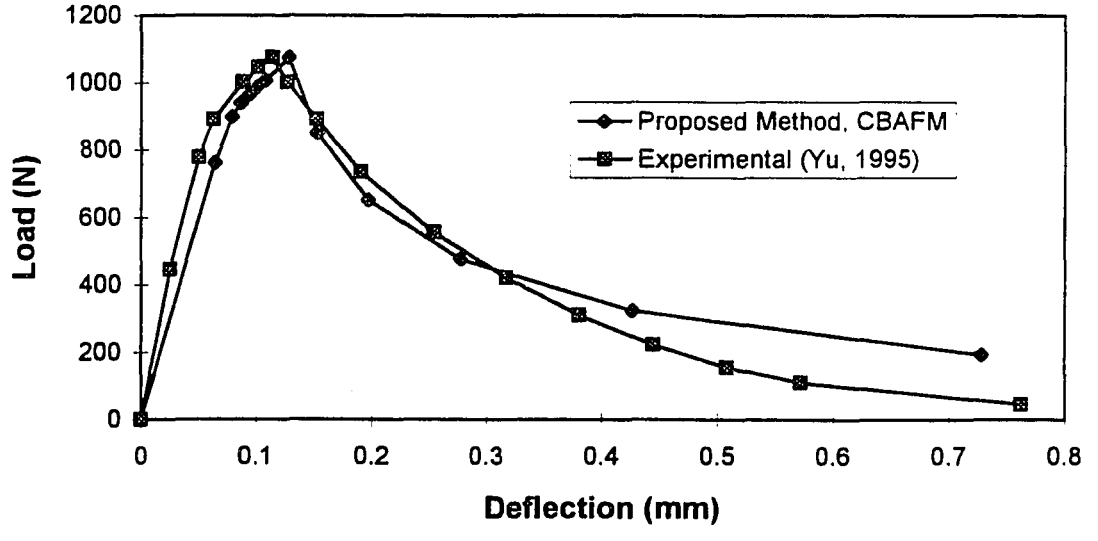

Figure 4.2(b) Comparison of computed (CBAFM), and experimental load-deflection relations for mid-size beam (Beam No. 2).

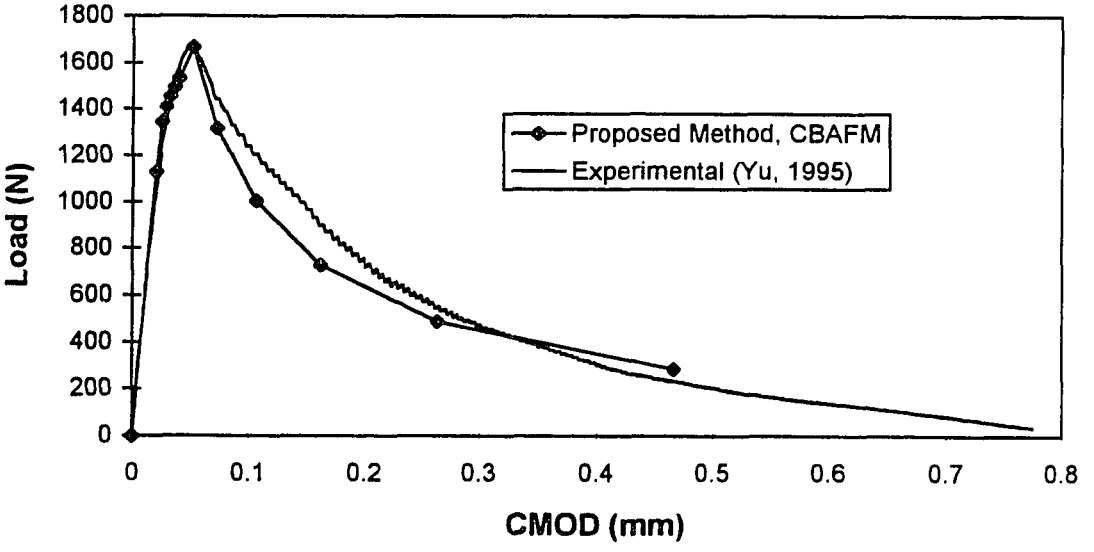

Figure 4.3 (a) Comparison of computed (CBAFM), and experimental load-CMOD relations for large size beam (Beam No. 3).

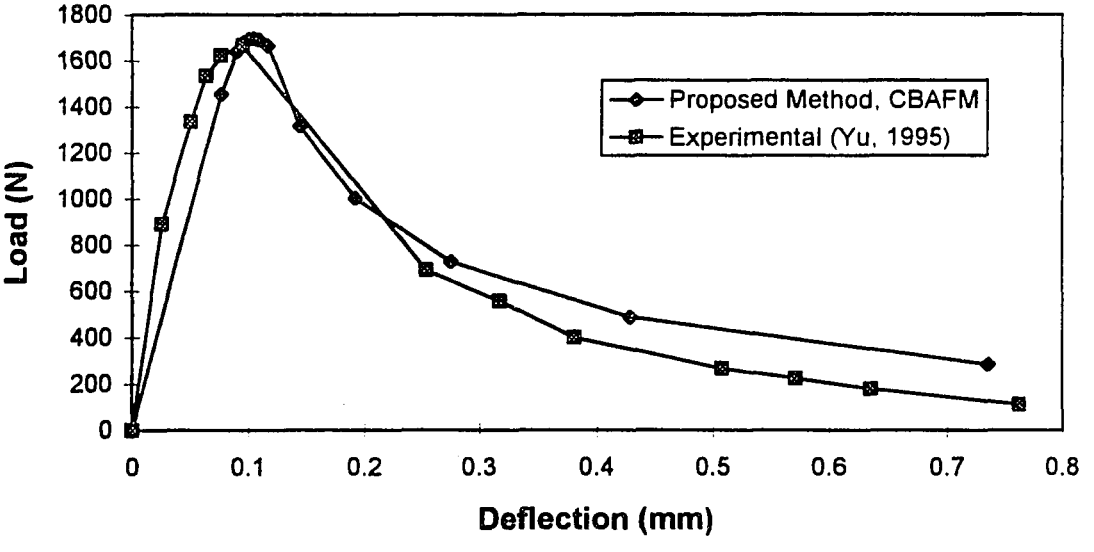

Figure 4.3(b) Comparison of computed (CBAFM), and experimental load-deflection relations for large size beam (Beam No. 3).

4.3 Comparison with Available Models

4.3.1 Comparison of Calculated K_{IC} and G_{IC} from Different Methods

The fracture parameters, critical stress intensity factor, K_{IC} and critical fracture energy release rate, G_{IC} are calculated by the proposed method for two different sizes of twelve precracked beams. The beam dimensions and experimental data are given in Table 4.2. Table 4.3 shows a comparison of calculated K_{IC} and G_{IC} values by four different methods which are TPFM (Jenq and Shah, 1985a), Go Method (Go, Cheer-Germ and Swartz, 1983), the Australian Method (Nallathambi and Karihaloo, 1985) and the proposed method. The calculated K_{IC} and G_{IC} values by TPFM, Go Method and the Australian Method are obtained from the reference (Refai and Swartz, 1987). The comparison of K_{IC} and G_{IC} values in Table 4.3 indicate that K_{IC} and G_{IC} values measured by all these techniques vary within a close range.

Table 4.3 Comparison of computed K_{IC} and G_{IC} values by different methods.

Beam Id.	Proposed Model (CBAFM)		Jenq/Shah (TPFM)[1]		Go Method[2]		The Australian Method[3]	
	K_{IC}	G_{IC}	K_{IC}	G_{IC}	K_{IC}	G_{IC}	K_{IC}	G_{IC}
	$MPa\sqrt{mm}$	N/m	$MPa\sqrt{mm}$	N/m	$MPa\sqrt{mm}$	N/m	$MPa\sqrt{mm}$	N/m
B31	45.4	53.75	36.0	34.0	33.2	28.8	43.7	46.4
B25	41.3	44.36	35.6	32.9	36.8	35.2	28.5	19.6
B24	36.9	35.50	36.5	34.8	38.2	38.0	35.6	29.0
C22	50.1	63.92	41.6	44.3	41.7	33.8	46.2	51.1
C2	51.4	67.04	42.3	45.5	36.8	34.4	43.3	44.4
C24	45.3	52.22	39.3	39.3	37.2	35.2	44.8	47.5
C20	40.4	41.56	38.8	38.4	36.5	34.1	29.8	21.1
C15	45.9	53.66	39.5	39.8	36.2	33.4	27.4	18.1
C5	49.2	61.63	41.3	43.4	36.6	34.2	54.4	68.6
C26	44.3	49.93	41.5	43.6	36.2	33.4	60.4	82.0
C27	38.0	36.68	33.3	28.0	34.5	30.1	49.2	51.9
C10	43.2	47.40	36.0	33.0	33.2	28.1	51.2	52.8

[1] (Jenq and Shah, 1985a); [2] (Go, Cheer-Germ and Swartz, 1987);
[3] (Nallathambi and Karihaloo, 1985)

4.3.2 Comparison among CBAFM, TPFM and Experimental Data

Figures 4.4 through 4.5 depict P-CMOD relations by the proposed model, CBAFM, the two-parameter fracture model, TPFM, and experimental data (Jenq and Shah, 1985b). Beam dimensions and other pertinent data are shown in Table 4.1. As shown in these figures, P-CMOD relations evaluated by the proposed model are in good agreement with the experimental results.

4.3.3 Comparison among CBAFM, FCM and Experimental Data

In Figures 4.6 through 4.7, P-CMOD relations by the proposed model, CBAFM, are compared with the fictitious crack model, FCM and the experimental data (Refai & Swartz, 1987). Beam dimensions and other pertinent data are given in Table 4.1. The predicted P-CMOD curves by the proposed model are in better agreement with the experimental results compared to predicted P-CMOD by FCM.

In Figures 4.8 through 4.9, P-CMOD relations by the proposed model, CBAFM, are compared with the fictitious crack model, FCM and the experimental data (Ratanalert and Wecharatana, 1990). Beam dimensions and other pertinent data are given in Table 4.1. In P-CMOD curves by FCM, three different softening relationships were assumed including (i) linear stress-displacement relationship, (ii) Reinhardt's empirical stress-displacement relationship, and (iii) Wecharatana's empirical stress-displacement relationship. These stress-displacement relations are discussed in Section 2.2, and are given here again for completeness:

Linear σ-w (Eq. 2.26): $\frac{\sigma}{f_t'} = (1 - \xi)$

where,

σ = closing pressure;

f_t' = maximum tensile strength;

ξ = ratio of crack opening displacement to maximum crack opening displacement at $\sigma=0$; $\xi = w/w_c$;

Reinhardt's empirical equation (Eq. 2.24): $$\frac{\sigma}{f_t'} = \left(1+(c_1\xi)^3\right)e^{(-c_2\xi)} - \xi\left(1+c_1^3\right)e^{-c_2}$$

where,

For concrete, c1 = 3.0 ; c2 = 6.93;

σ, ξ, f_t' are the same as defined above.

Wecharatana's empirical equation (Eq. 2.25): $$\frac{\sigma}{f_t'} = \frac{A}{\xi}\left(1-e^{-B\xi^C}\right)(1-\xi)^D$$

where

σ, ξ, f_t' are the same as defined above.

For concrete and mortar, A, B, C and D are equal to 0.052, 400, 1.75 and 0.5 respectively.

Figures 4.8 and 4.9 clearly describe that the accuracy of FCM significantly depends on the assumed post-peak stress-displacement relations. On the other hand, the predicted P-CMOD curves by the proposed model are in good agreement with the experimental data. Hence, the accuracy of the predicted P-CMOD by the proposed method are quite acceptable and satisfactory.

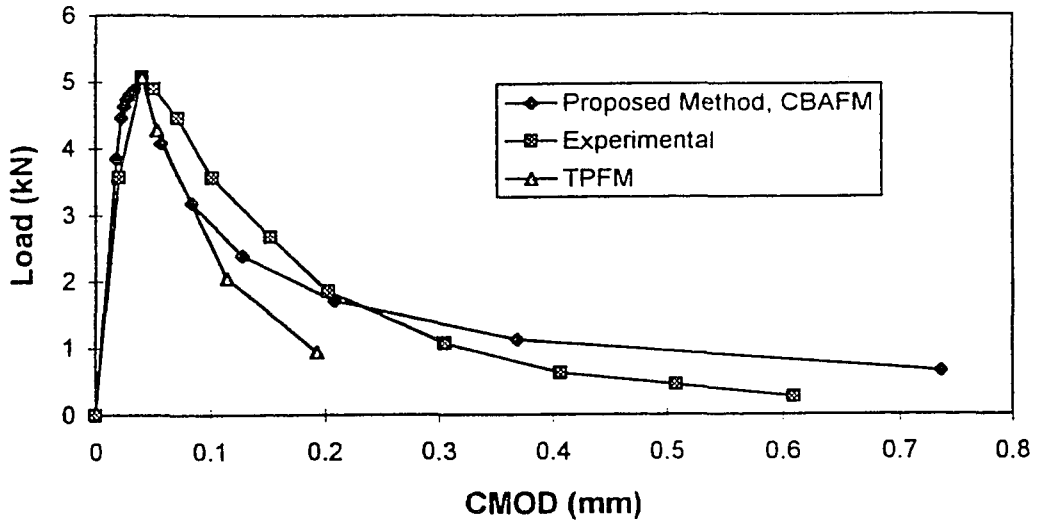

Figure 4.4 Load versus CMOD curves - Theoretical prediction by CBAFM, TPFM and experimental results (Jenq and Shah, 1985b) for Beam No. 4.

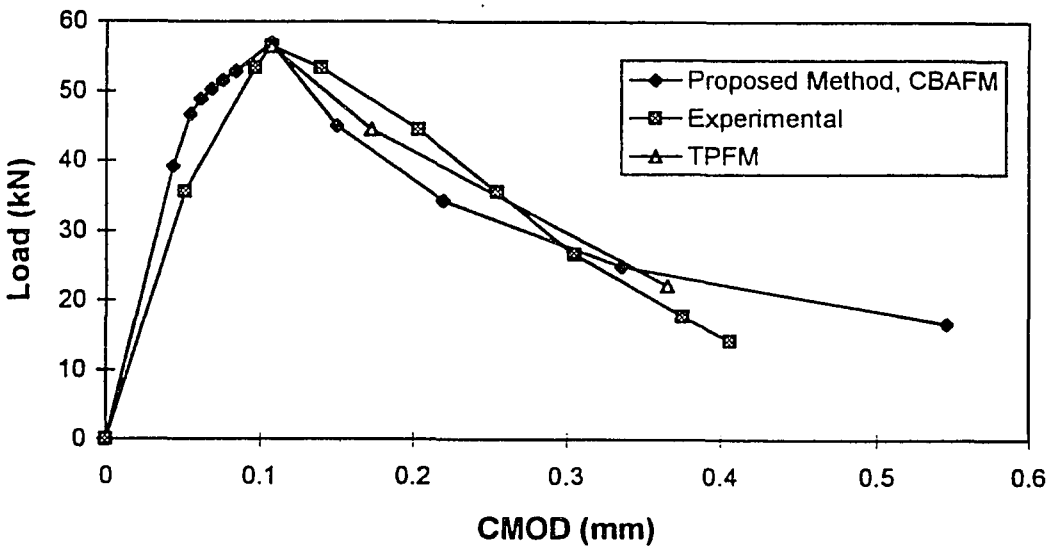

Figure 4.5 Load versus CMOD curves - Theoretical prediction by CBAFM, TPFM and experimental results (Jenq and Shah, 1985b) for Beam No. 5.

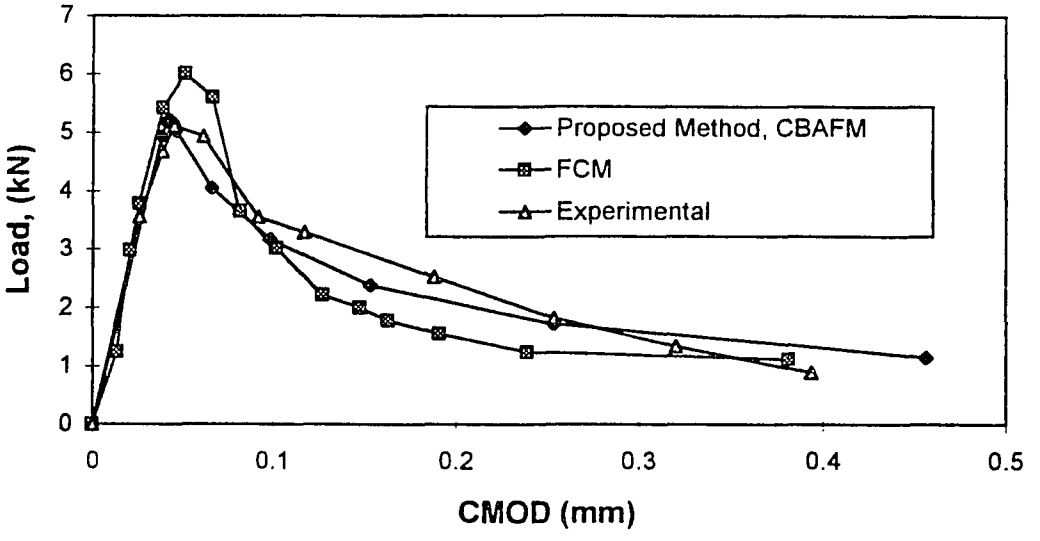

Figure 4.6 Load versus CMOD curves - Theoretical prediction by CBAFM, FCM and experimental results (Refai and Swartz, 1987) for Beam No. 6.

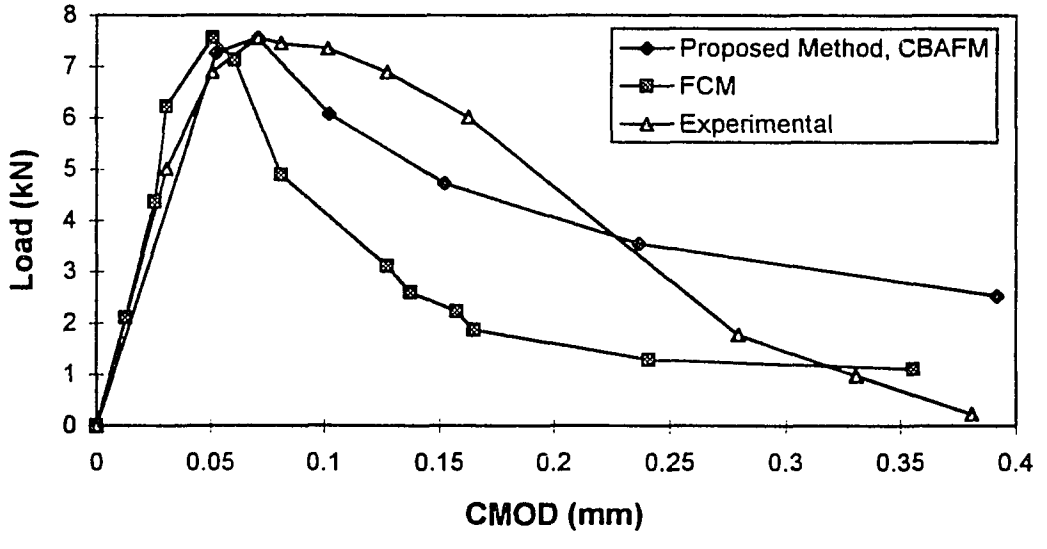

Figure 4.7 Load versus CMOD curves - Theoretical prediction by CBAFM, FCM and experimental results (Refai and Swartz, 1987) for Beam No. 7.

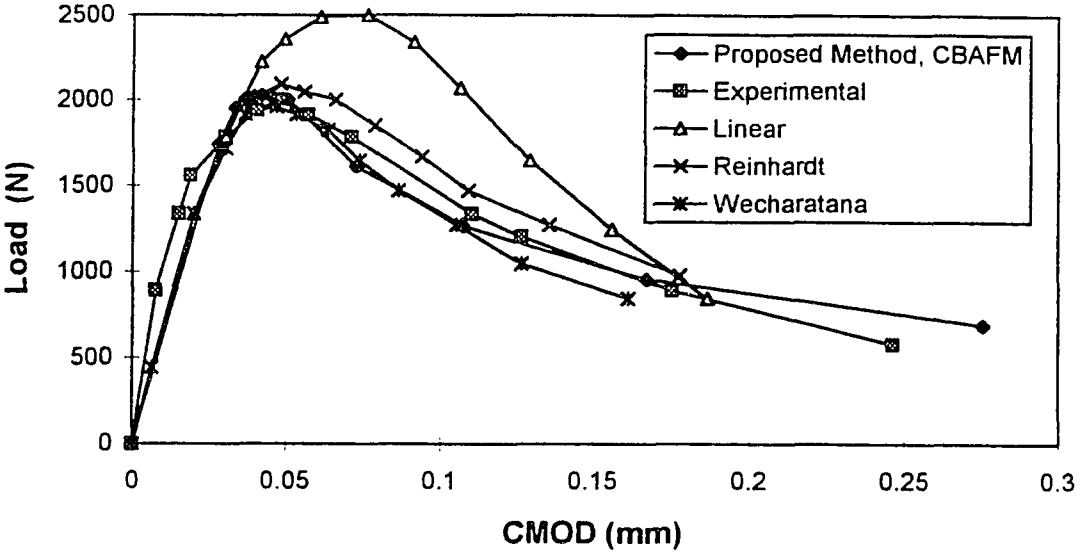

Figure 4.8 Load versus CMOD curves - Theoretical prediction by CBAFM, FCM and experimental results (Ratanalert and Wecharatana, 1990) for Beam No. 8.

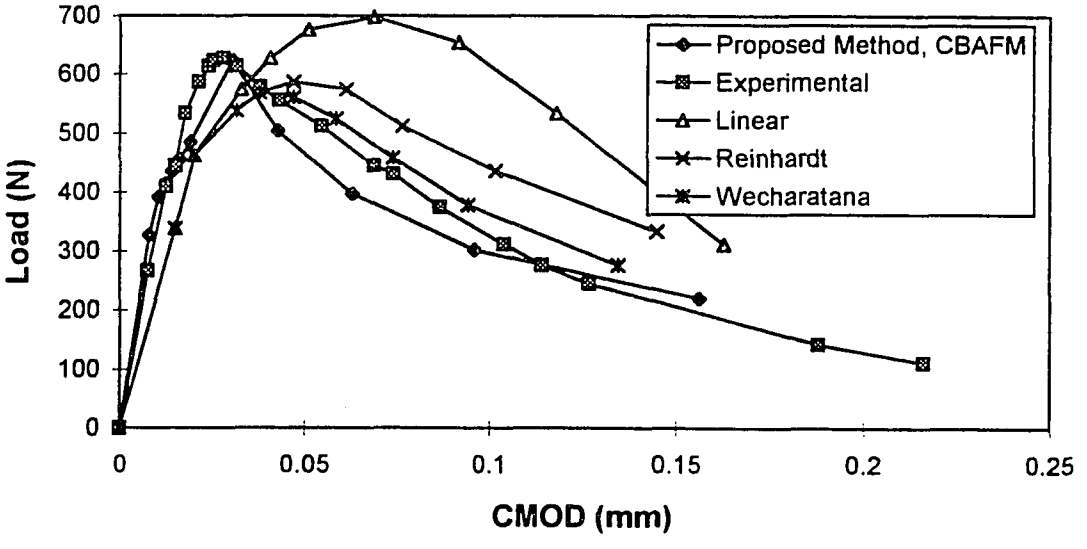

Figure 4.9 Load versus CMOD curves - Theoretical prediction by CBAFM, FCM and experimental results (Ratanalert and Wecharatana, 1990) for Beam No. 9.

4.4 Comparison of Fracture Energy

RILEM method, Equation (2.27) is employed for the determination of Fracture energy, G_F, by the proposed method (CBAFM), and the experimental data from three different beam sizes obtained by Yu, (1995). Theoretical and experimental load-deflection results given in Figures 4.1(b) through 4.3(b) are employed for this purpose. G_F values were also computed by using empirical equation given by Bazant (1983):

$$G_F = 0.0214\left(f_t' + 127\right)f_t'^{2} \cdot d_a / E$$

Where, d_a is the maximum size of coarse aggregate (inch), and the units for f_t' and E are PSI. Computed values are compared in Table 4.4, where close agreements are found between the experimental and computed G_F values by the proposed model.

Table 4.4 Comparison of Fracture Energy values, G_F

Beam No.	Fracture Energy, G_F (N/m)		
	Proposed Model	Experimental (Yu, 1995)	Bazant (1983)
1	94.50	101.50	75.25
2	94.50	101.50	75.25
3	99.75	98.00	75.25

4.5 Behavior of Crack Propagation

In order to obtain some useful information on the behavior of crack propagation, a set of dimensionless graphs (Figures 4.10 - 4.14) have been plotted based on the results from the proposed model for different sizes of beams.

In Figure 4.10, the theoretical post-peak load as a ratio of peak-load (P_u) is plotted against crack growth. Here crack growth is shown as a ratio of crack length (real crack + process zone length) and the beam depth. The plot shows similar behavior for all these beams.

In Figure 4.11, the theoretical post-peak CMOD as a ratio of CMOD at peak-load ($CMOD_u$) is plotted against crack growth. The graph shows that as the crack grows, the rate of change of CMOD increases faster. When the crack growth is about 85% of the beam depth which corresponds to about eight (8) times of $CMOD_u$, the CMOD increases very rapidly, and this point can be viewed as the critical crack-mouth opening displacement at complete failure (i.e. beam becomes two pieces), $CMOD_F$.

In Figure 4.12, the theoretical post-peak load as a ratio of peak-load (P_u) is plotted against CMOD as a ratio of CMOD at peak-load ($CMOD_u$). The graph shows that for larger beam, load carrying capacity drops more rapidly compared to smaller sizes of beams. This is a further proof of the effect of specimen size on brittleness of concrete specimen.

In Figure 4.13, the theoretical post-peak load as a ratio of peak-load (P_u) is plotted against post-peak process zone length (rp) as a ratio of process zone length at peak-load (rp_u). The graph shows that process zone length decreases more rapidly for smaller sizes of beams compared to larger sizes of beams.

In Figure 4.14, the theoretical post-peak process zone length (rp) as a ratio of process zone length at peak-load (rp_u) is plotted against CMOD as a ratio of CMOD at peak-load ($CMOD_u$). It shows that the theoretical $CMOD/CMOD_u$ versus rp/rp_u curve is independent of beam size. The graph shows that as the rp decreases as CMOD increases. By combining Figure 4.11 with Figure 4.14, it can be seen that the process zone decreases as the crack grows. It is interesting to note that the Figure 4.14 is nothing but the combination of Figures 4.12 and 4.13. The graphs of Figures 4.12 and

4.13 are beam size dependent where as graphs of Figure 4.14 are size independent. This means that the size dependency of P/P_u versus $CMOD/CMOD_u$ and P/P_u versus rp/rp_u are compensated in $CMOD/CMOD_u$ versus rp/rp_u.

The above concluding remarks, which are made based on the theoretical results of the proposed model for three different sizes of beams, should be further investigated experimentally, as well as, theoretically on more different sizes of beams.

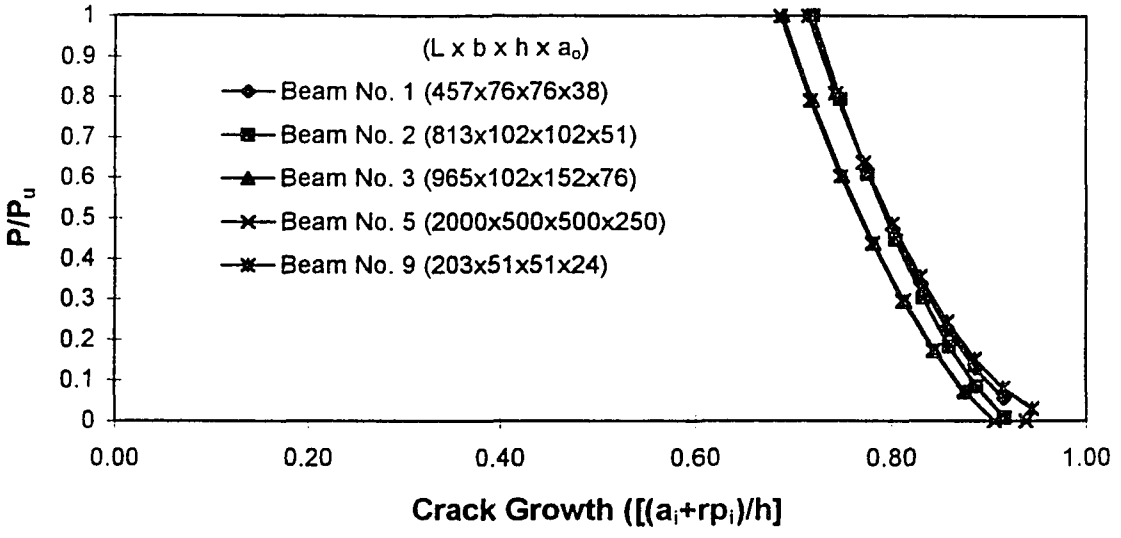

Figure 4.10 Plot of [P/P_u] versus Crack Growth, [(a_i + rp_i)/h] for different sizes of beams.

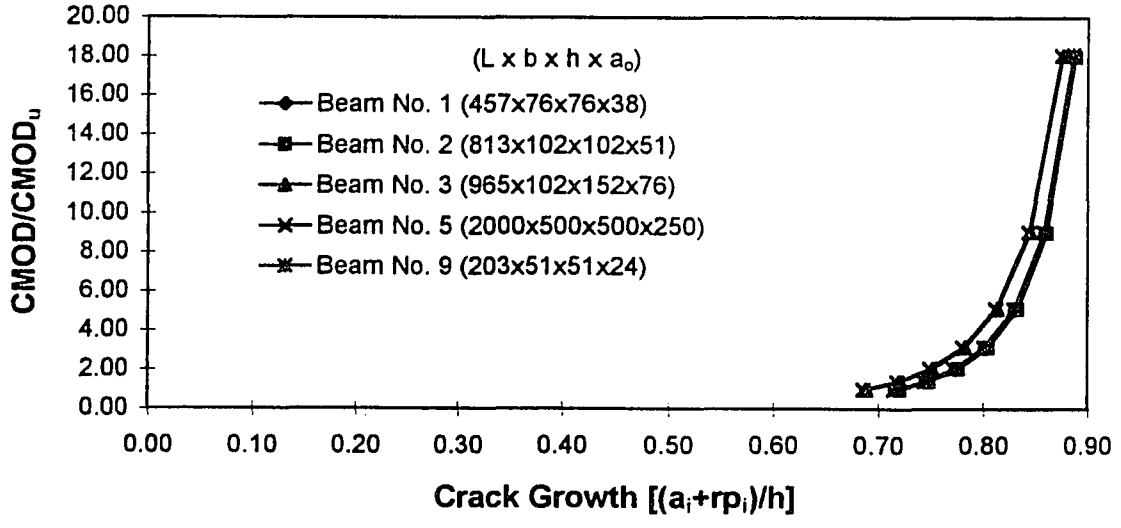

Figure 4.11 Plot of [$CMOD/CMOD_u$] versus Crack Growth, [(a_i + rp_i)/h] for different sizes of beams.

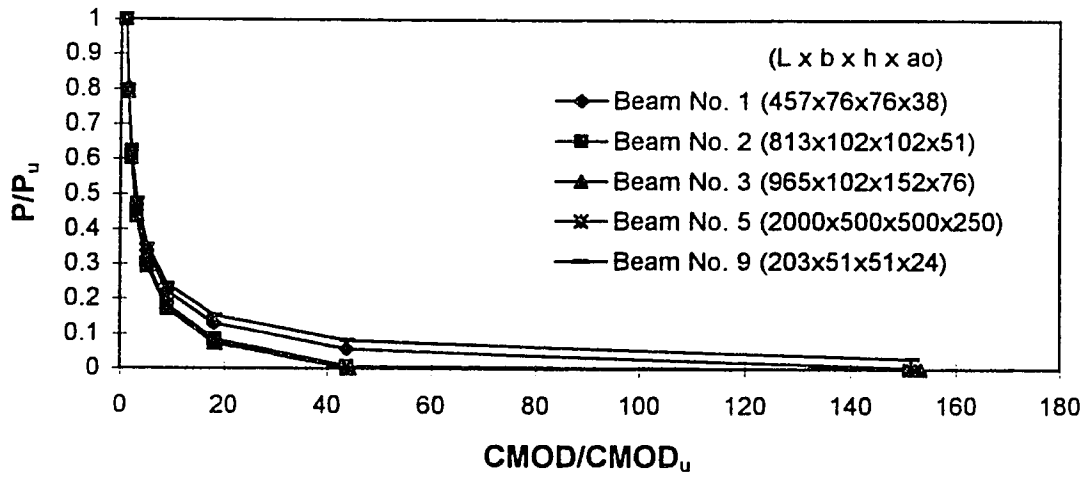

Figure 4.12 Plot of [P/P_u] versus [$CMOD/CMOD_u$] for different sizes of beams.

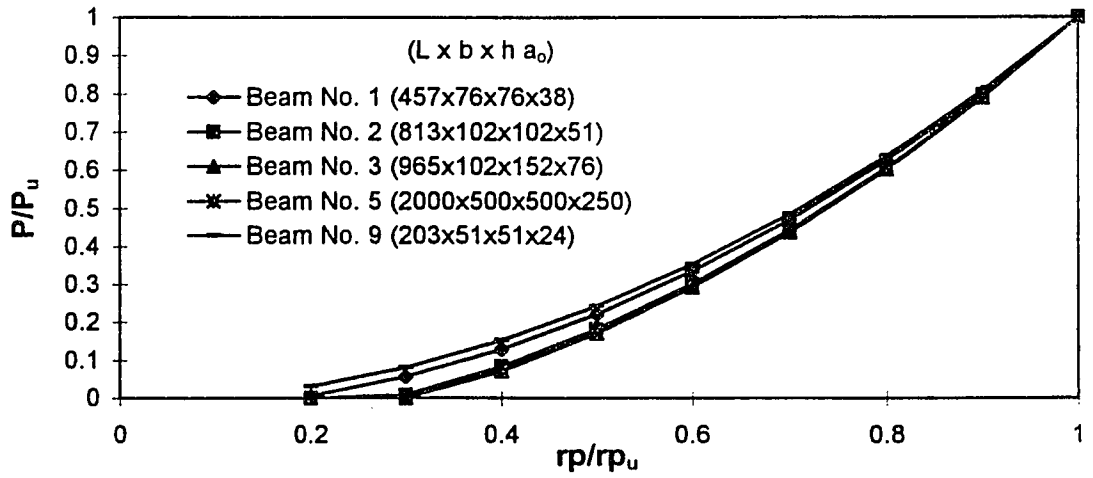

Figure 4.13 Plot of [P/P_u] versus [rp/rp_u] for different sizes of beams.

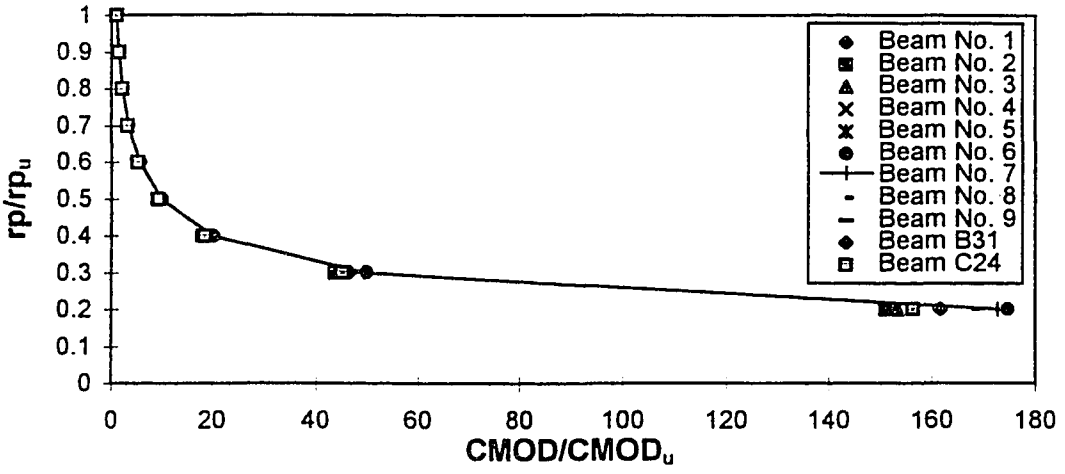

Figure 4.14 Plot of [CMOD/$CMOD_u$] versus [rp/rp_u] for different sizes of beams.

CHAPTER 5

CONCLUSIONS AND RECOMMENDATIONS FOR FUTURE RESEARCH

5.1 Summary and Conclusions

The main objective of this dissertation was to develop a simple non-linear fracture mechanics methodology for the determination of Fracture Energy (G_F) of concrete and it's non-linear fracture mechanics parameters, such as fracture process zone length (rp), critical fracture energy release rate (G_{IC}) and critical stress intensity factor (K_{IC}) for three point bend single-edge notch concrete beams. The validity of the concepts advanced in the proposed fracture model were demonstrated by an acceptable comparison of the theoretical prediction of the load versus CMOD, load versus load-point deflection (δ) relations and calculated G_F from theoretical P-δ with the experimentally measured values.

The conclusions of this dissertation can be summarized as follows:

1. The fracture energy (G_F) of concrete and non-linear fracture characteristics such as fracture process zone length (rp), critical fracture energy release rate (G_{IC}) and critical stress intensity factor (K_{IC}) can be determined according to the proposed model which is based on an analogous composite beam with continuously variable Young's modulus of elasticity within the fracture process zone.

2. The fracture process zone can be modeled as a damaged cohesive band where the extent of damage due to microcracking varies from no damage at the tip of FPZ to a complete damage (i.e. complete crack surface separation) at the tip of notch or pre-crack. Hence the fracture process zone can be defined as a material with a variable modulus of elasticity, E_V, where $E_V = 0$ at the tip of notch or pre-crack and $E_V = E$ (the modulus of elasticity of un-cracked zone) at the end of FPZ.

3. The proposed model can predict theoretically both the pre-peak and post-peak load versus crack-mouth opening displacement (CMOD) and load versus load-point deflection (δ) behavior for a three point bend (3-PB) single-edge-notch (SEN) beam. The accuracy of the predicted P-CMOD and P-δ relations are quite acceptable and satisfactory when compared with the experimental data.

4. The proposed model requires only Peak load (P_u) and corresponding crack-mouth opening displacement ($CMOD_u$). It does not require post-peak load-deflection or CMOD data. Furthermore, it does not require information as to the unloading characteristic of the beam. The testing machine does not need to be very stiff. No closed-loop displacement control is needed. This makes the testing procedure greatly simplified and makes it suitable not only for the testing laboratory but also for work sites where a closed-loop testing machine is not available.

5. The critical crack-mouth opening displacement at complete failure ($CMOD_F$) (i.e. the beam becomes completely fractured into two pieces) can be approximately estimated as eight times the crack-mouth opening displacement at peak load ($CMOD_u$).

5.2 Recommendations for Future Research

Most of the current analytical research to investigate the fracture behavior of concrete is based on the limiting states of plane stress or plane strain. Extending it to three dimensional case is necessary for further understanding and better simulation of fracture mechanics of concrete. The microcracking zone or the process zone is usually modeled analytically in one dimension (i.e. along the direction of crack propagation) and process zone length remains constant across the beam width. But some experimental results (Refai and Swartz, 1987) show that the microcracking zone

length varies across the beam width. Therefore, more effort both analytical and experimental is needed in this area.

For the sake of simplicity in the proposed model, the post-peak stress-displacement relation was assumed linear which is most widely used in analytical model. The proposed model can be further investigated by using bi-linear or other experimental result based empirical stress-displacement relations as discussed in literature survey, Section 2.2.

The contribution of tension reinforcement for reinforced concrete beam can be a new topic to be investigated by proposed fracture model.

The critical crack-mouth displacement at complete failure ($CMOD_F$) as obtained in this dissertation should be further investigated using more beam data and experimental results. Also, all concluding remarks which are made in this dissertation in Section 4.5 should be further investigated experimentally as well as theoretically on different sizes of beams.

APPENDIX - A

FORMULAE DERIVATION

A-1: **Moment at peak load, P_u**

Assuming unit weight of concrete = 150 pcf

Beam Dimensions, L,b,h are in inches, unit of Peak Load, P_u is pounds and unit of Peak Moment, M_u is lb-in

(Ref. Figure 3.1)

$$M_u = \frac{P_u \cdot L}{4} + \left[\frac{150}{12^3} b \cdot h\right]\frac{L^2}{8}$$

$$= 0.25P_u \cdot L + 0.010851b \cdot h \cdot L^2$$

A-2: **Elastic Moment Capacity, M_e**

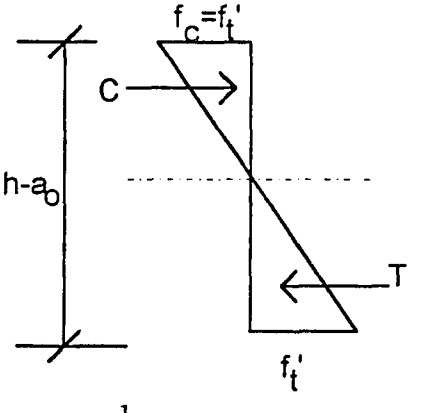

$$C = T = \frac{1}{4} f_t' \cdot b \cdot (h - a_0)$$

$$M_e = C(or\ T) \cdot Z$$

$$= \frac{1}{4} f_t' \cdot b \cdot (h - a_0) \cdot \frac{2}{3}(h - a_0)$$

$$= \frac{1}{6} f_t' \cdot b \cdot (h - a_0)^2$$

A-3: Boundary Limits for rp

Minimum value of rp = 0.

Derivation for the upper limit of rp:

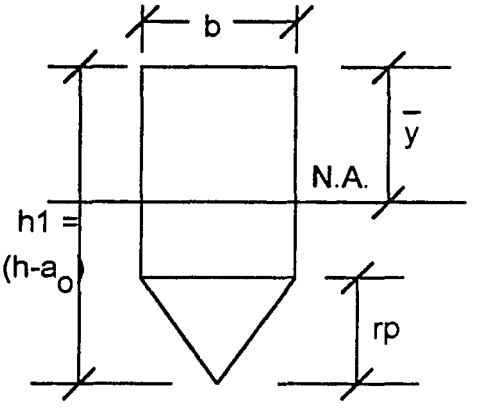

rp = fully developed fracture process zone length, (at peak load, Pu).

According to the composite section, the neutral axis, N.A. must lie above the process zone. Therefore,

$$\bar{y} < (h1 - rp)$$

$$\Rightarrow h1 > (\bar{y} + rp) \quad \text{.....(A3 - 1)}$$

R.H.S. of Eq. (A3 - 1):

$$(\bar{y} + rp) = \frac{3h_1^{\,2} + rp^2 - 3h_1 \cdot rp}{6\left(h_1 - \frac{1}{2}rp\right)} + rp$$

$$= \frac{3h_1^2 + 3h_1 \cdot rp - 2rp^2}{6\left(h_1 - \frac{1}{2}rp\right)}$$

Therefore, Eq.(A3 - 1) becomes

$$6h_1\left(h_1 - \frac{1}{2}rp\right) > \left(3h_1^2 + 3h_1 \cdot rp - 2rp^2\right)$$

$$\Rightarrow \left(3h_1^2 - 6h_1 \cdot rp + 2rp^2\right) > 0 \quad \text{.....(A3 - 2)}$$

Let us find out the real roots of

$$3h_1^2 - 6h_1 \cdot rp + 2rp^2 = 0$$

$$rp = \frac{6h_1 \pm \sqrt{36h_1^2 - 24h_1^2}}{2(2)}$$

$$= h_1 \frac{\left(3 \pm \sqrt{3}\right)}{2}$$

Therefore, $rp = 2.366h_1$ which is not possible.

$$= 0.63397h_1$$

$\therefore$ rp must be less than $0.63397h_1$

$$0 < rp < 0.63397h_1$$

A-4: <u>Section properties for the Composite section (Ref. Figure 3.5a)</u>

Composite Area:

$$A_c = b \cdot h_1 - \frac{1}{2} b \cdot rp$$

where $h_1 = h - a_0$

Location of neutral Axis:

$$\bar{y} = \frac{\frac{1}{2} b(h_1 - rp)^2 + \frac{1}{2} b \cdot rp\left(h_1 - \frac{2}{3} rp\right)}{A_c}$$

$$= \frac{h_1^2 + \frac{1}{3} rp^2 - h_1 \cdot rp}{2\left(h_1 - \frac{1}{2} rp\right)}$$

$$= \frac{3h_1^2 - 3h_1 \cdot rp + rp^2}{6\left(h_1 - \frac{1}{2} rp\right)}$$

Modulus of Inertia for the composite section,

$$I_c = \frac{1}{12}b(h_1 - rp)^3 + b(h_1 - rp)\left(\frac{h_1 - rp}{2} - \bar{y}\right)^2 + \frac{1}{36}b \cdot rp^3 + \frac{1}{2}b \cdot rp\left(h_1 - \frac{2}{3}rp - \bar{y}\right)^2$$

Section Modulus for the composite section at different levels:

$$S_{c1-1} = \frac{I_c}{\bar{y}}$$

$$S_{c2-2} = \frac{I_c}{(h_1 - rp - \bar{y})}$$

$$S_{c3-3} = \frac{I_c}{(h_1 - \bar{y})}$$

A-5: <u>Stresses at levels 1-1, 2-2 and 3-3</u>

Composite Beam Stresses (Ref. Figure 3.5b)

$$\sigma_{c1-1} = \frac{M_u}{S_{c1-1}}$$

$$\sigma_{c2-2} = \frac{M_u}{S_{c2-2}}$$

$$\sigma_{c3-3} = \frac{M_u}{S_{c3-3}}$$

Actual stresses (Ref. Figure 3.4b)

$$\sigma_{1-1} = \sigma_{c1-1}$$

$$\sigma_{2-2} = \sigma_{c2-2}$$

$$\sigma_{3-3} = \frac{\sigma_{c3-3}}{N_v(x = rp)} = \frac{\sigma_{c3-3}}{\infty} = 0$$

where $N_v(x) = \frac{E}{E_v(x)} = \left(1 - \frac{x}{rp}\right)^{-1}$, $0 \le x \le rp$

A-6: Static Equilibrium (Ref. Fig. 3.8b)

$$C = \frac{1}{2}\sigma_{c1\text{-}1} \cdot b \cdot \bar{y}$$

$$T = T_1 + T_2$$

where $T_1 = \frac{1}{2}\sigma_{c2\text{-}2} \cdot b(h - a_0 - \bar{y} - rp)$

and T_2 can be derived as following:

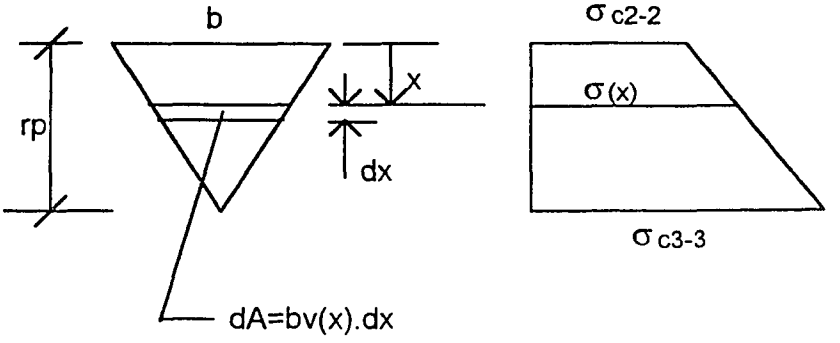

$$\sigma(x) = \sigma_{c2\text{-}2} + (\sigma_{c3\text{-}3} - \sigma_{c2\text{-}2})\left(\frac{x}{rp}\right), \quad 0 \le x \le rp$$

$$b_v(x) = \frac{b}{N_v(x)} = b\left(1 - \frac{x}{rp}\right)$$

$$T_2 = \int \sigma(x) \cdot dA$$

$$= \int_{x=0}^{rp}\left[\sigma_{c2\text{-}2} + (\sigma_{c3\text{-}3} - \sigma_{c2\text{-}2})\left(\frac{x}{rp}\right)\right]\left[b\left(1 - \frac{x}{rp}\right)\right]dx$$

$$= b \cdot \sigma_{c2\text{-}2}\int_0^{rp}\left(1 - \frac{x}{rp}\right)dx + b \cdot (\sigma_{c3\text{-}3} - \sigma_{c2\text{-}2})\int_0^{rp}\left(\frac{x}{rp} - \frac{x^2}{rp^2}\right)dx$$

$$= \frac{1}{2}b \cdot \sigma_{c2\text{-}2} \cdot rp + \frac{1}{6}b \cdot rp(2\sigma_{c3\text{-}3} - \sigma_{c2\text{-}2})$$

$$= \frac{1}{3}b \cdot rp\left(\sigma_{c2\text{-}2} + \frac{1}{2}\sigma_{c3\text{-}3}\right)$$

C.G. of T_1 :

$$y_{T1} = \frac{2}{3}(h - a_o - \bar{y} - rp)$$

G.G. of T_2 :

$$y_{T_2} = \frac{1}{T_2}\int_{x=0}^{rp} \sigma(x)\cdot b_v(x)\cdot x\cdot dx$$

$$= \frac{1}{T_2}\int_0^{rp}\left[\sigma_{c2-2} + (\sigma_{c3-3} - \sigma_{c2-2})\left(\frac{x}{rp}\right)\right]\left[b\left(1-\frac{x}{rp}\right)\right]xdx$$

$$= \frac{1}{T_2}\left[b\sigma_{c2-2}\int_0^{rp}\left(x-\frac{x^2}{rp}\right)dx + b(\sigma_{c33} - \sigma_{c2-2})\int_0^{rp}\left(\frac{x^2}{rp}-\frac{x^3}{rp^2}\right)dx\right]$$

$$= \frac{1}{T_2}\left[\frac{1}{6}b\cdot\sigma_{c2-2}\cdot rp^2 + \frac{1}{12}b(\sigma_{c3-3} - \sigma_{c2-2})rp^2\right]$$

$$= \frac{\frac{1}{12}b\cdot rp^2(\sigma_{c2-2} + \sigma_{c3-3})}{\frac{1}{6}b\cdot rp(2\sigma_{c2-2} + \sigma_{c3-3})}$$

$$= \frac{1}{2}rp\left(\frac{\sigma_{c2-2} + \sigma_{c3-3}}{2\sigma_{c2-2} + \sigma_{c3-3}}\right)$$

$$\bar{y}_1 = \frac{1}{T}\left[(T_1\cdot y_{T1}) + T_2\left\{(h - a_0 - \bar{y} - rp) + y_{T2}\right\}\right]$$

by substituting y_{T1}, y_{T2} and from similar triangles,

$$\frac{\sigma_{c3-3}}{\sigma_{c2-2}} = \frac{h - a_o - \bar{y}}{h - a_o - \bar{y} - rp}$$

$$\bar{y}_1 = \frac{1}{T}\left[\begin{array}{l}\frac{2}{3}T_1(h - a_o - \bar{y} - rp) + \\ T_2\left\{(h - a_o - \bar{y} - rp) + \frac{1}{2}\left(\frac{2(h - a_o - \bar{y}) - rp}{3(h - a_o - \bar{y}) - 2rp}\right)\right\}\end{array}\right]$$

Moment arm, $Z = \frac{2}{3}\bar{y} + \bar{y}_1$

Moment capacity, $M_{CAPACITY} = C(or\ \ T)\cdot Z$

Equations for static equilibrium:

$\sum H = 0 \qquad \Rightarrow T = C$

$\sum M = 0 \qquad \Rightarrow M_{CAPACITY} = M_u$

APPENDIX - B

COMPUTER PROGRAM BASED ON CBAFM

```
Program Composite_Beam_Analogy_Fracture_Model_CBAFM;
(* A Non-linear Fracture Mechanics Model for Three-Point Bend Beams *)
(* for Ph.D. Dissertation at NJIT -May 1995 *)
(* Programmed by : MOHAMMED ENAMUL HAQUE, NJIT ID # 000-84-2355 *)
Label 1,2,3;
var
a0,a,aa,h,alp,n,bta,ft,fc,Ec,GIc,
sig11,sig22,sig33,mu,pu,rp,L,cmodu,dna,ina,gf,me,pe,k1,
b,v,w,x,y,z,ctod,ctodu,cmod,cmode,
acom,ybar,icom,s11,s22,s33,comp,ten,
ae,a0h,aeh,KIe,KIc,delta,
dag,phi,wc,CTODE :real;
i,j,k,mm,bno,key,nob:integer;
file1,file11:text;

Procedure compsec(h,a0,b,rp:real;var Acom,ybar,Icom,s11,s22,s33:real);
var
h1:real;
begin
h1:=h-a0;
acom:=b*h1-0.5*b*rp;
ybar:=(3*h1*h1+rp*rp-3*h1*rp)/(6*(h1-0.5*rp));
Icom:=b/12*exp(3*ln(h1-rp))+b*(h1-rp)*exp(2*ln(abs((h1-rp)/2-ybar)))
   +b*exp(3*ln(rp))/36+0.5*b*rp*exp(2*ln(abs(h1-2*rp/3-ybar)));
s11:=icom/ybar;
s22:=icom/(h1-rp-ybar);
s33:=icom/(h1-ybar);
end;

Procedure PZL(h,a0,b,ft,mu:real;var rp,sig11,sig22,sig33,ybar,comp,ten:real);
var
x1,x2,tol,del,t1,t2,yy1,yy2,y1bar,Mcap:real;
i:integer;
begin
x1:=0.01;x2:=(h-a0)*0.7;
i:=0;
del:=999.0;tol:=0.1;
while (del>tol) do begin
```

```
i:=i+1;
IF(I=1) THEN RP:=X1;
IF(I=2) THEN RP:=X2;
IF (I>2) THEN
rp:=(x1+x2)/2;
compsec(h,a0,b,rp,Acom,ybar,Icom,s11,s22,s33);
sig22:=mu/s22;
del:=abs(sig22-ft);
if (sig22-ft) >0.0 then x1:=rp
else
x2:=rp;
end;
sig11:=mu/s11;sig33:=mu/s33;
comp:=0.5*sig11*b*ybar;
t1:=0.5*sig22*b*(h-a0-ybar-rp);
t2:=b*rp*sig22/3+b*rp*sig33/6;
ten:=t1+t2;
yy1:=h-a0-ybar-rp;
yy2:=0.5*rp*(sig22+sig33)/(2*sig22+sig33);
y1bar:=(t1*0.66667*yy1+t2*(yy1+yy2))/ten;
Mcap:=comp*(0.6667*ybar+y1bar);
end;

Procedure calculate_ctodu_cmodu(cmodu,sig33,h,ao,ec,ybar:real;var wc, ctodu:real);
begin
ctodu:=cmodu*(h-ybar-ao)/(h-ybar);
wc:=ctodu/(sig33/ec);
end;

Procedure Calculate_GIc_k1(h,b,a0,rp,ybar,ft,cmodu,ec:real;var gic,k1:real);
var
y1,sqk1:real;
begin
y1:=h-a0-rp-ybar;
gic:=ft*rp*cmodu*y1/(h-ybar)/b;
gic:=gic*(1/3+1/2*rp/y1+1/5*rp*rp/y1/y1);
sqk1:=gic*ec;
k1:=exp(0.5*ln(sqk1));
end;

Procedure ELASTIC_STRENGTH(ft,a0,h,b,l:real; var Me,Pe:real);
begin
(* length unit inch, force unit lb. *)
Me:=ft*b*(h-a0)*(h-a0)/6.0;
```

```
Pe:=(Me-0.01085*b*h*l*l)*4/l;
end;


Procedure P_Delta(l,b,h,a0,rpi,P,CMOD,ec,pu:real; var delta:real);
var
ai,gi,v1,v2,delcrk,delnock:real;
i,j:integer;
begin
(* Program Module 4 *)
ai:=a0+rpi;
gi:=ai/h;
(* for l/h =4 only *)
v1:=0.76-2.28*gi+3.87*gi*gi-2.04*gi*gi*gi+0.66/(1-gi)/(1-gi);
v2:=exp(2*ln(gi/(1-gi)))*(5.58-19.57*gi+36.82*gi*gi-
34.94*gi*gi*gi+12.77*gi*gi*gi*gi);
delcrk:=0.25*l/ai*cmod*v2/v1;

delta:=delcrk;
end;

Procedure P_CMOD_ascending_Model(L,h,a0,b,rpu,pu,pe,ybar,wc,ft,ec:real);
var
p,cmod,rpi,ybari,delyb,ac,ab,ang,h1,nn,area,a1,a2,a3,mom,
c,t1,t2,t3,delybar,ybarcal,T,yr,bp,xbar,delta:real;
i,j,m:integer;
begin
h1:=h-a0;
ang:=ft/rpu;
i:=1;  (* First Point  *)
P:=0.0; cmod:=0.0; delta:=0.0;
rpi:=0.0; ybari:=h1/2;
Writeln(file11,cmod,',',p,',',delta);
i:=2; (* rp = 0 Elastic limt  *)
p:=pe;
ybari:=h1/2; rpi:=0.0;
cmod:=ft/Ec*wc*(ybari+a0)/ybari;
P_Delta(l,b,h,a0,rpi,p,cmod,ec,pu,delta);
Writeln(file11,cmod,',',p,',',delta);
ybari:=h1/2;
m:=7;
for i:=3 to m do begin
ybari:=h1/2-(h1/2-ybar)*(i-2)/m;
rpi:=0.001;
```

```
delybar:=1.0;
while delybar>0.001 do begin
ac:=ft*(h1-ybari)/(h1-ybari-rpi);
ab:=ft-rpi*ang;
nn:=ac/ab;
(* calculate ybarcal *)
a1:=b*(h1-rpi);
a2:=rpi*b/nn;
a3:=0.5*rpi*(b-b/nn);
area:=a1+a2+a3;
ybarcal:=1/area*(a1*(h1-rpi)/2+a2*(h1-rpi/2)+a3*(h1-2*rpi/3));
delybar:=abs(ybari-ybarcal);
if(delybar>0.001) then rpi:=rpi+0.001;
end;
(* calculate Mom & P *)
C:=0.5*(ft/(h1-ybari-rpi)*ybari)*ybari*b;
T1:=0.5*ft*(h1-ybari-rpi)*b;
bp:=h1-ybari-rpi;
t2:=b*ft*rpi*(0.5*(1+1/nn)+rpi/(6*bp)*(1+2/nn));
xbar:=rpi*(1/6+1/(3*nn))+rpi*rpi/bp*(1/12+1/(4*nn));
xbar:=xbar/(0.5*(1+1/nn)+rpi/(6*bp)*(1+2/nn));
T:=t1+t2;
yr:=(t1*2*(h1-ybari-rpi)/3+t2*(h1-ybari-rpi+xbar))/T;
Mom:=C*(2*ybari/3+yr);
P:=4.0/l*(Mom-0.01085*b*h*l*l);
cmod:=ft/ec*wc*(h-ybari)/(h1-ybari-rpi);
P_Delta(l,b,h,a0,rpi,p,cmod,ec,pu,delta);
Writeln(file11,cmod,',',p,',',delta);
end;
end;

Procedure P_CMOD_Descending_Model(a0,h,rpo,b,l,ft,Gic,cmod0,ybar0,pu:real);
var
   ai,Pi,CMODi,c1,c2,lamda,aih,rpi,t1,t2,comp,yy1,yy2,y1bar,
   ten,ybar,Mmaxi,Pmaxi,y1i,cmod2:real;
   i,j,N:integer;
Begin
  lamda:=0.633;
  c1:=rpo/(h-a0)-lamda*a0/h;
  n:=10;
  for i:=1 to n-2 do begin
  aih:=a0/h+(1-(a0/h))*i/n;
  ai:=aih*h;
  (* 1st trial value of rpi  *)
```

```
  rpi:=rpo/(h-a0)*(h-ai);
  (* Calculate Mmaxi *)
  comp:=0.0; ten:=10.0;  (* make initial trial comp < ten *)
  compsec(h,ai,b,rpi,Acom,ybar,Icom,s11,s22,s33);
  sig22:=ft;
  sig11:=ft*ybar/(h-ybar-ai-rpi);
  sig33:=ft*(h-ybar-ai)/(h-ybar-ai-rpi);
comp:=0.5*sig11*b*ybar;
t1:=0.5*ft*b*(h-ai-ybar-rpi);
t2:=b*rpi*ft/3+b*rpi*sig33/6;
ten:=t1+t2;
yy1:=h-ai-ybar-rpi;
yy2:=0.5*rpi*(sig22+sig33)/(2*sig22+sig33);
y1bar:=(t1*0.66667*yy1+t2*(yy1+yy2))/ten;
Mmaxi:=comp*(0.6667*ybar+y1bar);
Pmaxi:=4.0/l*(Mmaxi-0.01085*b*h*l*l);
(* Calculate CMODi, assuming Gic Const. Material Property *)
y1i:=h-ai-rpi-ybar;
AA:=(h-ybar)*b/(ft*rpi*y1i*(1/3+1/2*rpi/y1i+1/5*rpi*rpi/y1i/y1i));
cmodi:=Gic*AA*rpo/rpi;
P_Delta(l,b,h,ai,rpi,pmaxi,cmodi,ec,pu,delta);
writeln(file11,cmodi,',',pmaxi,',',delta);
  end;
  end;

begin  (* MAIN *)
assign(file1,'a:DATA.PAS');
assign(file11,'a:RESULT.PAS');
reset(file1);
rewrite(file11);
(* Length unit is INCH, Force unit is POUND *)
readln(file1);
writeln('**** CBAFM.PAS is Running ****');
writeln('**** Programmed by: Mohammed E. Haque, Ph.D.,P.E. ****');
nob:=2; (* nob = total number of beams *)
for i:=1 to nob do begin
key:=123; (* key=123 for doing all the program modules *)
readln(file1,l,b,h,a0h,pu,ft,cmodu,Ec);  (* a0h=ao/h *)
a0:=a0h*h;  bno:=i;
(* Check for the Elastic Strength of the Beam *)
ELASTIC_STRENGTH(ft,a0,h,b,l,Me,Pe);
rp:=0.0;
Mu:=Pu*l/4+0.01085*b*h*l*l;  (* Unit Weight of Concrete = 150 PCF *)
(* Mu:=Pu*l/4.0;*)
```

```
If (Pe >= Pu) then begin
writeln('Elastic Moment Capacity Me = ',Me:10:3,' lb-in');
writeln('Moment due to Pu = ',Mu:10:3,' lb-in');
writeln('ELASTIC LOAD CAPACITY  Pe=',Pe:10:3,' #',' IS MORE THAN ACTUAL
LOAD Pu=',
     Pu:10:3,' #');
writeln('NO FRACTURE WILL BE DEVELOPED.  CHECK Pu OR TENSILE
STENGTH ft*');
writeln('******** PROGRAM TERMINATION DUE TO BAD DATA *********');
Goto 1
end;
(* Program MODULE-1 *)
PZL(h,a0,b,ft,mu,rp,sig11,sig22,sig33,ybar,comp,ten);
ae:=a0+rp;
aeh:=ae/h;
calculate_ctodu_cmodu(cmodu,sig33,h,a0,ec,ybar,wc,ctodu);
Calculate_GIc_k1(h,b,a0,rp,ybar,ft,cmodu,ec,Gic,k1);
writeln(file11,'BEAM SL. NO. ',BNO);
writeln('BEAM NO. ',BNO,' is now working');
writeln(file11,'l,','b,','h,','a0,','rp,','Ec,','ft,','Pu,','CMODu,','GIc,','K1');
writeln(file11,l,',',b,',',h,',',a0,',',rp,',',Ec,',',ft,',',Pu,',',CMODu,',',Gic,',',K1:10:3);
writeln(file11,'CMOD,','P,','delta');
while key=123 do begin
(* Program MODULE-3 *)
P_CMOD_ascending_Model(L,h,a0,b,rp,pu,pe,ybar,wc,ft,ec);
P_Delta(l,b,h,a0,rp,pu,cmodu,ec,pu,delta);
Writeln(file11,cmodu,',',pu,',',delta);
(* Program MODULE-2 *)
P_CMOD_Descending_Model(a0,h,rp,b,l,ft,Gic,cmodu,ybar,pu);
writeln(file11);
key:=99;
end;
end;
writeln('**** SUCCESSFUL COMPLETION ****');
close(file1);
close(file11);
1: end.
```

Note: The Output file "Result.Pas" is formatted in such a way that after each output, there will a "," . This is done in order to down load the Output file "Result.Pas" into Microsoft EXCEL or Lotus 1-2-3, which will provide graphic applications (such as prepare graphs etc.).

APPENDIX - C

SI UNIT CONVERSION FACTORS

The following SI Unit Conversion Factors have been used in this dissertation:

Quantity	Multiply	by	to obtain
Length	Inch (in)	25.4	Millimeter (mm)
Force	Pound-force (lb)	4.448222	Newton (N)
Bending Moment	Pound-force-inch (lb-in)	0.112985	Newton-Meter (N-m)
Stress	Pound-force per Sq. inch (lb/in^2)	0.00689475	Megapascal (MPa)
Fracture Energy	Pound-force per Inch (lb/in)	175.127	Newton per Meter (N/m)
Stress Intensity Factor	$PSI\sqrt{in}$	0.034748	$MPa\sqrt{mm}$

REFERENCES

Ansari, F. 1987. "Stress-Strain Response of Microcracked Concrete in Direct Tension," *ACI Materials Journal*, Technical Paper, Title no. 84-M42, pp. 481-490.

Ansari, F. 1989. "Mechanism of Microcrack Formation in Concrete," *ACI Materials Journal*, Technical Paper, Title no. 86-M41, pp. 459-464.

Bazant, Z.P., and B.H. Oh. 1983. "Crack Band Theory for Fracture of Concrete," *RILEM, Materials and Structures*, Vol. 16, No.93, pp.155-177.

Bazant, Z.P. 1986. "Mechanics of Distributed Cracking (1986)," *Applied Mechanics Reviews*, ASME, Vol.39, No.5, pp. 767-705.

Bazant, Z.P., and P.A. Pfeiffer. 1987. "Determination of Fracture Energy from Size Effect and Brittleness Number," *ACI Material Journal*, Title No. 84-M41.

Carpinteri, A., and A.R. Ingraffea (editors) 1984. *Fracture Mechanics of Concrete: Material Characterization and Testing*, Martinus Nijhoff Publisher.

Go, Cheer-Germ, and Stuart E. Swartz. 1983. "Fracture Toughness Techniques to predict Crack Growth and Tensile Fracture in Concrete," *Report No. 154, Engineering Experiment Station*, Kansas State University, Manhattan, KS.

Gopalaratnam, V.S., and S.P. Shah. 1985. "Softening Response of Plain Concrete in Direct Tension," *ACI Journal*, Vol.82, No.3, pp. 310-323.

Hillerborg, A.E., M. Moder, and P.E. Petersson. 1976. "Analysis of Crack Formation and Crack Growth in Concrete by means of Fracture Mechanics and Finite Elements," *Cement and Concrete Research*, Vol. 6, pp. 773-782.

Hillerborg, A. 1983. "Analysis of One Single Crack," *Fracture Mechanics of Concrete* edited by F.H. Wittmann, Elsevier Science Publishers B.V., Amsterdam.

Ingraffea, A.R., and W.H. Gerstle. 1984. "Non-Linear Fracture Models for Discrete Crack Propagation," *Proceedings of NATO Advanced Workshop "Application of Fracture Mechanics to Cementitious Composites*, edited by S.P. Shah.

REFERENCES
(Continued)

Jenq, Y.S., and S.P. Shah. 1985a. "Two Parameter Fracture Model for Concrete," *Journal of Engineering Mechanics*, ASCE, Vol. 111, No.10, Oct. , pp.1227-1241.

Jenq, Y.S., and S.P. Shah. 1985b. "Nonlinear Fracture Parameters for Cement Based Composites: Theory and Experiments," in *Application of Fracture Mechanics to Cementitious Composites*, S.P. Shah, Ed., Martinus Nijhoff Publishers, pp. 319-359.

Jenq, Y.S., and S.P. Shah. 1985c. "A Fracture Toughness Criterion for Concrete," *Engineering Fracture Mechanics*, Vol.21, No.5, pp.1055-1069.

Kaplan, M.F. 1961. "Crack Propagation and the Fracture of Concrete," *Journal of the American Concrete Institute*, Vol. 58, No. 5, pp. 591-610.

Mindess, Sidney. 1983. "Application of Fracture Mechanics to Concrete," *Proceedings, Fourth Engineering Mechanics Division Specialty Conference*, Purdue University.

Nallathambi, P., and B.L. Karihaloo. 1985. "Determination of Specimen Size Independent Fracture Toughness of Plain Concrete", *Proceedings, Fracture Energy of Concrete*, Switzerland.

Petersson, P.E. 1981. "Crack Growth and Development of Fracture Zones in Plain Concrete and Similar Materials," *Report TVBM- 1006, Division of Building Materials, Lund Institute of Technology*, Sweden.

Petersson, P.E. 1980. "Fracture Energy of Concrete: Method of Determination and Practical Performance and Experimental Results," *Cement and Concrete Research*, Vol. 10, pp. 78-101.

Ratanalert, S., and M. Wecharatana. 1990. "Evaluation of Existing Fracture Models in Concrete," *American Concrete Institute, SP-118-5*, pp. 113-146.

Refai, T.M.E, and S.E. Swartz. 1987. "Fracture Behavior of Concrete Beams in Three-Point Bending Considering the Influence of Size Effects," *Kansas State University, Engineering Experiment Station, Report No. 190.*

REFERENCES
(Continued)

Reinhardt, H.W., H.A.W. Cornelissen, and D.A. Hordijk. 1986. "Tensile Tests and Fracture Analysis of Concrete," *Journal of Structural Engineering*, ASCE, Vol. 112, No. 11, pp. 2462-2477.

RILEM Technical Committee 50-FMC. 1985. "Determination of the Fracture Energy of Mortar and Concrete by means of Three-point Bend Tests of Notched Beams," Proposed RILEM recommendation, *Materials and Structures*, Vol. 18, No. 106.

Shah, S.P., and F.J. McGarry. 1971. "Griffith Fracture Criterion and Concrete," *Journal of Engineering Mechanics Division (ASCE)*, pp 1663-1675.

Swartz, S.E., K.K. Hu, and G.L. Jones. 1978. "Compliance Monitoring of Crack Growth in Concrete," *Journal of Engineering Mechanics Division, ASCE*, Vol. 104, No. EM4, pp. 412-417.

Swartz, S.E., K.K. Hu, M. Fartash, and C.M.J. Huang. 1982. "Stress Intensity Factors for Plain Concrete in Bending- Pre-notched versus Precracked Beams," *Experimental Mechanics*, Vol. 22, No. 11.

Swartz, S.E., and T.M.E. Refai. 1987. "Strain Distribution Ahead of The Crack Front in Concrete Beams in Three-Point Bending," *Proceedings, BSSM SEN International Conference on Advanced Measurement Techniques*, London.

Tada, H., P.C. Paris, and G.R.Irwin. 1976. *The Stress Analysis of Cracks Handbook*, Del Research Corporation, Hellertown, Pa.

Wecharatana, M., and S.P. Shah. 1982. "Prediction of Nonlinear Fracture Process Zone in Concrete," *Journal of EMD, ASCE* , pp. 1100-1113.

Wecharatana, M., and S.P. Shah. 1982. "Slow Crack Growth in Cement Composites," *Journal of the Structural division, ASCE*, Vol. 108, No. 5T6, pp. 1400-1413.

Wecharatana, M., and S.P. Shah. 1983. "Non-Linear Fracture Process Zone in Concrete," *Proceedings, Fourth Engineering Mechanics Division Specialty Conference*, Purdue University.

Wecharatana, M., and W.J. Chiou. 1986. "Fracture Energy and the Complete Tensile Softening Response of Concrete," *Proceedings of the 1986 SEM Spring Conference on Experimental Mechanics*, New Orleans, pp. 23-30.

REFERENCES
(Continued)

Yu, Been-Jyh. 1995. "A Nondestructive Method for the Determination of Fracture Energy in Concrete Structures," *Ph.D. Dissertation in Civil Engineering*, New Jersey Institute of Technology.